Structural and spectroscopical investigation of metallothionein 1 from *Cicer arietinum*.

Dissertation

zur

Erlangung der naturwissenschaftlichen Doktorwürde

(Dr. sc. nat.)

vorgelegt der

Mathematisch-naturwissenschaftlichen Fakultät

der

Universität Zürich

von

Oliver Schicht

aus

Österreich

Promotionskomitee

Prof. Dr. Heinz Berke (Vorsitz)

Dr. Eva Freisinger (Leitung der Dissertation)

Prof. Dr. Roland K.O. Sigel

Zürich, 2008

We are what we think. All that we are arises with our thoughts. With our thoughts, we make our world.

Buddha

Acknowledgements

My first acknowledgement goes to Dr. Eva Freisinger for accepting me as a part of her group and giving me to opportunity of conducting research in this interesting field.

Prof. Dr. Heinz Berke for the continuous support of our group and research.

I thank Estevão Aun Peroza, Augusto C. dos Santos Cabral and Xiaoqiong Wan for the excellent atmosphere in the lab, the friendship we share and for keeping the aquarium intact.

My thanks go to the whole Sigel-group for their cooperation, daily help and support.

Ms Beatrice Spichtig for the perfect organization of every thing concerning bureaucracy.

I thank all the members of the ACI, especially Tanja Spörri, for their uncomplicated interactions and help.

Thank you all for the incredible gift to my 30th birthday.

Special thanks to my parents and my brother, for their continuous support through all the years.

My gratefulness goes to Ms Ada Carbone, for supporting me in my life and through the time of writing this thesis.

Thank You.....

1 Index of content

2 Abstract

Only a couple of years ago, existence of plant metallothioneins (MTs) was uncertain and research on this subject was almost inexistent. The metal ion binding abilities of the plant metallothionein 1 (MT1) from *Cicer arietinum* (chickpea) has not been described ambiguously in the literature so far. Plant MTs are small gene encoded ~7-8 kDa proteins with a high cysteine content. Differing form their mammalian isoforms, plant metallothioneins feature a Cys-devoid linker region of up to 42 amino acids, which might even contain aromatic amino acids. Coordination of d^{10} metal ions is assumed to occur predominantly via thiol groups of the cysteine residues and most likely of metal-thiolate clusters are formed.

The aim of this work was to characterise the chickpea metallothionein 1 by spectroscopic methods. For the first time the plant metallothionein 1 (MT1) from *Cicer arietinum* (chickpea) has been described. The metal ion binding capacities were studied via metal ion titration experiments of the apo-, zinc- and cadmium-forms. Absorption (UV), circular dichroism (CD) and magnetic CD reveal an exceptional high divalent d^{10} metal ion binding ability of 5, requiring a new type of cluster, unprecedented in the literature so far. This was not expected with respect to only 12 Cys-residues, which are equally distributed among the C- and N-terminal domains.

pH titrations show a two-step behaviour, with a minor step over a broad pH range and a major step. As expected, the pH value at which complete release of Cd(II) ions was achieved is lower than for the Zn(II) forms.

The binding capacity of copper(I) is 6 as seen from UV- and CD-spectroscopy, leading to unusual high Cu(I) to Cys ratios for MTs of 2.

The secondary structure of MT1 from C. *arietinum* shows a high content of about 30% β-sheets, which are expected to form the linker region. Large amounts of defined secondary structural elements are only to be found in plant MTs.

3 Zusammenfassung

Noch vor einigen Jahren war die Existenz von Metallothioninen (MTs) in Pflanzen zweifelhaft und Forschung auf diesem Gebiet wurde nur vereinzelt durchgeführt. Daher wurde zum Beispiel die Bindungskapazität von Metallothionein 1 aus *Cicer arietinum* bis jetzt noch nicht beschrieben. Pflanzliche MTs sind gencodierte, ~7-8 kDa grosse Proteine, mit einen hohen Cysteinanteil. Sie unterscheiden sich von den Isoformen der Säugetiere durch einen bis zu 42 Aminosäuren langen Cys-freien Linker, welcher sogar aromatische Aminosäuren enthalten kann. Die Koordination von vorwiegend d^{10} Metallionen erfolgt über die Schwefelgruppen der Cystein-Seitenketten in Form von Metall-Thiolat-Clustern.

Das Ziel dieser Arbeit ist die Charakterisierung des MT1 der Kichererbse (*Cicer arietinum*) mit Hilfe spektroskopischer Methoden, welches in dieser Arbeit zum ersten mal beschrieben wird. Die Bindungskapazitäten wurden über verschiedene Titrationsexperimente der apo-, Zink und Cadmium-Formen bestimmt. Absorptions- (UV), circular Dichroismus (CD) sowie magnetische CD Spektroskopie zeigen eine unerwartet hohe Bindungskapazität von 5 divalenten d^{10} Metallionen. Durch die gleichmässige Verteilung und geringe Gesamtzahl von 12 Cysteinen in der Primärstruktur auf zwei Domänen wurde eine geringere Kapazität erwartet.

In pH-Titrationen wird ein 2-stufiges Verhalten mit einem kleinen und einem grösseren Schritt bei der Metallionenabgabe deutlich. Wie erwartet sind die pH-Werte, die eine vollständige Freigabe aller gebundenen Metallionen wiederspiegeln, für Cadmium tiefer als für Zink.

Bis zu 6 Kupfer(I)-Ionen können an MT1 binden, wie durch UV- und CD-Spektroskopie bestätigt wurde. Dies führt zu einem bis dahin in der Literatur unbekannten höheren Cu(I) zu Cys Verhältnis von 2.

Der sekundäre Anteil von 30% β-Faltblatstruktur welcher der Linkerregion zugeschrieben wird, ist aussergewöhnlich für MTs. Bis jetzt weisen nur MTs aus Pflanzen höhere Anteile definierter Sekundärstrukturen auf.

4 Abreviations

AAS	Atomic Absorption Spectrometry
CD	Circular dichroism
cicMT1	Metallothionein 1 from *Cicer arietinum*
Cys	Cysteine residues
DTT	Dithiothreitol
E_c-1	Early cysteine-labeled protein
ESI-MS	Electrospray Ionisation Mass Spectrometry
FPLC	Fast Protein Liquid Chromatography
FTIR	Fourier transform infrared spectroscopy
LMCT	Ligand-to-metal charge transfer
MCD	Magentic circular dichroism
MT	metallothionein
MT1	Metallothionein 1
PC	Phytochelatine
2-PDS	2,2'-Dithio-dipyridine
SDS-PAGE	sodium dodecyl sulfate polyacrylamide gel electrophoresis
Tris	2-amino-2-hydroxymethyl-1,3-propanediol
UV	Ultra violett
Vis	visible

5 Introduction

5.1 Metal ion uptake and defense mechanisms in plants

A number of factors influence the growth of plants in their natural habitat, one of which is the exposure to different essential and non-essential metal ions. Specifically sufficient supply with zinc or copper is vital to plants. Growth conditions with potential toxic levels of metal ions can basically have three effects: unrestricted uptake, exclusion and (hyper)accumulation [1]. Naturally, the largest amount of metal ions present in the soil are excluded by the cell membrane of the plant roots, acting as a kind of cation exchanger [2]. Nevertheless, controlled uptake of micronutrients such as copper, nickel and zinc ions is ensured by specific mechanisms[3]. Unfortunately, cadmium, lead and mercury ions, metal ions for which there is no essential role known in plants, can also reach the inner cell compartment where they very often bind irreversible to the available ligands, blocking important ligands even at low concentrations [4]. Recently however, a role of cadmium under zinc deficient growth conditions in marine diatoms has been stated [5, 6]. Mercury, lead(IV) and copper(I) are classified as class B ions with a pronounced affinity to sulfur and nitrogen in biological systems, whereas copper(II), cadmium, nickel and zinc, classified as class A metal ions, are borderline metal ions forming stable complexes with sulfur, nitrogen and oxygen as donor atoms [7]. Zinc ions are required in a large number of enzymes and play an essential role in DNA transcription [8]. A typical symptom of zinc deficiency is stunted leave growth, commonly known as "little leaf" and is caused by the oxidative degradation of the growth hormone auxin [9-11]. Toxicity of cadmium and mercury may result from the binding of these metal ions to sulfydryl groups in proteins, leading to an inhibition of activity or disruption of structure. This might also be accompanied by the displacement of essential metal ions from their binding sites resulting in additional deficiency effects [4]. Furthermore, an excess of heavy metal ions may stimulate the formation of free radicals and reactive oxygen species (ROS), thereby resulting in oxidative stress conditions [12, 13].

The distribution of zinc and copper ions in plants and their specific tissues remains still unknown [14]. For copper two types of transporters are known [15, 16]. However, an integrated picture combining all metal ion transport mechanisms is still inexistent, but necessary to engineer plants with specific metal ion binding abilities to improve human health

[14]. Since plant foods contribute at least 70% of the cadmium uptake in humans, an understanding on how plants take-up this metal ion and distribute it among their different tissues is of major interest [17]. Especially seeds such as rice, durum wheat, sunflower kernels and flax seeds but also shellfish tend to naturally hyper-accumulate Cd(II) in amounts 100-fold higher than the maximum dose of <10 µg/kg which is not considered to be a health risk [18].

Plants feature various methods of defense against metal toxicity. Extracellularly they include roles for mycorrhizas (a symbiotic association between a fungus and the roots of a plant), as well as for the cell wall and extracellular exudates [19]. Interestingly, metal tolerant species seem not to posses an enhanced tolerance towards free radicals and reactive oxygen species (ROS), but rather rely on improved mechanisms for metal ion homeostasis [12].

Importantly, the cell membrane is the first barrier for protection and uptake of essential and non-essential metal ions. This is ensured by repulsion and reduced permeability, or alternatively active efflux is used to ensure metal ion uptake required for nutrient needs [20]. However, direct evidence for active metal ion transport through the plasma membrane in plants is scarce [19]. Gene analyses have revealed the existence of metal ion transporters in plants such as CPx-ATPase, the Nramps and the CDF (cation diffusion facilitator) family, which could play a role in metal trafficking [21]. Nevertheless, knowledge of the transport function, specificity and cellular locations of these proteins in plants are unknown. Even though uptake of metal ions is not specific for a given transporter, translational and post-translational regulation of these active pumps is [14]. There are indications for a copper induced leakage of the plasma membrane, indicating a certain toxicity of this essential metal ion to plants [22]. This damage could result from various mechanisms such as oxidation and cross-linking of protein thiols, inhibition of key membrane proteins or changes in the fluidity of membrane lipids [23]. Direct effects of copper and cadmium treatments on the lipid composition of the membrane and thus the membrane permeability have been discribed [22, 24-26]. Furthermore, ATPase function is reduced by cadmium in wheat and sunflower roots [26], while, in *Nitella gracilis (green algae)*, copper-induced changes in cell permeability were attributed to non-selective conductance increases and inhibition of the light-stimulated H^+-ATPase pump [27]. It is important to note, that effects on the plasma membrane of plants are metal ion specific, since zinc in contrast to for example copper does not cause membrane leakage and is protective against oxidation [3, 28]. Additional factors that may be involved in the maintenance of plasma membrane integrity involve heat shock proteins and plant metallothioneins in an enhanced membrane repair machinery [29].

Designed by nature to help withstand thermal stress, heat shock proteins (HSP) are also expressed as response to heavy metal ion stress [30, 31]. It could be shown, that a short heat stress given prior to heavy metal ion stress prevents membrane damage [32]. Still further investigations are needed for a detailed analysis or support of a repair or protective role of HSP [19].

In contrast to mammalians, plants feature non-translational enzymatically synthesized phytochelatins (PCs). Synthesis requires metal ion glutathion complexes as substrate and is considered to be the major response of plants to heavy metal stress [33]. The general structure of PCs is $(\gamma\text{-Glu-Cys})_n\text{-Gly}$ with n = 2-11. Exposure of *Brassica juncea*, Indian mustard, to cadmium showed rapid induction leading to PC biosynthesis and PC concentrations theoretically sufficient to chelate all Cd^{2+} taken up [34]. Furthermore, also genes encoding for PC synthases in yeast have been identified, and it has also been shown that introduction of the *Arabidopsis thaliana*, mouse-ear cress, PC gene could confer substantial increases in metal ion tolerance in yeast [35, 36]. To investigate the function of PCs in metal ion detoxification, the sensitivity of several PCsynthase mutants was tested for a range of heavy metal ions in both, *A. thaliana* and *Schizosaccharomyces pombe*, fission yeast, and revealed a role of PCs against cadmium ions and arsenate, but not against zinc and nickel [37]. Also, copper does not seem to influence the level of PCs and questions a general role of PC in copper detoxification. More likely seems a chelation of copper ions by plant metallothioneins [38].

The final step in cadmium detoxification in higher plants involves compartmentalization of cadmium-PC complexes in the vacuole [39]. This accumulation appears to be mediated by both, a Cd/H^+ antiporter and an ABC-transporter, located at the tonoplast [40]. The stabilization of the Cd-PC complex in the vacuole is facilitated by the incorporation of acid-labile sulfide [41, 42].

5.1.1 The role of MTs in metal homeostasis

The role of MTs in plants is still a matter of debate. Within the protoplast chelators such as organic acids, amino acids, phytochelatins (PCs) or metallothioneins (MTs) all respond to elevated metal ion levels [19]. Since even essential metal ions can develop toxicity when occurring in too high concentrations, effective homeostasis is essential [14]. On the one hand non-accumulating plants scavenge the majority of cadmium and arsenate using PCs [38]. On the other hand, a positive correlation was found between MT gene expression and Cu tolerance in a number of *A. thaliana* populations [43]. MTs are small, gene-encoded proteins

with an exceptional high content of cysteine (Cys) residues of up to 33%. First described in 1957 [44], they fetched a huge attention due to their ability to bind remarkable amounts of d^{10} metal ions. Today, MTs are accepted as shuttles for essential metal ions, such as Zn^{2+} and Cu^{+}, to various metalloenzymes and transcription factors, as well as influencing cell proliferation, tissue regeneration and repair [45-47]. Figure 1 gives an overview of potential cellular mechanisms involved in metal ion detoxification and tolerance in higher plants [19].

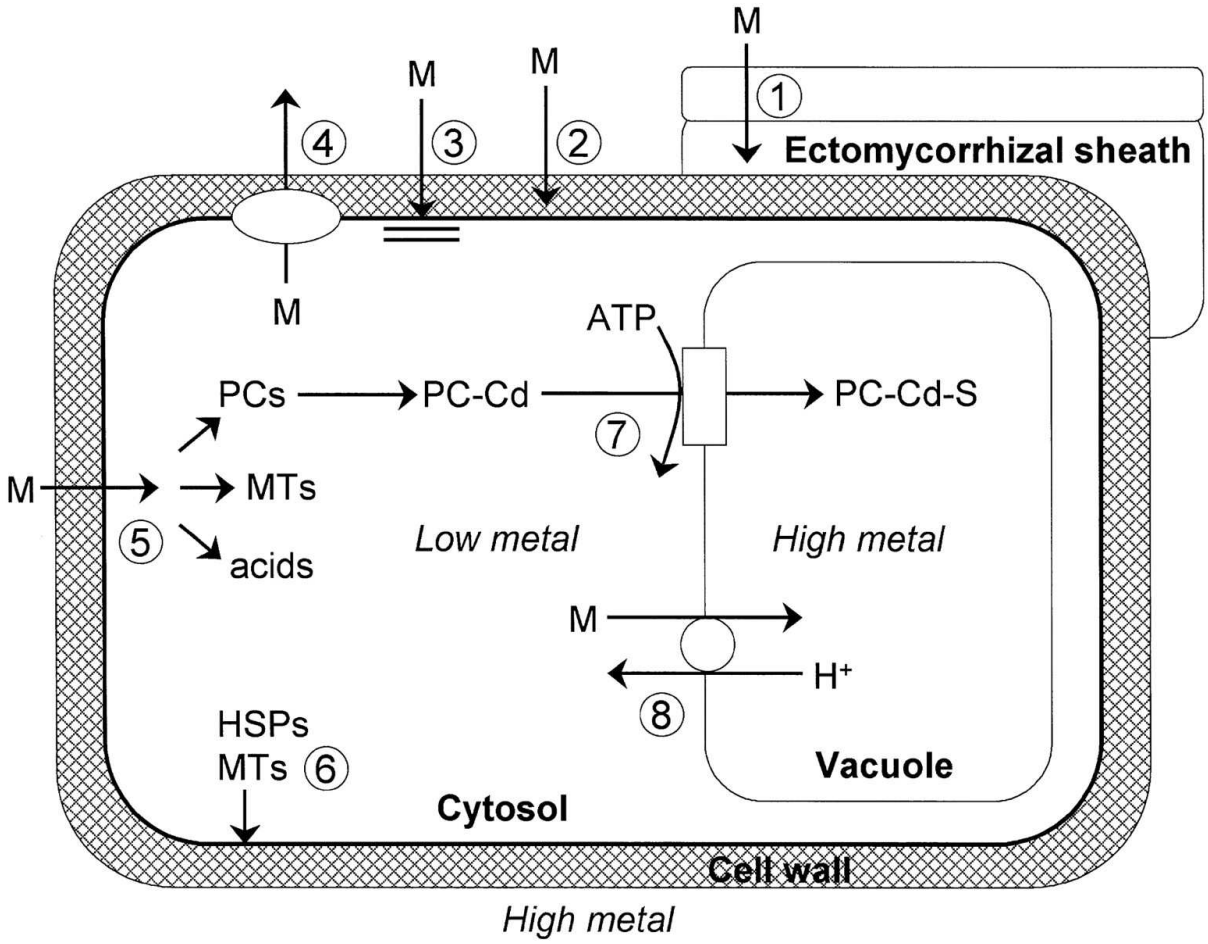

Figure 1: Summary of potential cellular mechanisms involved in metal ion detoxification and tolerance in higher plants. 1. Restriction of metal ion movement to roots by mycorrhizas. 2. Binding to cell wall and root exudates. 3. Reduced influx across plasma membrane. 4. Active efflux into apoplast 5. Chelation in cytosol by various ligands. 6. Repair and protection of plasma membrane under stress conditions 7. Transport of PC-Cd complex into vacuole. 8. Transport and accumulation of metal ions in the vacuole (taken from [19]).

The binding of Zn^{2+} to MTs has been shown to be physiological relevant [48-52]. *In vivo*, MTs are an ideal zinc reservoir, since metal ion binding is thermodynamically stable. The uptake and release of zinc ions is most likely controlled by the redox potential regulation of glutathione (GSH) and glutathione disulfide (GSSG) [53]. For example in mammalians, thes transfer of zinc from holo-MTs (= metal ion loaded MT) to apo-MTs (= metal-free MTs) or

various other apo-zinc proteins was shown *in vitro* [54]. The more oxidative the redox states becomes the more efficiently zinc is released from MT as the metal ion coordinating thiolate ligands get oxidized to disulfide bridges in a principally reversible process [54]. Zinc release is also a stress response to NO and reactive oxygen species (ROS) probably due to the same oxidative mechanism [55]. It has been stated that zinc release from MT under either physiological or stress conditions occurs in a random manner with no preference of certain cluster position [53]. In general, regulation of Zn^{2+} in the cell is tightly controlled, limiting free zinc ion concentrations. Interestingly, studies with $^{65}Zn^{2+}$ *in vivo* show that transfer of this essential metal ion to different zinc requiring proteins solely occurs via ^{65}Zn-MT but not directly by the salt $^{65}ZnCl_2$ [56], indicating the need of some kind of direct MT-protein interaction. Nevertheless, still two major concerns exist regarding Zn^{2+} transfer from MTs to other proteins. Firstly, the energetic feasibility and secondly, the specificity of the transfer. As mentioned above, the energetic barrier of Zn-MT binding could be overcome by redox reactions at the Zn-thiolate cluster [53]. Conformational changes induced by possible MT-protein interaction could provide an additional mean to increase zinc lability. A direct interaction between rabbit liver MT and a zinc acceptor protein has been demonstrated by following the Zn^{2+}-transfer reaction from Zn-MT to an apo-zinc-binding peptide in presence and absence of a membrane separating both enzymes [57]. Zn^{2+}-transfer was only observed in the latter case. This direct interaction between zinc-donor and -acceptor might ensure the required specificity of the metal ion transfer. However, the role of MT in hyper-accumulators is not understood [1].

5.2 Classifications of MTs

Generally, the members of the metallothionein superfamily show a huge heterogeneity in their amino acid sequences. However, a classification system based on 15 MT families is possible, taking into account taxonomic parameters and the Cys-distribution patterns as well as sequence homologies of MTs from certain classes of organism (Table 1) [58].

Table 1: Typical Cys-distribution patterns in the 15 MT families [59].

Family	Cys-distribution pattern
1 vertebrate MTs	K-x(1,2)-C-C-x-C-C-P-x(2)-C
2 mollusc MTs	C-x-C-x(3)-C-T-G-x(3)-C-x-C-x(3)-C-x-C-K
3 crustacean MTs	P-[GD]-P-C-C-x(3,4)-C-x-C
4 echinodermata MTs	P-D-x-K-C-V-C-C-x(5)-C-x-C-x(4)-C-C-x(4)-C-C-x(4,6)-C-C
5 diptera MTs	C-G-x(2)-C-x-C-x(2)-Q-x(5)-C-x-C-x(2)-D-C-x-C
6 nematoda MTs	K-C-C-x(3)-C-C
7 ciliata MTs	-
8 fungi-I MTs	C-G-C-S-x(4)-C-x-C-x(3,4)-C-x-C-S-x-C
9 fungi-II MTs	-
10 fungi-III MTs	-
11 fungi-IV MTs	C-X-K-C-x-C-x(2)-C-K-C
12 fungi-V MTs	-
13 fungi-VI MTs	-
14 prokaryotic MTs	K-C-A-C-x(2)-C-L-C
15 plant MTs	-

Each family is divided into several subgroups sharing a particular set of sequence specific characteristics, being strictly monophyletic. They are thought to be evolutionary related [58, 60, 61].

Although, the content of secondary structural elements as investigated so far has been found to be generally rather low in MTs and their functional influence is not clear, some features have been observed: SmtA from *Syneccochoccus* PCC7942 (β-sheets, α-helix) [62], mammalian MT3 (β-sheets) [63], echinoderma SpMTA (α-helix) [64], fish *Notothenia Coriiceps* (black rockcod) MT (β-sheets) [65] and *Homarus anmericanus* (crustacean) MTH (β-sheets) [66].

MTs show a variety of tertiary structures. Based on the few three-dimensional structures known up to date MTs show either a single-domain structure, as in the yeast and prokaryotic isoforms [62, 67] or they feature two domains as e.g. in vertebrates, echinodermata and crustacean MTs [64, 68, 69]. No conclusive data are available for plant MTs, but two possible three-dimensional structures have been proposed: firstly a dumbbell structure similar to that of vertebrate MTs [70, 71] or a hairpin structure, in which two Cys-rich domains interact to form a unique metal-thiolate cluster [72-75].

Intermolecular interactions between different MT molecules have been scarcely taken into account. Dimerization and oligomerization processes have been observed and attributed to several molecular mechanisms [76]. Formation of an intermolecular disulfide bridge at the C-terminal end under aerobic conditions has been observed in mammalian MT [77]. In case of metal ion excess, a N-terminal metal ion-bridged dimer exists for mammalian MTs [63]. In MTs metal ions were found to bridge histidine residues of different protein molecules [77] and also intermolecular interactions between separate metal-thiolate clusters mediated by phosphate ions have been reported [77]. These dimers have shown to acquire novel properties on metal detoxification [77]. However, their physiological significance has only been demonstrated in the case of prokaryotic *Synechococcus* SmtA, which forms a MT dimer structurally similar to what is found for Zn-fingers, which develop Zn-regulatory activities [75]. Also from experiments conducted with mass spectroscopy it is known that MTs are able to form disulfide bonds at least *in vitro* [78].

5.3 MTs in plants

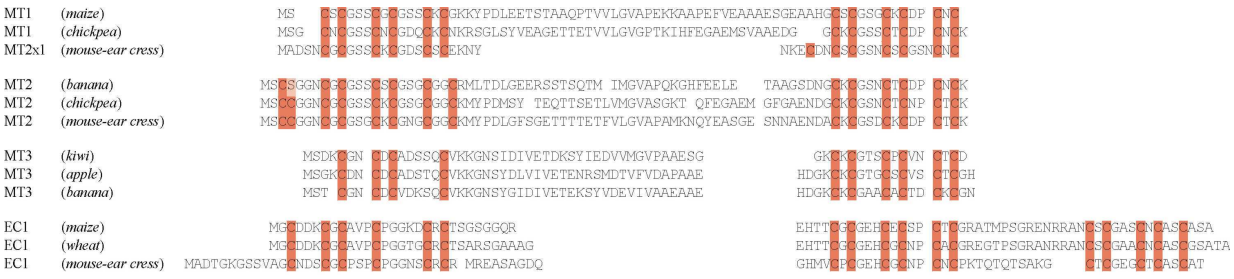

Figure 2: Alignment of the four different subclasses of MT family 15.

Plant MTs constitute family 15 of the metallothionein superfamily and are further subdivided into the four subfamilies p1, p2, p3 and pec depending on the Cys content and distribution in the primary structure (Figure 2) [79].

Type 1 plant MTs (p1), which show higher expression levels in roots than in shoots, contain a total of six Cys-x-Cys motifs that are equally distributed among the two domains at the C- and N-terminal end. These domains are separated by an approximately 40 amino acid Cys-free long linker.

In type 2 MTs (p2), more abundant in shoots than in roots, the two domains are separated by an equally long linker as in MT1 and also the Cys-distribution pattern at the C-terminal domain is conserved. However, the first pair of cysteine residues in the N-terminal domain at

positions 3 and 4 shows a Cys-Cys motif. Additionally, at the end of the N-terminal Cys-rich domain a Cys-Gly-Gly-Cys motif is present. Overall, part of the sequence of the N-terminal domain of MT2s is highly conserved (MSCCGGNCGCS) [38].

In ripening fruits or leaves of plants that do not produce fleshy fruits such as *A. thaliana*, members of the p3 subfamily (MT3s) are expressed. They contain only 4 Cys residues in the N-terminal domain. The consensus sequence for the first three residues is Cys-Gly-Asn-Cys-Asp-Cys. The fourth cysteine is not part of a pair of cysteines, but is contained within a highly conserved motif, Gln-Cys-x-Lys-Lys-Gly. The C-terminal domain equals those from p1 and p2. The linker region also consists of approximately 40 amino acids.

The first plant MTs was discovered in *T. avestivum* and named "early-Cys-labeled" (E_c) protein [80] and is restricted to developing seeds [38]. The Cys-distribution pattern did not match any of the so far known MT isoforms from mammalians [81]. Experiments showed that Zn^{2+} could be replaced by Cd^{2+} as in other MTs, showing the typical Cd-mercaptide UV spectrum [82]. This protein was found to bind up to 5% of the total zinc in the wheat embryo, indicating an unlikely role in detoxification [48]. These proteins are regulated in the same way as a lot of other genes that are expressed during maturation of embryos and whose mRNAs persist until inhibition and germination. So far, a role in zinc ion homeostasis is suggested, thereby interacting with Zn-dependent DNA and RNA polymerases and *trans*-acting Zn-finger proteins. Such functions would be accentuated during embryogenesis [48, 49]. After germination, the E_c protein- and mRNA–levels decline [2]. Differing from all other plant MTs type 4 MTs (pec subfamily) feature three Cys-rich domains, each containing 5 or 6 Cys distributed in a Cys-x-Cys manner. The linker region is considerably shorter than those found in all other plants MTs ranging from 10 to 15 amino acids. The diversity of the plant MT gene family suggests that the encoded proteins may differ not only in sequence but also in function. Up to now little is known about putative MT genes from nonflowering plants.

Apart from the different cysteine distribution pattern, the elongated cysteine free linker region, which might even contain aromatic amino acids is the most distinguishing feature of plant MTs to MTs from other families. The role of these linker regions is still not known, but they have been proposed to affect cellular functions via their interaction with other metal-ion processing proteins [72]. It seems, that a number of properties are differing considerably between the plant MT subclasses. For example, elevated Cd(II) and Cu(II) levels increase expression of MT1 from *A. thaliana*, underlining a role in metal detoxification and homeostasis [83, 84]. In contrast metal ions such as zinc(II) have no such influence on the seed specific MT from *T. aestivum*, common bread wheat [48].

The gene expression of plant MTs in general occurs at high levels, but varies strongly depending on plant, tissue and MT genotype [38].

Recombinant methods allow expressing plant MTs in various expression systems. The analysis of $PsMT_A$, a MT from *Pisum sativum* (green garden pea), over-expressed in *Escherichia coli* showed proteolytic cleavage of the inner linker region [74, 85]. As long linker regions are notoriously prone to proteolytic cleavage *in vivo*, it was proposed that cleavage of the linker region in $PsMT_A$ is generally taking place *in vivo* after the metal-thiolate clusters haven been formed [74]. As more attention is paid to nutritional composition of foods as opposed to simple calorific value, MTs may provide one mechanism to manipulate metal ion concentrations in seeds [86]. When expressed in *E. coli*, the pea MT1 bound to copper, cadmium and zinc, with the highest affinity for copper [85].

5.4 Phytoremediation and MT

Phytoremediation is a promising technique for the decontamination of heavy metal polluted soils. Principally, this can be achieved in two different ways: phytostabilization and phytoextraction. Phytostabilization uses plants to transform metal ions in the soil into less toxic compounds without actually removing them from the soil. For example toxic chromium(VI) compounds can be reduced to Cr^{3+} by reduction by deep rooted plants to Cr^{3+} [87] while lead can be transformed into chloropyromorphite ($Pb_5(PO_4)_3Cl$) which is not bioavailabe [88, 89]. Phytoextraction is the method of choice for cadmium and zinc [88], as these metal ions can be easily chelated and compartmentalized by plants [90]. Even though over-expression of (mammalian) MTs in plants showed an increase in cadmium tolerance, metal ions were not hyper-accumulated and thus no benefit for phytoremediation is gained [91]. Furthermore, expression of mammalian MT1 as full-length protein, in form of the "α-domain" or fused to β-glucuronidase (GUS) under several promoters increased the cadmium tolerance of tobacco and other plants, but had little effect on cadmium transport to shoots [92-95]. However, there is an increased ability to store Cd^{2+} in roots. A pea MT gene over-expressed in *A. thaliana* enhanced Cu^{2+} accumulation [96]. So far, naturally occurring hyper-accumulators are much more efficient extracting metal ions from soils than genetically modified plants, but their specificity towards generally only one metal ion is not suitable for soils polluted with multiple metal ions [1]. In most cases, metal ion uptake was not markedly altered in transgenic plants. However, when the MT used for transgenic modifications was

itself of plant origin, higher amounts of metal ions were accumulated in the roots of the transformed plants than in control plants [97]. Still MTs are only one small piece in the whole picture ofplant detoxification and thus their putative role in phytoremediation will be limited.

5.5 Plant MT1

The first plant MT1 gene was described in 1990 found in a Cu-tolerant ecotype of *Mimulus guttatus* (yellow monkey flower) [98]. Knockout experiments of MT1 genes from *A. thaliana* show that MT1 is needed for cadmium tolerance, but is not essential for homeostasis of essential metal ions [84]. The concentrations of Cd^{2+} and Zn^{2+} in aerial parts of plants were dramatically reduced in MT1 knockdown lines, suggesting a role for MT1 proteins in metal ion translocation. They are believed to participate in cell-to-cell movement of these metal ions via plasmodesmata, microscopic channels of plants [99]. Trichomes, plant hairs, have been found to show very high expression levels of MT1 and MT2 [100, 101] and the accumulation of toxic metal ions such as Cd^{2+} in trichomes is known [102]. Even though it is not really understood which metal ions bind to MTs in plant tissues, MTs might actually be necessary for detoxification in trichomes. Another hypothesis is states that specific metal ion requiring enzymes are highly expressed in trichomes and plant MTs are involved in the delivery of metal ions into these specialized cells [100]. In *A. thaliana* expression of MT genes is also found in the phloem, a living tissue that transports nutrients in plants, indicating a role in metal ion transport [101]. However, so far MTs have never been found among the phloem exudate proteins characterized from various plants, but the detection of expressed MT proteins is known to be challenging and thus might be the ultimate criterion [38].

There are also indications showing that MT1 might be involved in the root-to-shoot translocation of essential metal ions via the xylem sap, one of the two types of transport tissue in vascular plants [103]. However, there is little direct evidence that plant metallothioneins function in the short- or long-distance transport of essential or toxic metal ions in plants [19].

MT1 levels are reported to increase dramatically in senescing leaves in *B. napus* [104], *A. thaliana* [101] and Oryza sativa, rice [50], where the protein seems to be necessary to chelate copper ions released from catabolized metalloproteines. Since other proteins, which are involved in copper homeostasis, are expressed at the same time, MT1 has been proposed to play the following roles: delivery of copper ions to the trans-Golgi network to enable incorporation into copper-requiring proteins, as well as chaperoning for copper ions for long-

distance transport from leaves to storage “areas” such as developing seeds by MT1 expressed in the phloem [38]. These roles would make MT1s an integral part of a system regulating uptake and distribution of copper [105]. These tight regulation mechanisms ensure a level of less than one “free” copper ion per cell, which is crucial for preventing cellular damage due to ROS formed by reactive copper [106], underlining the importance of the drastic increase of MT1 levels observed in senescing leaves. Additionally, MT1 gene expression has been observed in processes involving apoptosis and leaf abscission [107] as well as during the hypersensitive response to pathogens [108]. Type 1 MTs are reported to be expressed under copper stress for *A. thaliana*, rice, wheat and tobacco (*Nicotiana glutinosa*) [50, 51, 109, 110]. Furthermore, stress conditions such as an excess of aluminium and cadmium ions, nutrient deprivation, and heat shock induce MT1 expression in wheat and rice [50, 110].

CicMT1 is exemplary for plant MT1s and since its gene sequence is known and could easely be maipulated to be expressed in *E.coli* (MSGCNCGSSC NCGDQCKCNK RSGLSYVEAG ETTETVVLGV GPTKIHFEGA EMSVAAEDGG CKCGSSCTCD PCNCK), this protein has been choosen for further investigation.

5.6 Metal ion binding sites in MTs

For mammalian MTs, one solid state structure determined by single crystal X-ray analysis and solution structures determined by NMR spectroscopy are known [69, 111-113]. From both methods it is established that the divalent d^{10} metal ions are coordinated in two separate clusters. The so-called α-domain hosts a tetranuclear M_4Cys_{11} cluster (Figure 3), and a trinuclear M_3Cys_9 in formed by the β domain. In both cluster, the coordinated Zn^{2+} or Cd^{2+} show (distorted) tetrahedral tetrathiolate coordination spheres [114].

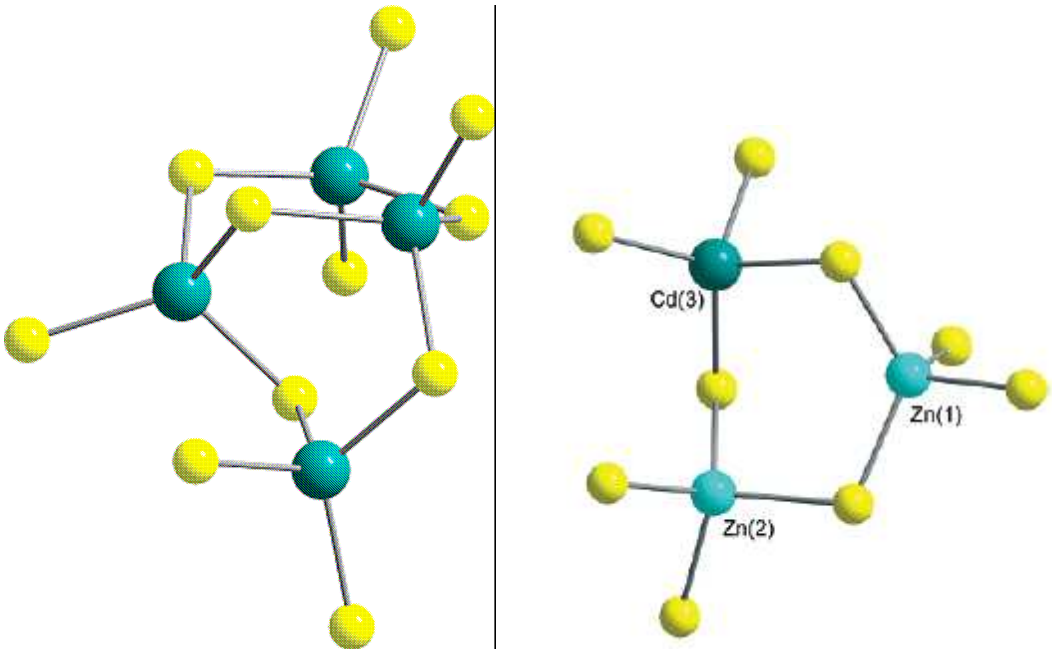

Figure 3: The tetranuclear Cd_4Cys_{11} (left) and trinuclear cluster(right) of M_7MT2 from rat liver (taken from PDB 4mt2).

In contrast to reconstituted proteins and mammalian MT1 and MT2 isolated from natural sources, naturally occurring MT3 from bovine brain has been shown to contain a mixture of monovalent and divalent metal ions, specifically four Cu^+ and three Zn^{2+} ions in the α- and β-domain, respectively [115]. Extended X-ray absorption fine structure (EXAFS) Cu and Zn K-edge investigations of MTs are indicative of distinct homometallic clusters with trigonal and tetrahedral metal ion coordination geometries, respectively [116, 117]. The latest example of vertebrate MTs, which solution structure has been determined, is Cd_7MTA from the antarctic fish *N. coriiceps* [65]. Comparing the α- and β-domains with those of the mammalian isoforms the close structural similarities are obvious, which is not surprising as they all belong to the family of vertebrate MTs. Besides the NMR structures of these vertebrate proteins, also solution structures were solved for the invertebrate Cd_6MT1 proteins from crustacean blue crab (*Callinectes sapidus*) [118] and lobster (*Homarus americanus*) [119] as well as for Cd_7MTA from echinodermata purple sea urchin (*Strongylocentrotus purpuratus*) [68]. All of the latter feature two separate metal-thiolate clusters as in the vertebrate isoforms. The major difference though is that the two metal-thiolate clusters in blue crab and lobster both show a Cd_3Cys_9 stoichiometry similar to the β-domain of the vertebrate isoforms. The echinodermata sea urchin MT however, features the usual Cd_4Cys_{11} and Cd_3Cys_9 clusters known from vertebrates although in reversed arrangement. As a consequence, also the connectivity patterns of the Cd-thiolate clusters are different, accompanied by a new fold of the peptide backbone. Additionally, the topology of the Cd_4Cys_{11} cluster of sea urchin does

not match the principal structural characteristics of the M_4Cys_{11} units of identical composition present in the α-domains of all vertebrate M_7MTs (Figure 4).

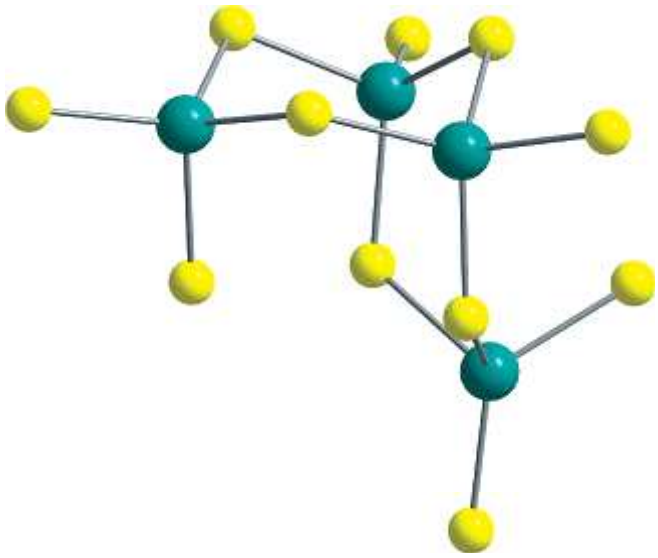

Figure 4: The tetranuclear Cd_4Cys_{11} cluster of Cd_7MTA from equinodermal sea urchin (taken from PDB 1qjk).

In contrast to Zn(II) and Cd(II) containing proteins, the knowledge about the architecture of Cu-MTs was for a long time limited to two solution structures from yeast [120] and fungus (*Neurospora crassa*) [121]. Recently, also the solid state structure of a truncated copper yeast thionein was determined by X-ray crystallography [122]. It reveals that copper ions show both trigonal and linear coordination environment within the same cluster. Interestingly, two Cys residues located at the C-terminus of the protein are not involved in the copper-thiolate cluster formation [123, 124] and were therefore also truncated in the protein used for crystallization [122]. The low resolution NMR data obtained for fungal MT was only sufficient to postulate a hexanuclear Cu(I)-thiolate cluster of unknown structure [121]. The first direct evidence for the Cu(I) coordination mode in MTs was obtained by EXAFS studies [125]. Apart from showing coordination of Cu(I) by both, terminal and bridging thiolate groups, they also indicate trigonal coordination environments with Cu(I)-S distances of approximately 2.25 Å. This is in accordance to findings from inorganic model compounds showing that copper ions are usually monovalent in their thiolate complexes with trigonal planar or linear coordination geometries [114].

Structural studies of apo-MTs are a difficult task due to their oxygen sensitivity leading to the formation of disulfide bridges. Up to day, there is no solid-state or solution available. Informations available are based on classical spectroscopic methods such as circular dichroism (CD) or molecular dynamics calculations. The latter method revealed that human

apo-MT still retains a considerable amount of secondary structure (β-turns) [126]. In particular, circular dichroism spectroscopy is able to provide invaluable information on the metal-protein stoichiometries, metal-binding dynamics, and metal coordination geometries by probing the chirality of the metal-thiolate cluster in the protein [127-131]. A chiroptical signal such as the circular dichroism signal is observed for an electronic transition only when the chromophores exists in an asymmetric electric field. Significant enhancement is observed for the three-dimensional asymmetric environments found in proteins [132].

6 Experimental section

6.1 Protein expression and purification

6.1.1 Expression vector construction

The MT1 gene (MSGCNCGSSC NCGDQCKCNK RSGLSYVEAG ETTETVVLGV GPTKIHFEGA EMSVAAEDGG CKCGSSCTCD PCNCK) from *Cicer arietinum* (Swiss-Prot Accession Number Q39458 (http://www.expasy.ch)) was optimized for *E. coli* codon usage by manually exchanging plant codons by codons more frequently used by the expression host. The gene sequence including restriction sites for MdeI and XmaI was constructed from 7 oligo nucleotides (nt) of approximately 45-53 nts length via PCR.

Primer 1: 50bp, Tm = 66.6 °C

3´- ggaattcCAT ATGtctggct gcaactgtgg cagtgctgc aattgtggcg -5´

Primer 2: 50 bp, Tm = 66,2 °C

3´- gtagctgcaa ttgtggcgat cagtgcaaat gcaataagag atcagggttg -5´

Primer 3: 53 bp, Tm = 65.9 °C

3´- gcaataagag atcagggttg agctatgtcg aagccggcga aaccacagag acg -5`

Primer 4: 48 bp, Tm = 64.9 °C

3`- gcgaaaccac agagacggtg gttttaggcg taggtccgac caagatcc -5`

Primer 5: 52 bp, Tm = 65.9 °C

3`- ggtccgacca agatccattt tgagggagcg gaaatgagtg tggcagctga ag -5`

Primer 6: 51 bp. Tm = 64.9 °C

3´- gagtgtggca gctgaagatg gtggctgcaa atgtgggtca agctgcacct g -5`

Primer 7: 45 bp, Tm 63.5 °C

3`- ggtcaagctg cacctgtgac ccttgcaact gcaaacccgg gtccg -5`

1µL of primer (n) and inverse complimentary (n+1) (100 pmol/µL, Microsynth AG, Balgach, Switzerland), 5 µL of 10x buffer, 1 µL dNTP (10mM, Eppendorf, Schönenbuch, Switzerland), 0.5 µL Pfu polymerase (Promega, Wallisellen, Switzerland) and 41.5 µL H_2O were set to 30 PCR cycles of 60 s 95 °C, 30 s 55 °C, 60 s 73 °C (Figure 5). After each PCR step, the mixture was purified using a 2% agarose gel (100 mL 5 µL ethidiumbromide 10 mg/mL). The cutout gel piece was purified using the Gel cleanup Kit (Qiagen, Hombrechtikon, Switzerland). The synthetic gene was cloned into the pTYB2 vector using NdeI and XmaI restriction sites. Ligation was performed using the "LigaFast™ Rapid DNA Ligation System" (Promega, Wallisellen, Switzerland) amplified followed by transformation into the *E. coli* cell line XL1Blue. This cloning strategy adds two vector derived additional amino acids, Pro and Gly, to the C-terminus of the protein. The additional mass was taken into account for MS spectra.

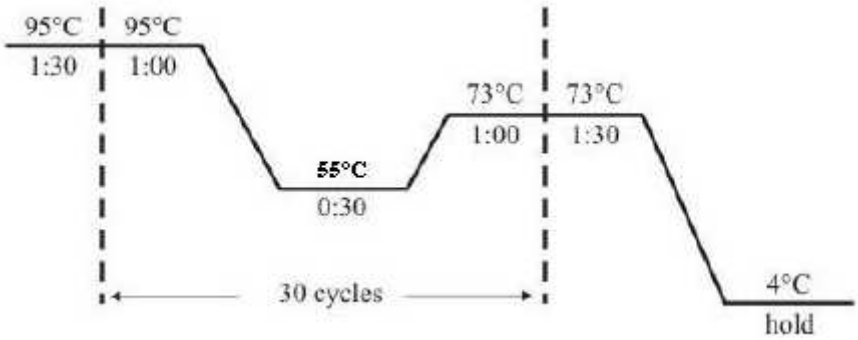

Figure 5: Schematic illustration of PCR cycles.

6.1.2 Protein overexpression and purification

Recombinant overexpression of MT1 as a fusion protein with a C-terminal self-cleavable intein-tag (IMPACT system, New England Biolabs) was performed in the *E. coli* cell line BL21(DE3) in LB media. 2 L flasks were filled with 800 mL LB medium and were inocculated with 4 mL overnight culture (20 mL LB medium, 20 µL ampicilin (100 mg/L), one colony picked from freshly prepared agarplate, 37° C) and 800 µL ampicillin stock solution (100 mg/L). Cells were grown to OD_{600} of 0.6 and induced with 1 mM isopropyl-β-D-thiogalactopyranosid (IPTG). 30 and 90 min after induction a solution of $ZnCl_2$ or $CdCl_2$ was added to a final concentration of 400 µM. Cells were harvested 6 hours after induction by centrifugation (15 min, 4000g) and stored at –80 °C. All following steps were carried out under a constant flow of nitrogen using degassed nitrogen saturated solutions. For purification, cell pellets of two 800 mL cell cultures were resuspended in 25 mL buffer A (20

mM Tris-HCl pH 8.6, 500 mM NaCl) and ruptured by sonification (30 s pulse, 90 s pause, for 15 min, micro tip). After centrifugation (30 min, 35000g) the supernatant was applied to a chitin affinity column (New England Biolabs) and washed with 200 mL buffer A followed by 200 mL high salt buffer B (20 mM Tris-HCl pH 8.6, 1 M NaCl). On-column self-cleavage of the intein-tag was induced with 30 mM DTT over night at 4 °C and additionally for 4 hours at room temperature. Eluted (buffer A) crude MT1 was dialyzed (Snake Pleated Dialysis Tubing, Pierce, USA) first against 10 mM Tris-HCl (pH 8.6) for 4 hours followed by dialysis against 1mM Tris-HCl pH 8.6 over night and finally lyophylized over night. The chitin column was regenerated by incubation in 20 mL 0.3 M NaOH and 10% sodium dodecyl sulfate (SDS) solution under constant mixing for 1 h. The sample was then further purified with a size exclusion chromatography column (Highload 16/60 Superdex 75 pg, Amersham Bioscience; flowrate 0.7 mL/min, 4° C, 10 mM Tris-HCl pH 8.6, 50 mM NaCl) using a an Äkta prime FPLC instrument (Amersham Bioscience). Monomeric MT1 eluted as a single peak (retention volume = 68 mL) and was dialyzed against 1 mM Tris-HCl 8.5 and either used directly or lyophilized and stored at –20 °C. Protein purity was examined by tricine SDS-PAGE as described [133]. Monobromobimane- (mBBr-) modified MT1 was prepared according to the literature [134], but without addition of EDTA or a reducing agent during the modification procedure. Polyacrylamide gels were either coomassie [135] or silver stained [136] according to given protocols (see chapter 10).

6.1.3 Protein and metal ion quantification

Due to its low content of aromatic amino acids and in order to avoid inaccuracies caused by superposition of thiolate-metal LMCT bands and the absorption bands of aromatic amino acids at ~280 nm, MT1 concentrations were determined by quantification of thiolate groups with 2,2`-dithiopyridine (2-PDS) at pH 4.0 [5]. Stoichiometric formation of thiopyridone was followed via its absorption maximum at 343 nm (absorption coefficient 7600 M^{-1} cm^{-1}). With the known content of 12 cysteines in MT1 and assuming a completely reduced state of the protein as shown by ESI-MS (see chapter 7.1), the concentration was calculated. To measure the metal ion content MT1 solutions were diluted with salpetric acid (0.2 M HNO_3) to 1 µM MT1 and analyzed by flame atomic absorption spectroscopy (F-AAS) on an AA240FS spectrometer (Varian AG, Zug, Switzerland) using Zn(II)/Cd(II) standards of 0.1, 0.25, 0.5 and 1 mg/L.

6.1.4 Apo-MT1 preparation

Freshly prepared MT1 was dissolved in 285 µl of nitrogen saturated water (≈ 500mM MT1), incubated with DTT (60 µM final) on ice for 1 h and acidified to pH 1 with 1 M HCl. To separate the apo-protein from its released metal ions and the DTT gel filtration using a Sephadex G-50 column (self-packed) (10 mM HCl, 4 °C, 0.8 mL/min, retention time: 30 min) was performed and the apo protein was collected under a constant flow of argon followed by lyophilization. All following steps were carried out in a nitrogen-purged glove box. For the experiments lyophilized metal-free apo-protein was dissolved in 10 mM HCl and the concentration was determined by the 2-PDS-assay.

6.2 Spectroscopic measurements and protein analysis

6.2.1 UV absorption, CD and MCD spectroscopy

UV absorption measurements were carried out on a Cary 500 scan spectrophotometer (Varian AG, Zug, Switzerland) using scan speeds of 600 nm min^{-1} in the range of 200-500 nm (Co^{2+} titrations 200-800 nm) with 1 nm increments. CD spectra were recorded on a J-810 spectropolarimeter (Jasco Inc., Groß-Umstadt, Germany). For MCD spectra a J-715 spectroploarimeter complemented with a magnet of 1.5 T was used. The scanning speed for CD and MCD was set to 10 nm min^{-1} in the range of 210-450 nm (3 spectra accumulation, 0.2 nm increments). All spectra were recorded at 20 °C.

6.2.2 pH titrations of Zn_5- and Cd_5MT1

800 µL of 10 µM Zn_5- or $Cd_{4,5}$MT1 (2 mM Tris-HCl pH 8.5, 10 mM NaCl) were titrated with increments (typically 1µL) of a diluted HCl (1 mM) solution. After each addition pH and the correlated UV spectra were recorded. Handling of samples throughout each experiment was carried out under a constant flow of nitrogen. Dilution effects due to HCl addition were negligible. Curve fitting of experimental data was performed with Origin® 7.0 (Originlab Corporation, Northampton, USA). Equations ((Equation 1 p. 34) were derived as described in [137] without using the Hill coefficient.

6.3 Metal ion titrations of Zn_5- and apo-MT1

6.3.1 Titrations with $CdCl_2$

10 µM Zn_5MT1 (2 mM Tris-HCl pH 7.5, 10 mM NaCl) was titrated with increasing amounts (0-7 equivalents) of $CdCl_2$ (1 mM). After each metal ion addition, the solution was incubated for 5 min at 20 °C and subsequently a spectrum was recorded. Metal ion reconstitution reactions of apo-MT1 were performed from freshly lyophilized protein redissolved in 10 mM HCl inside a nitrogen-purged glove box. Apo-MT1 solutions were supplemented with 10 mM NaCl and increasing amounts of $CdCl_2$. Finally, the pH was raised by addition of 2 mM Tris to a pH of 7.5 (±0.2).

6.3.2 Titrations with $HgCl_2$

15 µM Zn_5MT1 (2 mM Tris-HCl pH 7.5, 10 mM NaCl) was titrated with increasing amounts (0-15 equivalents) of $HgCl_2$ (5 mM). After each metal ion addition, the solution was incubated for 30 min at 20 °C and subsequently a spectrum was recorded. For each equivalent a corresponding baseline had do be recorded, to compensate for interactions of the metal ions with the buffer, and subtracted from the corresponding spectrum. For apo-protein titrations, Zn_5MT1 was acidified with 1 M HCl to a pH of 2. Then $HgCl_2$ titrations were carried out as described for pH 7.5.

6.3.3 Titration with $[Cu^I(CH_3CN)_4]BF_4$

To prevent oxidation of Cu(I) to Cu(II) all titrations had to be performed in a nitrogen-purged glove box. 20 µM Zn_5MT1 (2 mM NH_4OAc pH 7.5, 10 mM NaCl) was titrated with increasing amounts (0-15 equivalents) of $[Cu^I(CH_3CN)_4]BF_4$ (1 mM) dissolved in an aqueous solution containing 2% acetonitrile. After each addition of $[Cu^I(CH_3CN)_4]BF_4$, the solution was incubated for 30 min at 20 °C and subsequently a spectrum was recorded. For each equivalent a corresponding baseline had do be recorded and subtracted from the corresponding spectrum. Apo-MT1 solutions were supplemented with 10 mM NaCl and

increasing amounts of $[Cu^{I}(CH_3CN)_4]BF_4$ were added. Finally, the pH was raised by addition of 2 mM NH_4OAc to a pH of 7.5 (±0.2).

$[Cu^{I}(CH_3CN)_4]BF_4$ was prepared according to the literature [138]. 1 g of $Cu(BF_4)_2$ and 2 g of copper powder were stirred for 3 h under reflux at 30 °C in 20 mL CH_3CN under nitrogen atmosphere. The crude product was vacuum filtrated and recrystallized from CH_3CN yielding 82 % $[Cu^{I}(CH_3CN)_4]BF_4$ and stored under argon atmosphere.

6.4 ESI-MS

Samples were diluted with 0.2% formic acid/50% acetonitril (pH 2) or NH_4OAc in 50% methanol (pH 7.0-7.5) and mass spectra were recorded in a Q-TOF Ultima API spectrometer (Waters, UK). Deconvolution of spectra was performed with the MaxEnt1 software.

6.5 Protein crystallization

Cd_5MT1 was either concentrated by lyophilization and redissolved in water or concentrated using protein concentrators (3 kDa cutoff) to a final concentration of 10 mg/mL. A buffer concentration below 1 mM was ensured. 1µL drops mode were tested in batch with the commercially available protein crystallization screens Index, Crystal 1 and Crystal 2 from Hampton Research (Aliso Viejo, CA, USA). Additionally, an automated screening was performed at the Hauptman Woodward Medical Research Institute (Buffallo, NY, USA) testing 1536 different conditions. For this, 600 µL of a protein solution with a concentration of 10 mg/mL were required and shipped on dry ice. All plates were incubated at 23 °C.

6.6 Secondary structural analysis of MT1 by CD spectroscopy

A lyophilized sample of Cd_5MT1 was dissolved in 200 µL ddH_2O to give a final concentration of 10 µM. Gel filtration using a G-10 column (self-packed) in 10 mM sodium phosphate buffer pH 7.5 was performed to ensure proper buffer exchange (flowrate 1.8 mL/min, 4 °C, elution time: 20 min) . Samples were used immediately after gel filtration, diluted to 1 µM (3.3 mM buffer) and spectra taken in the range from 190-250 nm. Data were

analyzed using the k2d program and algorithm (http://www.embl-heidelberg.de/~andrade/k2d.html).

6.7 Secondary structural analysis of MT1 by FTIR spectroscopy

Fourier transform infra red (FTIR) spectroscopy was performed either as KBr pellet using the lyophilized protein or in solution (10 µM MT1, 2 mM Tris-HCl pH 7.5, 10 mM NaCl). Measurements with KBr pellets were done on a Digilab FTS 40 Pro Spectrometer (Canton, MA, USA). The system was purged with nitrogen gas to avoid resonances from CO_2 and H_2O vapor. For each spectrum, a 1024 scan interferogram was collected in single beam mode with a 4 cm^{-1} resolution from 4000 cm^{-1} to 1000 cm^{-1}. Background correction was performed as described elsewhere [139]. The transformed spectra where truncated in the region between 1560 cm^{-1} and 1860 cm^{-1}. Second-derivative spectra where used to verify the peak assignment of the deconvolved spectra [140]. Fourier self-deconvolution of the amide I band was performed by gaussian curve fitting with a 18 cm^{-1} half-bandwidth, a resolution enhancement factor of 2.4 and a Happ-Genzel apodization (Resolutions Pro Version 4.0.0.030, Digilab). This procedure showed neglectable signs of over deconvolution such as side lobes. Iterative gaussian fitting to the deconvoluted spectra was carried out with Origin® 7.0. Assignment was performed according to known values described in the literature [141-143].

Measurements performed in the solubilized state where performed on a Bruker Bio-ATR FTIR spectrophotometer (Fällanden, Switzerland). The system was purged with nitrogen to exclude resonances from CO_2 and H_2O vapor. 20 µL of sample where applied to the surface of the ATR-crystal. After temperature equilibration 1024 scans where performed. Data assignment and calculations where performed by the OPUS® software from Bruker.

7 Results

7.1 Expression, purity and metal ion content of C. arietinum MT1.

Both Zn(II)- and Cd(II)-forms of *C. arietinum* MT1 (cicMT1) were overexpressed in the protease-deficient *E. coli* cell line BL21(DE3) as recombinant protein fused to an intein-tag. After thiol-mediated self-cleavage of the fusion-tag and several dialysis steps to reduce buffer and salt concentrations, the protein was lyophilized. Redissolved MT1 was then purified over a size exclusion column (Figure 6) to yield the monomeric form.

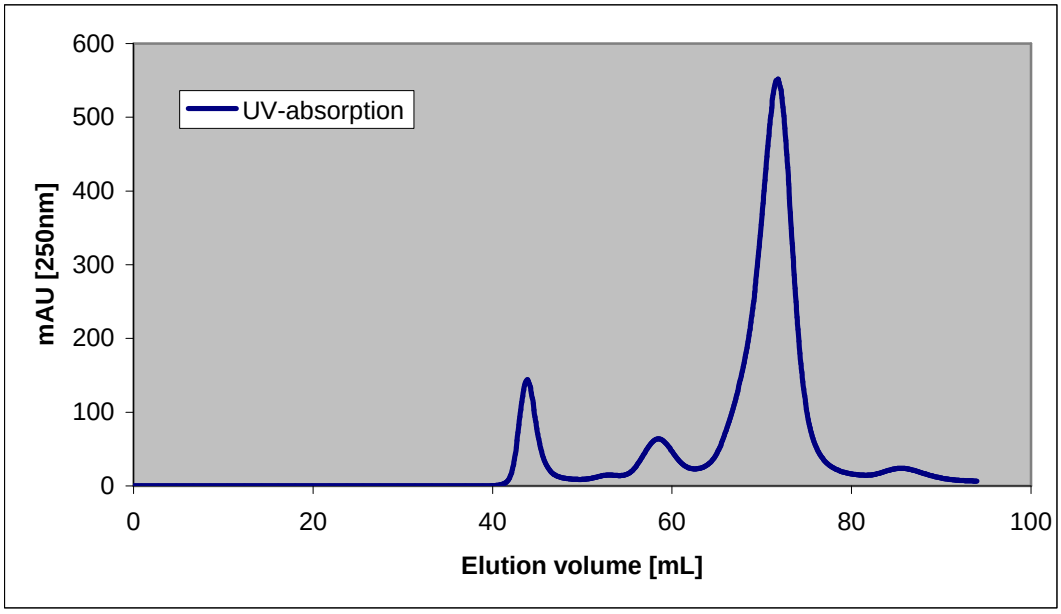

Figure 6: Elution profile of Cd_5MT1 in 10 mM Tris-HCl pH 8.6 and 50 mM NaCl.

Protein yield was 800 µg per 800 mL cell culture for the monomeric form. To confirm the purity of the sample cicMT1 was subjected to SDS-PAGE and ESI-MS.

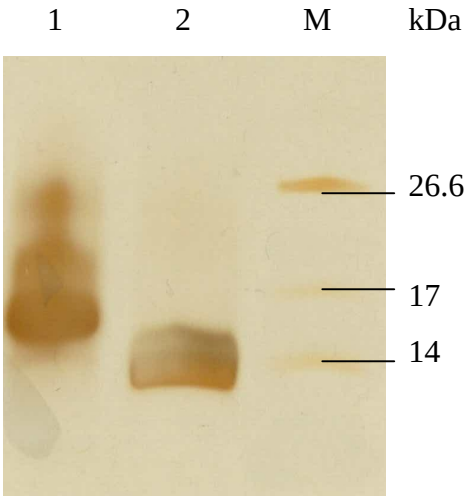

Figure 7: Silver-stained SDS-PAGE (12%) of unmodified (lane 1) and of mBBr-modified Cd_5MT1 (lane 2) relative to a protein marker (M).

Since it is known that MTs tend to have unusual migration behaviors due to their compact structure, high cysteine and metal ion content [73, 144, 145] the SDS-PAGE gels of cicMT1 were only performed in the mBBr-modified form. Importantly, the reactivity of mBBR is only directed towards the thiol groups and not towards disulfide bridges [137]. Silver staining (Figure 7) reveals that the protein shows no impurity up to the detection level of 5 ng of protein [146].

Purity was also confirmed using ESI-MS, which shows, that purified cicMT1 is monomeric.

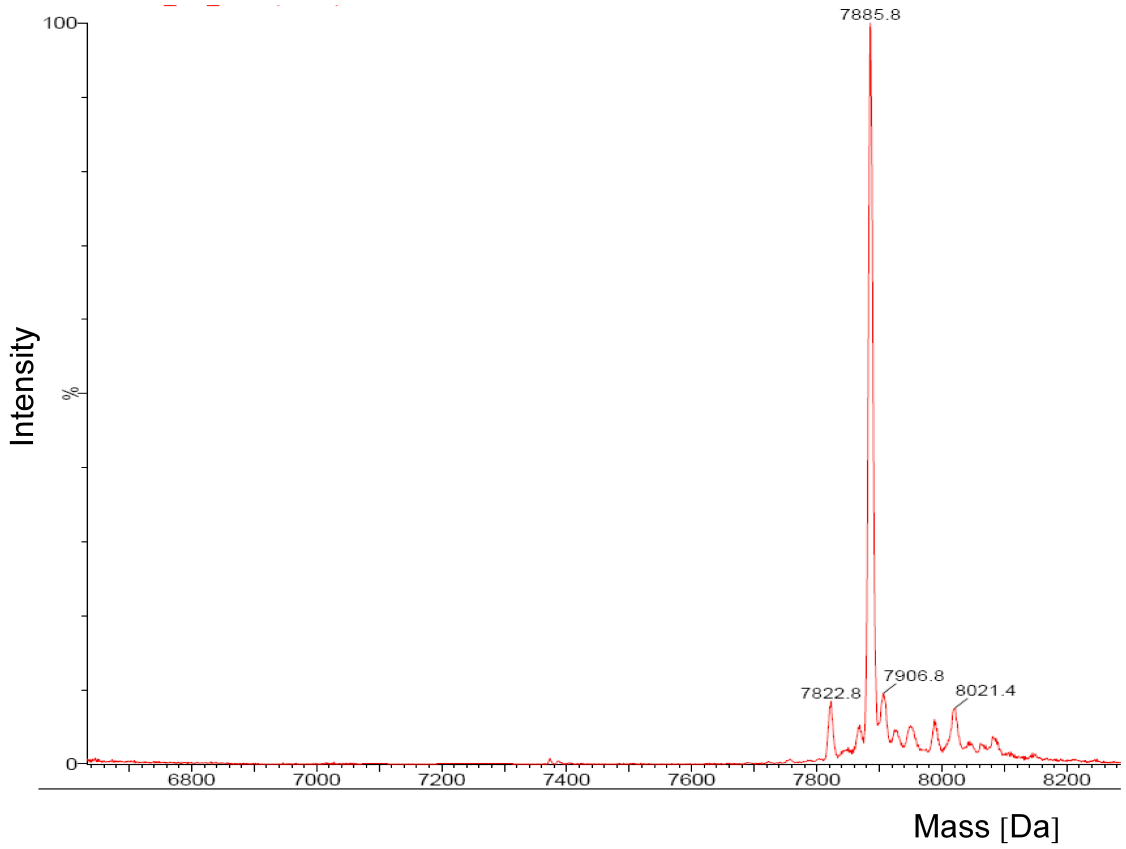

Figure 8: Deconvoluted ESI-MS of $Zn(II)_5$-MT1 at pH 7.

Figure 8 clearly shows, that cicMT1 only forms very low amounts a Tris-aduct as seen for wheat E_c-1 [73] and banana MT3 [137]. The signal at 7885.8 Da (calc. 7895.1 for Zn_4MT1) corresponds to Zn_4cicMT1, devoid of the N-terminal methionein, which is usually cleaved in *E. coli* expression hosts [147, 148]. In general, only Zn_4- or Cd_4cicMT1 are observed in ESI-MS spectra in contrast to results obtained from flame atomic absorption spectroscopy (F-AAS) and UV titrations which mainly resulted in Zn_5- or Cd_5cicMT1. However, due to the ionization process during ESI-MS the 5^{th} equivalent could get lost. This might be also an indication for a weaker binding site for the 5^{th} equivalent of Zn(II)- or Cd(II)cicMT1.

7.1.1 Crystallization of MT1

In order to obtain the solid state structure of cicM1 and thus to get a closer look upon the three dimensional arrangement of the metal ion cluster and the peptide backbone, the protein was tested in a huge set of 1536 different crystallization conditions.

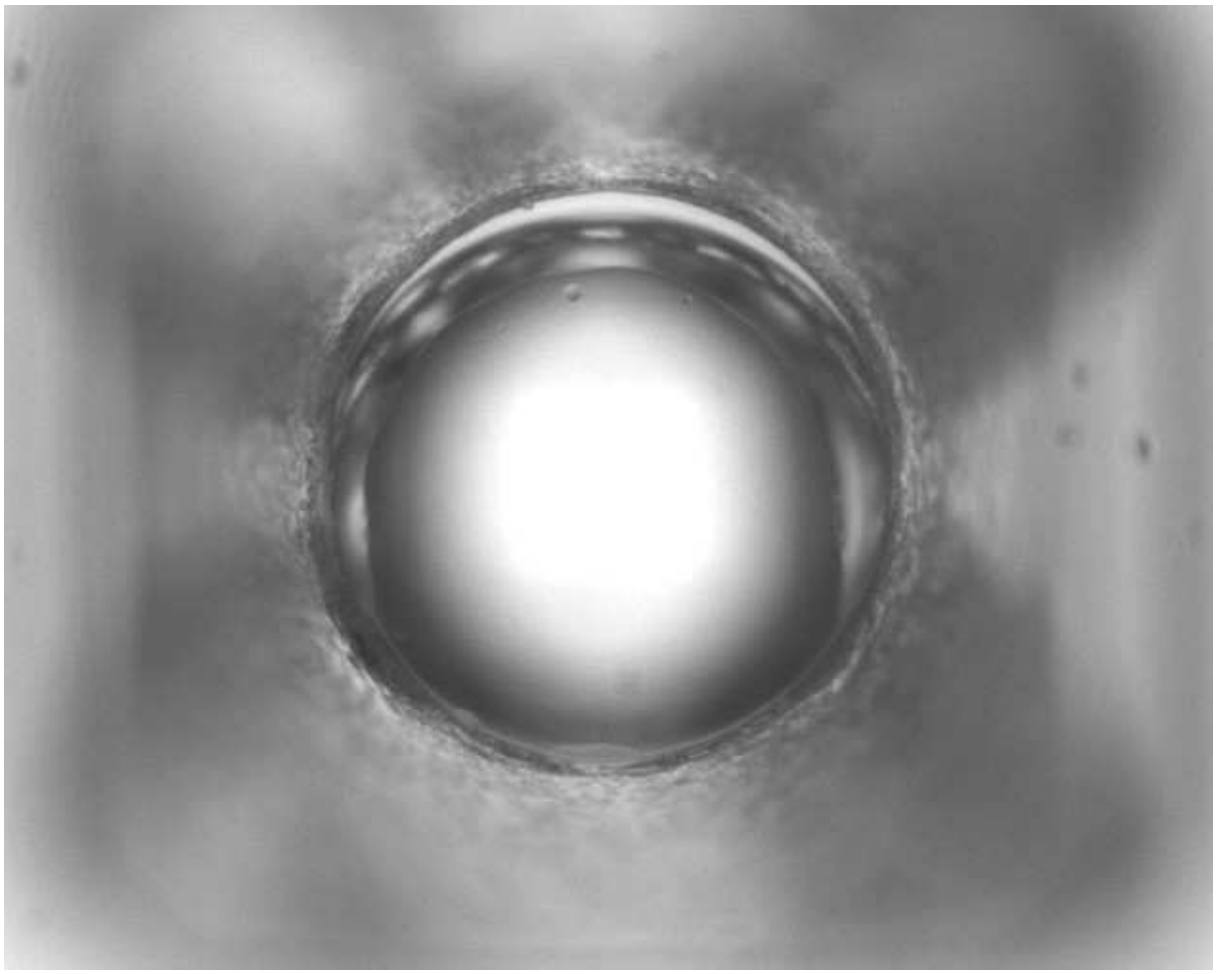

Figure 9: Typical clear drop seen in crystallization trials with MT1.

So far it was not possible to obtain a protein crystal of the full-length cicMT1. Either clear drops (Figure 9) or complete precipitation (Figure 10) were observed in crystallization trials. However, it has been stated that crystallization of MTs in general is difficult and failed frequently [149] due to its unique structural properties.

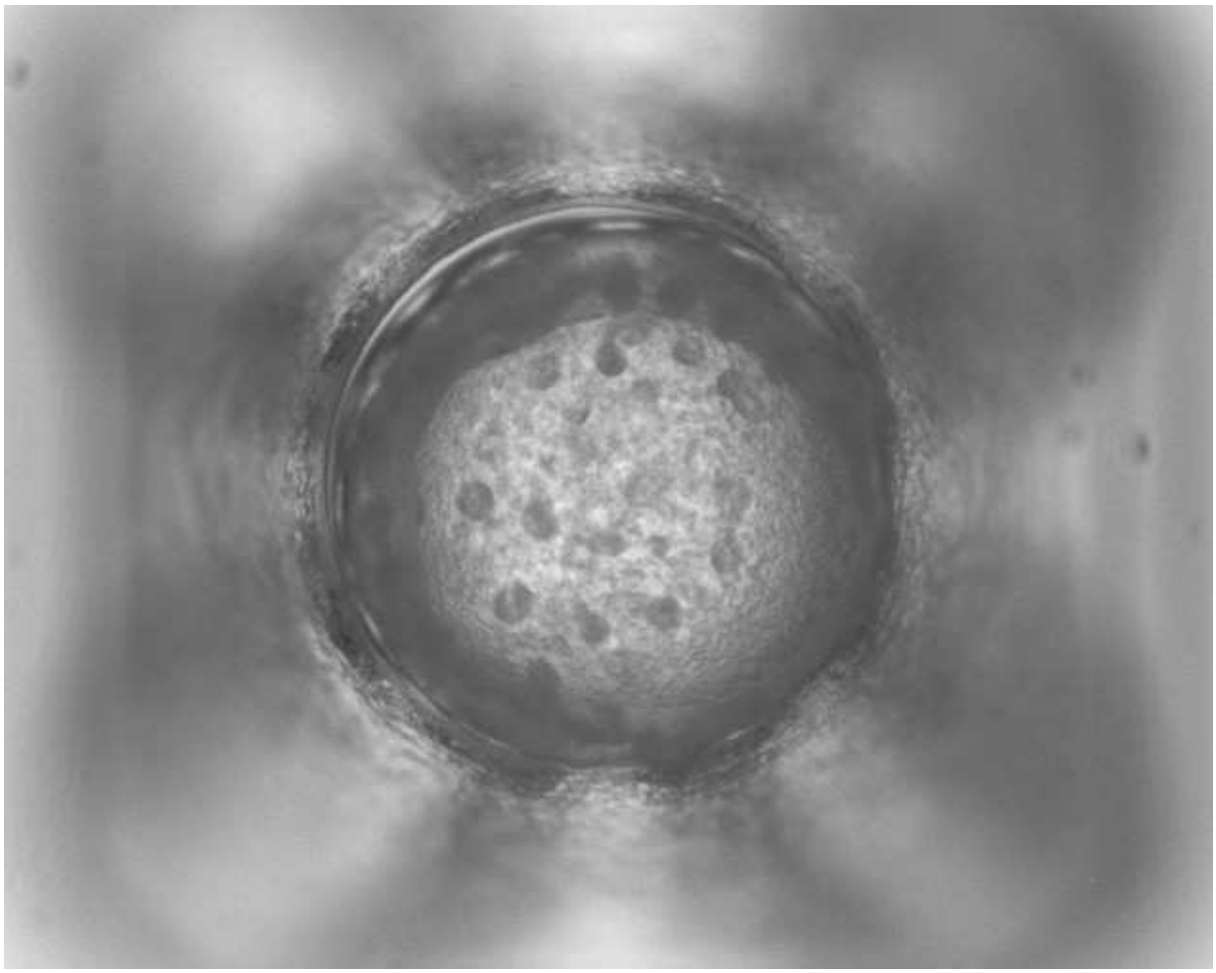

Figure 10: Typical drop with precipitate seen for crystallization trials with MT1.

A truncated version of cicMT1 might reduce flexibility and thus could increase the likelihood of crystallization. Truncation should be performed at C- and N-terminus removing all amino acids prior to the first or last cysteine residue, respectively.

7.1.2 Time depended stability of the metal ion cluster

To determine the stability of the metal ion cluster in Cd_5MT1, the protein (~ 10µM, 2mM Tris-HCl pH 7.5) was incubated with an approximately 100-fold excess (related to metal binding capacities) of Chelex100 for different periods of time. For each sample the protein concentration was determined by PDS assay and the metal ion content by F-AAS.

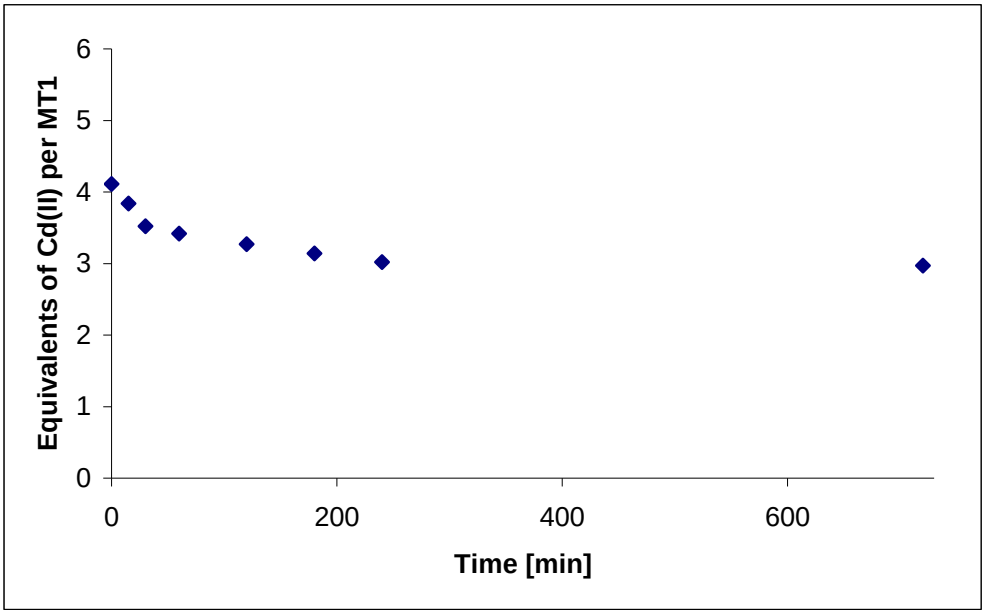

Figure 11: Time dependent Cd(II) content of MT1 after incubation with Chelex100.

Figure 11 summarizes the effect of Chelex100 on the metal ion cluster of Cd_5MT1. It is obvious that the fifth equivalent is removed readily by contact with Chelex100. Further treatment leads to a withdraw of an additional equivalent of Cd(II), resulting in a stable Cd_3MT1 form. However, the loss of the 4^{th} equivalent requires up to 3 hours, indicating an slightly lower affinity of MT1 towards 4 Cd(II) ion compared to Chelex100.

7.2 Spectroscopic titrations

Soon after their discovery it has been found out that MTs are very eligible to absorption measurements [150]. The mammalian isoforms, lacking aromatic amino acids, showed very distinct shoulders at neutral pH with the position and intensity of the shoulders depending on the metal ion coordinated to the deprotonated cysteine residues [151]. These ligand to metal charge transfer (LMCT) bands are visible in the UV region of the spectrum. Additionally, due to the existence of aromatic amino acids in plant MTs from subfamilies p1,p2 and p3, absorptions in the UV range at around 280 nm appear as well. Lowering the pH value of the protein solution will lead to a competition reaction between protons and metal ions bound eventually causing complete protonation of the thiolate groups and metal ion release. This release can be followed by monitoring the disappearance of the characteristic LMCT shoulders. The final spectrum represents the apo-form of the protein. At the pH of the

measurements (7.5) no significant spectroscopic contribution from deprotonated thiolate groups (pK_a . 8.9) to the absorption properties occurs [152].

7.2.1 Zn_5MT1 pH titration

The stability of the metal-thiolate coordination bond strongly depends on the pH and the metal ion. *In vivo,* local pH changes can most likely facilitate an easier release of the metal [84]. Zinc-thiolate cluster give rise to a characteristic LMCT band centered around 230 nm. This band is superimposed with the stronger absorption bands of the amide bonds of the protein backbone resulting in a mixed spectrum, where the S → Zn LMCT band is not clearly observed. Deconvolution of difference absorption spectra, i.e. in which the spectrum of the apo-form is subtracted form each spectra, in gaussian components and their comparison to calculated values of allowed CT bands according to the semi-empirical theory by Jorgensen [153] showed that the relevant transitions indeed derive from several LMCT transitions.

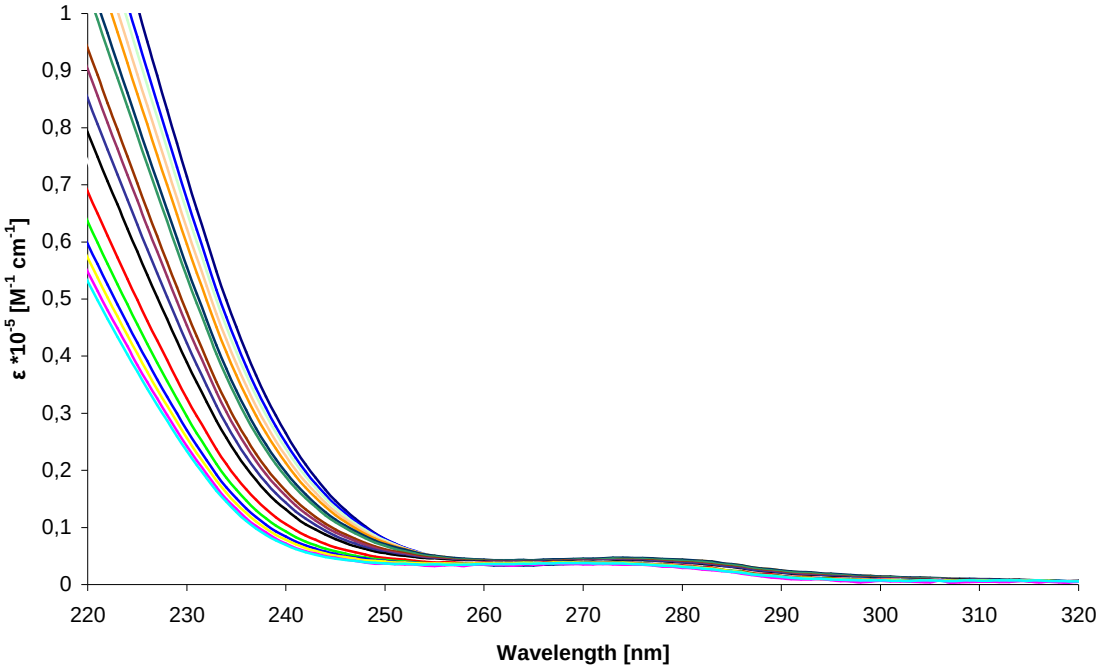

Figure 12: UV spectra of pH titration of Zn_5MT1 (10µM) in 2 mM Tris-HCl (starting pH 8.5, end pH 1.9) and 10 mM NaCl.

Figure 12 shows the typical decrease of the S→Zn LMCT band at 230 nm with decreasing pH values. Up to pH 5.5 a smooth continuous loss of the LMCT transition is observed followed

by a steep drop, between 5.5 and 4.0, and the complete loss of the metal ions from the protein at pH < 4. At low pH values the electronic spectra of metal depleted MT1 resemble the apo-cicMT1 spectra at pH 7.5 (Figure 26). The band at 280 nm deriving form. Tyr and Phe slightly increases with decreasing pH. However, the changes remain marginal (0,05%), compared to the changes of the S → Zn transitions. The point of half dissociation of Zn(II) ions from Zn_5MT1 is at pH 4.9 determined on the basis of half-maximum absorption at 230 nm.

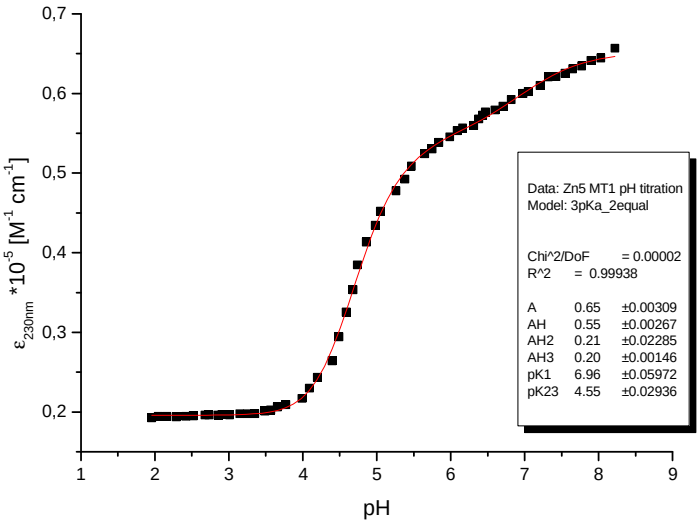

Figure 13: Plot of molar absorption at 230 nm against pH for the pH titration of Zn_5MT1 and fitted data to a model considering 3p*K*a values of which 2 are equal (see text). Curve fitting was performed with Origin®.

The smooth and constant decrease of the LMCT band and the two protonation steps become are clearly visible in the data plot in Figure 13. As mentioned above, complete protonation of the cysteinyl groups in MT1 is achieved at pH values below ~ 4 as evident from the constant absorptivity values, which are caused by a small, but constant contribution of the protein backbone. Plotting molar absorptivity at 230 nm against the pH and then fitting it to various equations describing different acid-base equilibria enables the determination of apparent pK_a values of the cysteine residues in presence of the metal ion under investigation. A detailed description of curve-fitting procedures can be found in the literature [137]. Curve fitting for the Zn_5MT1 pH-titration showed the best results for an equation considering 3 pK_a values, two of them being equal (Equation 1), resulting in values of pK_{a1} at 6.96 (± 0.06) and p$K_{a2,3}$ at 4.55 (±0.03), respectively.

$$y = (A+AH*10^{(pK1-x)}+AH2*10^{(pK23+pK1-2*x)}+AH3*10^{(2*pK23+pK1-3*x)})/(1+10^{(pK1-x)}+10^{(pK1+pK23-2*x)}+10^{(2*pK23+pK1-3*x)}) \quad \text{(Equation 1)}$$

(Equation 1 is constituted by the absorbance value A to AH3 indicating the different protonation steps of the metal ion cluster as well as the apparent p*K*as. Due to the steepness of the slope 2 p*K*a values (2 and 3) are considered to be similar.

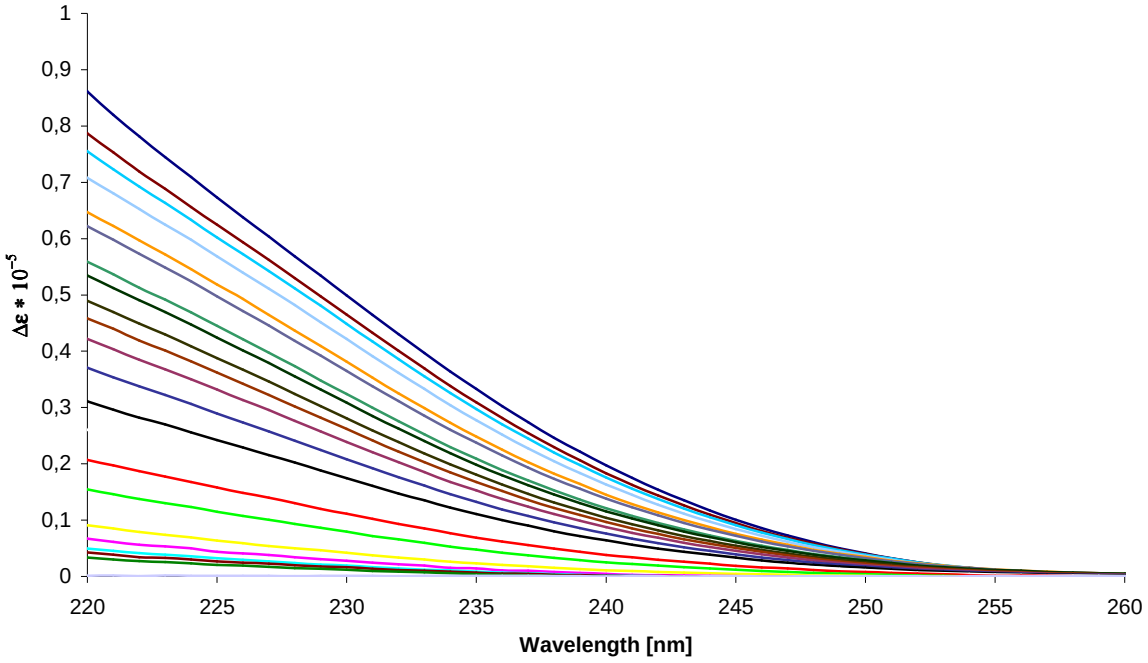

Figure 14: Difference spectra of Zn_5MT1 pH titration, where the spectrum of the apo-form (pH 1.96) has been subtracted from all other absorption spectra.

The difference spectra (Figure 14) show the contribution of the thiolate-zinc LMCT to the UV spectrum (Figure 12) and reveal the limited influence of the peptide chain to the overall electronic absorption in this region. Figure 14 clearly reflects the pH-titration in its behavior, with a slow decrease at pH values above 6 and rapid protonation of the twelve cysteinyl groups and Zn(II) release at lower pH values. However, due to the higher energy of the sulfur zinc transition compared to cadmium no distinct shoulder is formed.

7.2.2 Cd_5MT1 pH titration

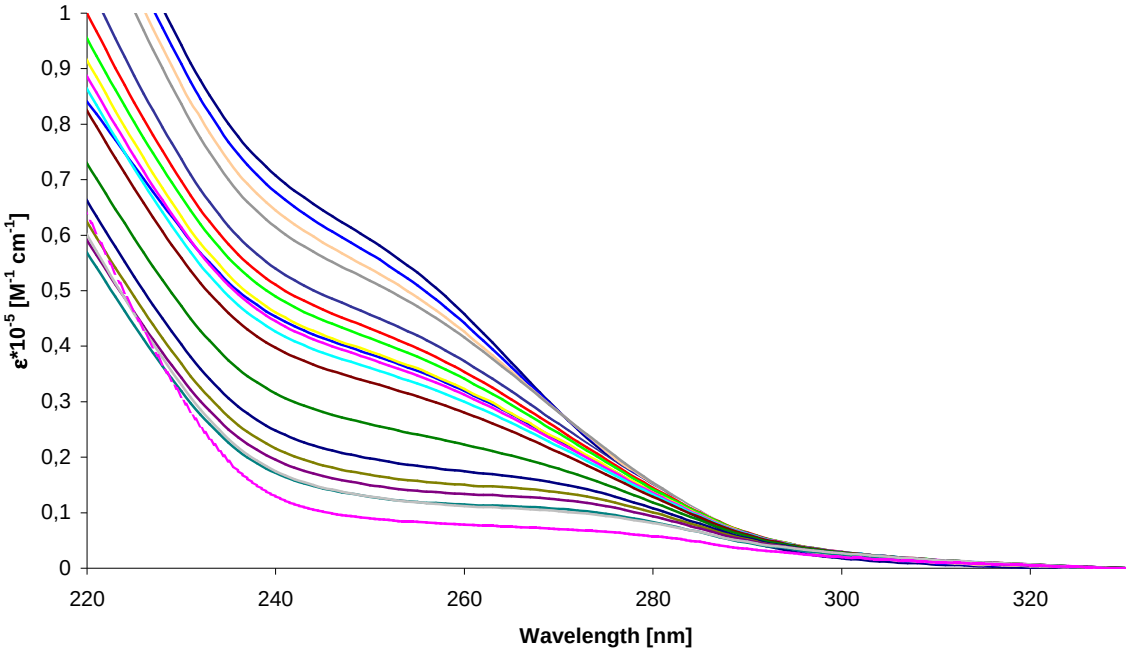

Figure 15: UV spectra of pH titration of Cd_5MT1 in 2mM Tris-HCl (starting pH 8.5, end pH 1.9) and 10 mM NaCl.

Absorption (Figure 15) and difference absorption spectra (Figure 17) of Cd_5MT1 in dependence of the pH reveal the expected shoulder at 250 nm. This LMCT band has already been described in the early stages of MT research [150]. By lowering the pH cadmium is subsequentially released from the protein and the cysteine residues become protonated. The apparent pK_a values compared to the zinc form are shifted by approximately 1 pH unit, being in accordance to the higher affinity of cadmium towards thiolate ligands. The observed absorption around 280 nm is caused by the aromatic amino acids tyrosine and phenylalanine. The general behavior of Cd_5MT1 in pH titration studies resembles that of the zinc form (Figure 12). The molar absorbance at 250 nm is 5.8 * 10^4 M^{-1} cm^{-1} (pH 8.5). Looking at Figure 16 the slightly different behavior of Cd_5MT1 compared with Zn_5MT1 becomes obvious. The continuous decrease of the S → Cd LMCT is less steep than in the case of zinc and shifted by one pH unit to ~ 5. These findings correlate very well to the higher affinity of cadmium towards sulfur ligands and are an indication of one very pronounced and one minor demetalation step. The slope around the second inflection point of around 3.8 is steeper than the one found for Zn_5MT1. Protonation ends with a plateau representing the apo- form of MT1.

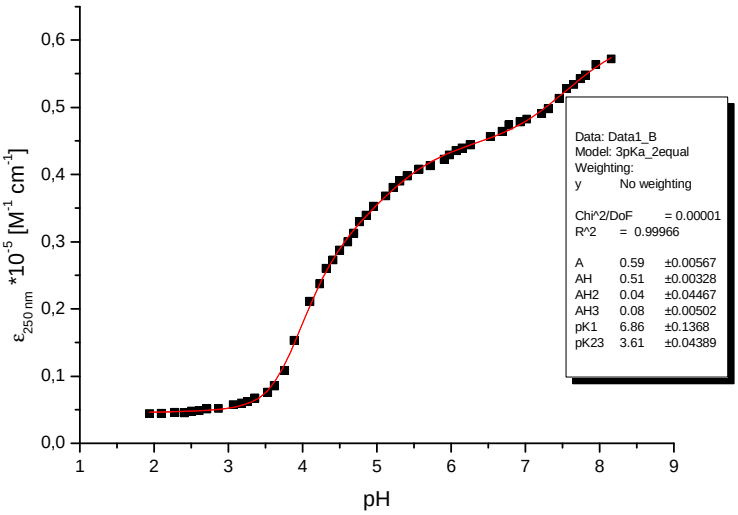

Figure 16: Plot of molar absorption at 230 nm against pH for the pH titration of Cd_5MT1 and fitted data to a model considering 3p*K*a values of which 2 are equal (see text). Curve fitting was performed with Origin®.

As it has been stated before [73, 137] the steep slope suggest that the majority of metal ions is released at a given pH, implementing similar pK_a values for the involved cysteine residues. Therefore single protonated species can be neglected. The plot of pH versus the S → Cd LMCT band can be fitted to an equation describing 3 pK_a with two equal ones. This results in the presence of 2 pK_a values of –6.9 and 3.6, respectively. The half dissociation of Cd(II) from MT1 is 3.9 as determined on the basis of half-maximum absorption.

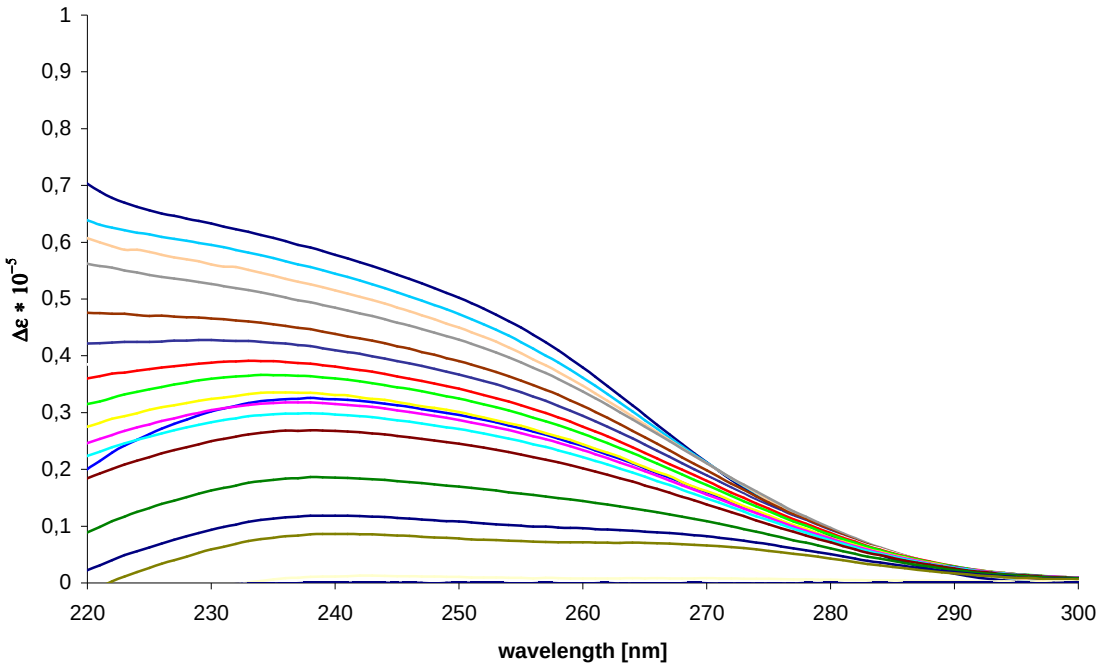

Figure 17: Difference spectra of Cd_5MT1 pH titration, where the apo-form (pH 1.9) has been subtracted from all other absorption values.

The difference spectra (Figure 17) show the strong influence of the cadmium-thiolate chromophores on the electronic spectra originating from the metal ion cluster. The molar difference absorption coefficient at pH 7,5 lying at around 236 nm is 5.8 * 10^4 M^{-1} cm^{-1}. When converted to a metal molarity of 1.2 * 10^4 [M^{-1} cm^{-1}] these values compares quite well to published data of cadmium mercapto-ethanol complexes [154].

7.2.3 pH titration of Cd(II) reconstituted apo-MT1

The cadmium content of fully reconstituted apo-MT1 was determined by flame AAS yielding 5.1 equivalents of Cd(II) per MT1. Progressive acidification leads to a similar titration profile as exhibited by the recombinant Cd-form of cicMT1 (Figure 15). The expected S → Cd LMCT band displays it self as a clear and distinct shoulder. The molar absorbance at 250 nm is 5.2 * 10^4 M^{-1} cm^{-1} (pH 8.3).

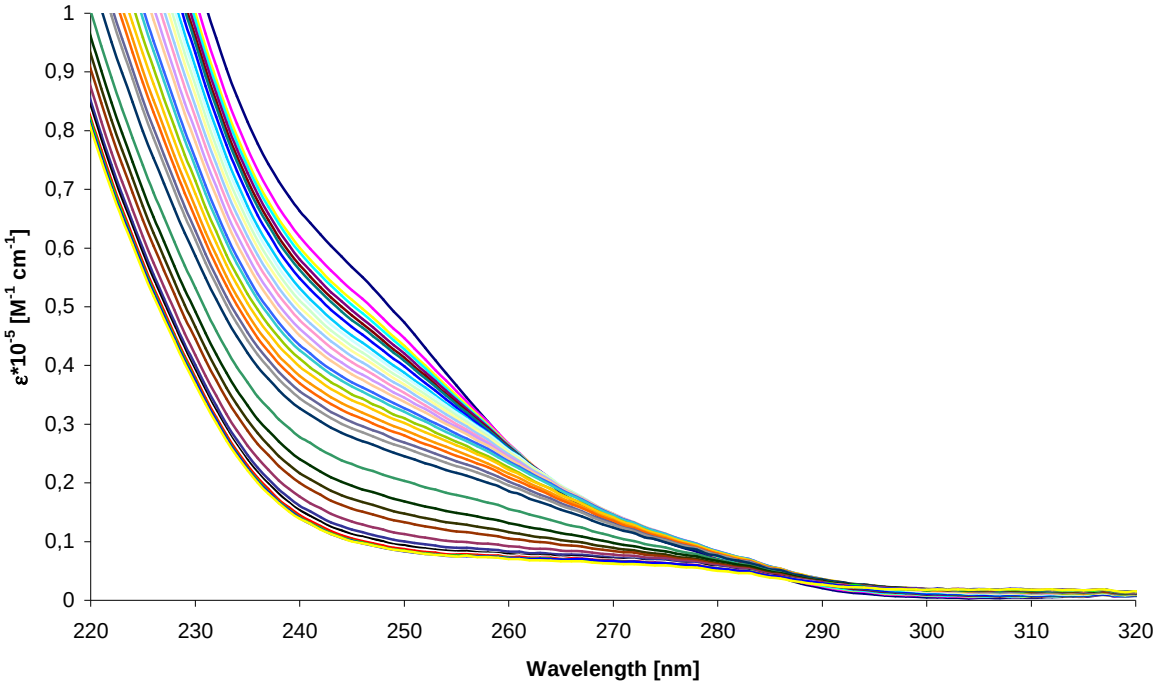

Figure 18: UV spectra of pH titration of reconstituted Cd_5MT1 in 2mM Tris-HCl starting pH 8.5 and 10 mM NaCl.

A two-step behavior as seen for recombinant Cd_5MT1 (Figure 16) is also to be found in the reconstituted form (Figure 19). This clearly shows that a full reconstitution cicMT1 is not necessary to achieve reliable results in contrast to most mammalian MTs [155]. However, due to the high secondary structure content of cicMT1 (see chapter 7.3), which might not be completely restored after the low pH metal ion depletion step, pH titrations of reconstituted MT1 turn out to be difficult to obtain exactly matching spectrum profiles (Figure 15 and Figure 18). Therefore slight different appearance is to be expected.

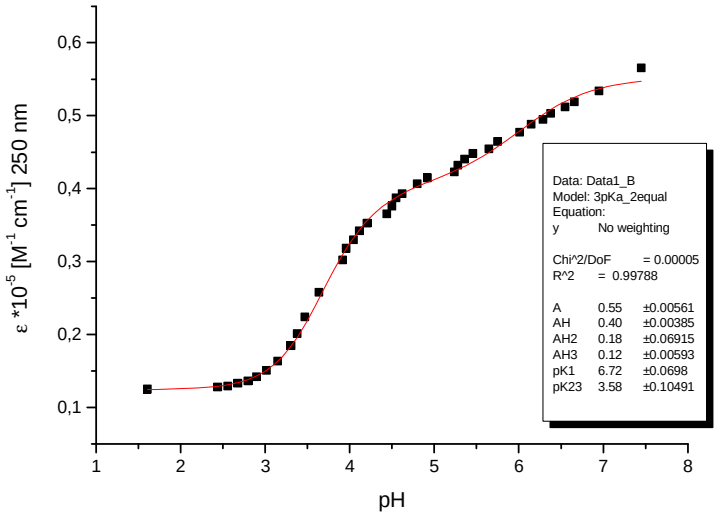

Figure 19: Plot of molar absorption at 230 nm against pH for the pH titration of Cd_5MT1 and fitted data to a model considering 3p*K*a values of which 2 are equal (see text). Curve fitting was performed with Origin®.

Plotting the pH versus the respective absorption of the S → Cd LMCT band also underlines the similarity of the fully reconstituted form to the native one. Fitting can be done by using a 3 pK_a equation with two equal values, as done for Cd_5MT1 obtained directly from expression (see Figure 16). Calculated values are 6.72 and 3.58, respectively. These values are in good agreement with data for recombinant Cd_5MT1 (see Figure 15).

It is worthwhile noting that, spontaneous proteolytic cleavage *in vitro* of the linker in plant MTs has been observed [85] and a cleavage *in vivo* after the formation of a homogeneous cluster has been speculated [72]. For *C. arietinum* MT1 proteolytic cleavage *in vitro* has never been observed during the course of the studies, even at pH 2 the protein was found to be stable for more than 24 h. However, the ability of binding up to 5 equivalents of divalent metal ions does not exclude a linker cleavage *in vivo* of MT1 from chickpea.

7.2.4 Stepwise substitution of Zn(II) ions by Cd(II) in Zn_5MT1

Stoichiometric replacement of Zn(II) in MTs by metals with a higher thiol affinity is a widely used method to study cluster rearrangement and gather information about binding abilities..

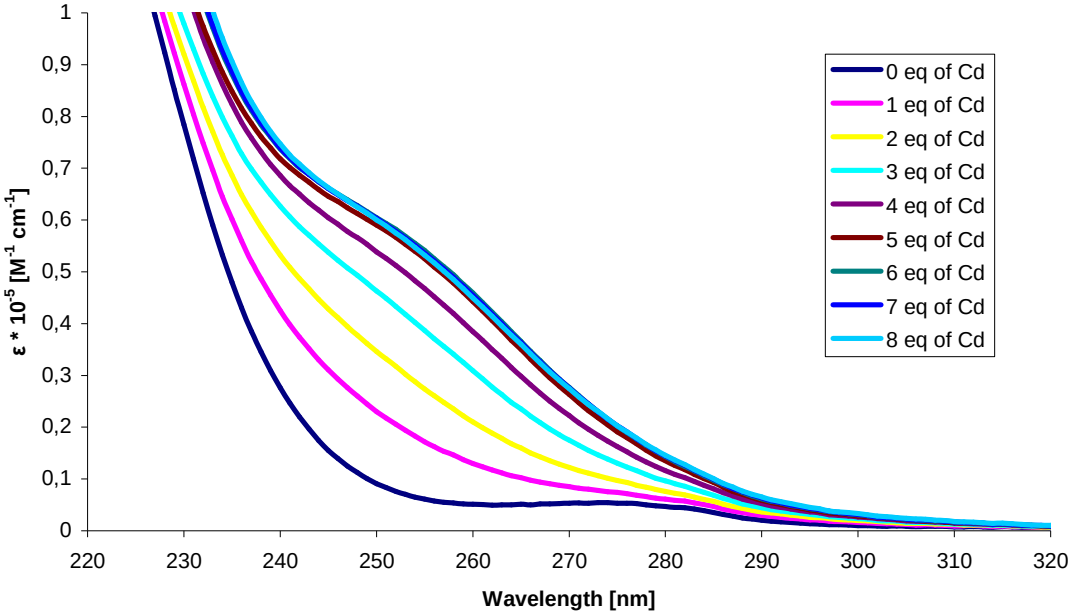

Figure 20: UV-Spectra of the stepwise substitution of Zn(II) ions in Zn_5MT1 by Cd(II) in 2 mM Tris-HCl pH 7.5 and 10 mM NaCl.

Due to a smaller optical electronegativity of zinc compared to cadmium the first LMCT band of S → Zn appears at higher energy than the according S → Cd band [151]. This enables the UV observation of the incorporation of cadmium into Zn_5MT1. *In vivo*, Zn(II) is very often replaced by Cd(II) isostructurally [151, 156]. Figure 20 shows the stoichiometric replacement of zinc by cadmium at physiological pH and salt concentration. The characteristic LMCT band increases with each addition until saturation at 5 mol equivalents of Cd(II) is reached (Figure 21). Further addition leads to a marginal decrease, a phenomena observed with MTs [157] which is derived from the contribution of chloride ligands to the metal cluster.

Since cicMT1 contains one tyrosine as well as one phenylalanine residue, a small clear absorption at 280 nm is visible in the UV spectra. This band is overlaid by the S → Cd LMCT band with increasing cadmium content, and after addition of the third equivalent of Cd(II) it becomes undistinguishable.

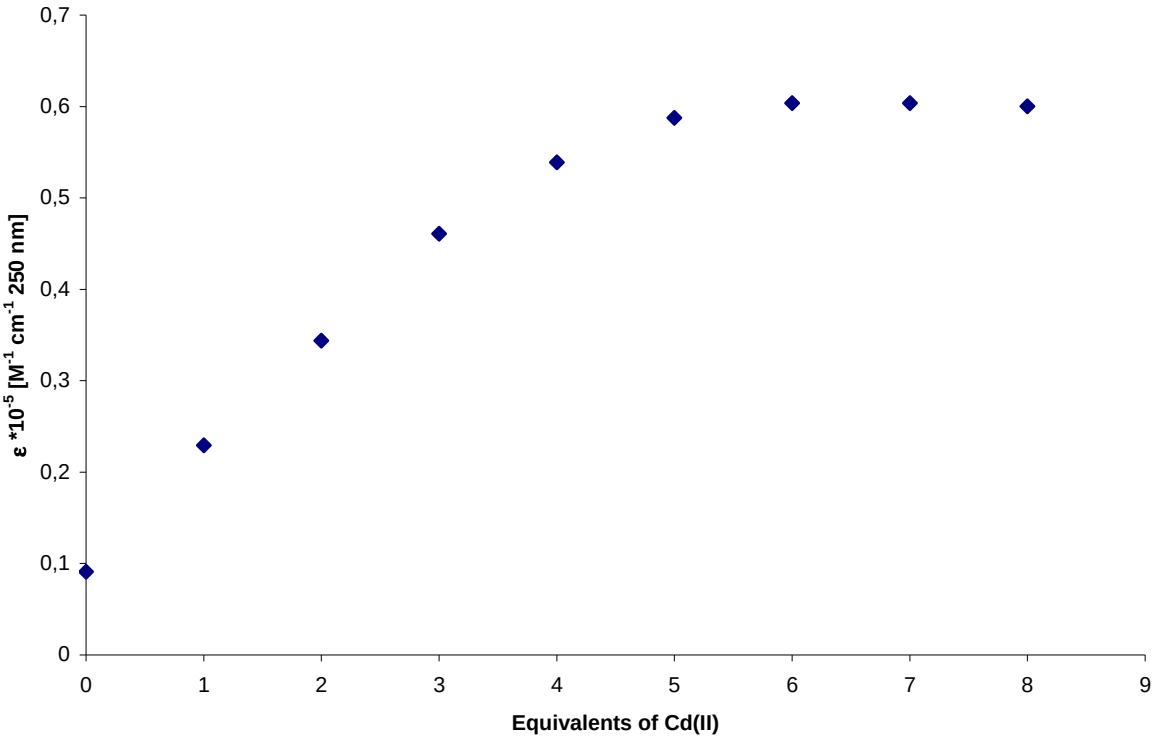

Figure 21: Added equivalents of Cd(II) to Zn_5MT1 versus molar absorptivity at 250 nm.

Previous studies showed that bridging thiolate groups absorb at slightly higher wavelengths than terminal ones [158]. This shift is caused by a higher polarization at the sulfur atom by the two divalent metal ions bound. Cd(II) in MT1 reflects this behavior in the substitution of Zn(II). Further, the S → Cd LMCT band does not strictly increase evenly with added molar equivalents of Cd(II). From Table 2 it becomes obvious that the first three equivalents of cadmium give an average increase in molar absorptivity of 0.12 * 10^5 M^{-1} cm^{-1} indicating coordination to groups bridging Zn(II) and Cd(II) ions but not two Cd(II) ions. The polarization effect becomes visible with the addition of the forth equivalent and is completed with saturation at five equivalents of Cd(II).

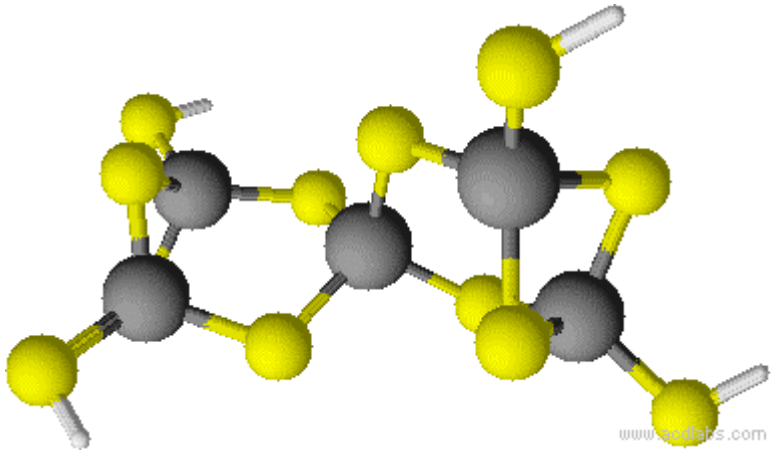

Figure 22: Possible Cd_5Cys_{12} cluster for Cd_5MT1. Modeled with Chemscetch 10 from ACD-labs.

Table 2: Comparison of molar absorptivity per equivalent of Cd(II) added to Zn_5MT1

Equivalents of Cd^{2+}	ε_{250nm} *10^{-5} [M^{-1} cm^{-1}]	$\Delta\varepsilon_{250}$(n+1)-n
0	0,09	-
1	0,23	0,14
2	0,35	0,12
3	0,46	0,12
4	0,54	0,08
5	0,59	0,05
6	0,60	0,01
7	0,60	0,00
8	0,60	0,00

Evaluating the substitution results (Figure 20) and considering the primary structure of cicMT1 as well as the metal ion content one could speculate that the two cysteine rich domains are in close proximity in space corroborating the predicted “hairpin” fold for plant MTs [72]. In this way 3 Cd(II) could be coordinated by MT1 solely making use of terminal thiolate groups, and the entire protein could then accommodate 5 tetrahedral coordinated zinc or cadmium ions with 4 terminal and 8 bridging groups (Figure 22).

7.2.5 Stepwise substitution of Zn(II) ions by Cd(II) Zn_4MT1

Caused by factors, that could neither be evaluated nor controlled so far, occasionally the Zn(II) or Cd(II) content of recombinantly expressed holo-cicMT1 was found to be four equivalents per cicMT1 instead of five. Further addition of Zn(II) or Cd(II) did not facilitate the formation of a $M(II)_5$MT1 species. Subsequent substitution of zinc ions in Zn_4MT1 with Cd(II) leads to different results than observed for Zn_5MT1.

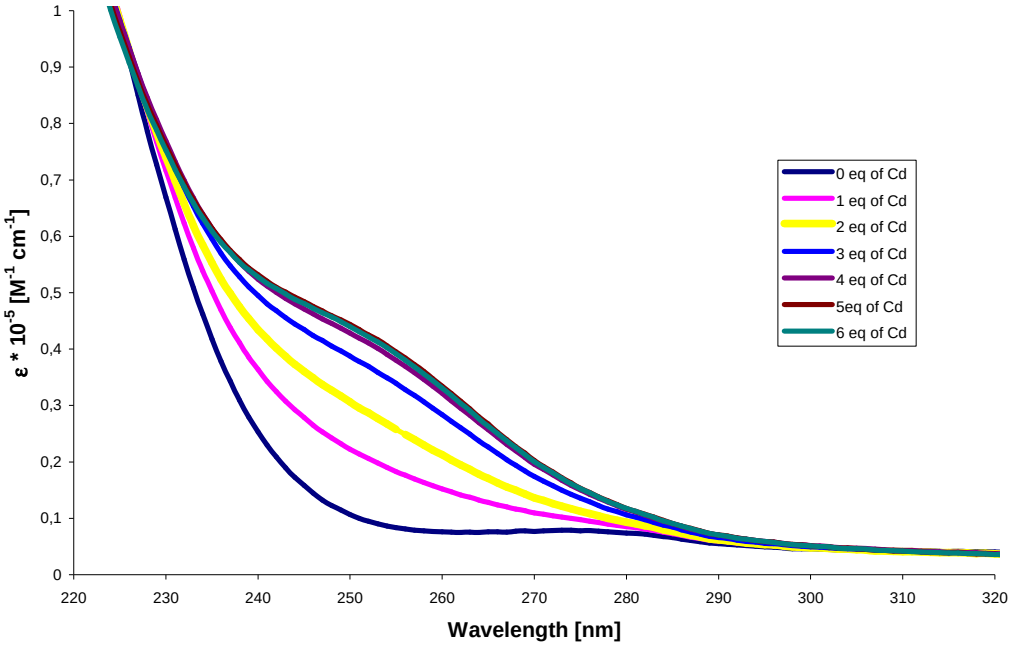

Figure 23: UV-Spectra of the stepwise substitution of Zn(II) ions by Cd(II) in Zn_4MT1in 2 mM Tris pH 7.5 and 10 mM NaCl.

The UV spectra (Figure 23) reveal that a maximum of 4 equivalents of cadmium are bound by the protein. After the addition of the second equivalent of Cd(II) the aromatic absorption at 280 nm is completely superimposed by the S → Cd LMCT band evolving. The slight increase upon addition of the fifth equivalent in absorption at the S → Cd specific LMCT band at 250 nm lies within the normal error range of the titration experiment. Even the addition of an excess of cadmium (of 10 equivalents total) did not facilitate the formation of a Cd_5MT1 species, so that on a speculative basis the two ends of the protein are too far apart from each other to form a homogenous single cluster. Therefore, in this case the formation of two separate clusters instead of one as predicted for the Cd_5MT1 species would be required. While the molar absorptivity after the addition of the first equivalent if Cd(II) is nearly equal for both, the Zn_4- and the Zn_5MT1 species, the addition of further Cd(II) ions causes a less pronounced increase at 250 nm. Finally, also the molar absorptivity at 4 equivalents is significantly lower of the Cd_4-form ($0.43*10^5$ M^{-1} cm^{-1}) compared to the Cd_5-form ($0.54*10^5$ M^{-1} cm^{-1}).

Table 3: Comparison of molar absorptivity per equivalent of Cd(II) added to Zn_5MT1

Equivalents of Cd^{2+}	ε_{250nm} *10^{-5} [M^{-1} cm^{-1}]	$\Delta\varepsilon_{250}$(n+1)-n
0	0,11	
1	0,22	0,12
2	0,31	0,08
3	0,39	0,08
4	0,43	0,04
5	0,44	0,01

Treatment of the Cd_5-form with Chelex100 resin showed the immediate remove of one equivalent. This indicates a Cd(II) binding site with a lower affinity. This might be caused by a somehow different coordination mode of the metal ion and/or might be an indication for a strained cluster structure. The Cd(II) ion released might actually be the cation holding the two separate metal thiolate clusters of the $M(II)_4$-forms together to result in the $M(II)_5$-form. Additionally, it has been reported that the role of the spacer is not to facilitate the independency of the two Cys-rich domains, but rather to make them mutually dependent when binding to zinc [72]. This indicates that the $M(II)_5$-form could be the native one.

Why the linker region is able to assist formation of a single cluster in Cd_5MT1 but fails to do so in Cd_4MT1 remains to be investigated.

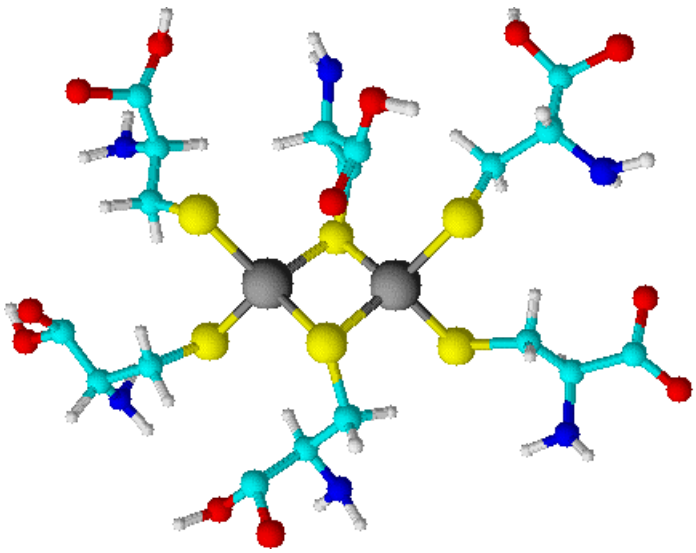

Figure 24: Possible model for the $Cd(II)_2Cys_6$ cluster at C- and N-terminal end of *C. arietinum* MT1. Modeled with Chemscetch 10.

7.2.6 Comparison of CD-spectra of Zn_5MT1 and Cd_5MT1

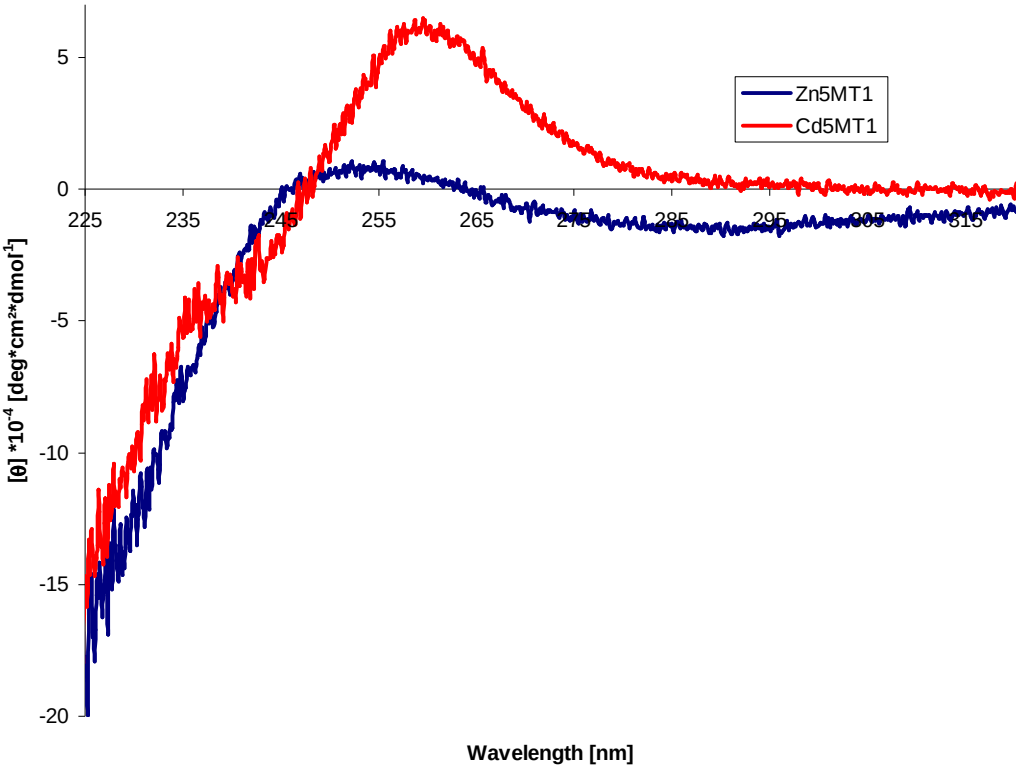

Figure 25: Comparison of spectropolarimetric properties of recombinantly expressed Zn_5MT1 and Cd_5MT1. Spectra were recorded in 2 mM Tris-HCl pH 7.5 and 10 mM NaCl.

CD spectra (Figure 25) of Cd_5MT1 and Zn_5MT1 show that the thiolate-cadmium LMCT band lies at lower energy than the thiolate-zinc band. However, while Cd_5MT1 features a small shoulder around 240 nm, (which in the mammalian isoforms is the maximal negative ellipticity leading to a weakly pronounced positive ellipticity around 220 nm [152, 155]. Zn_5MT1 does not show this pattern. This may arise from the fact that on the one hand the thiolate-zinc transition is shifted to higher energy increasing the overlay of the LMCT bands with the peptide backbone contributions. On the other hand, zinc is bound weaker to thiolates, has a smaller ionic radius and lower optical electronegativity than Cd(II)-ions, leading to different transition surroundings for Zn_5MT1 compared to Cd_5MT1 [149, 155]. The biphasic signal of the cadmium-thiolate chromophores with its positive transitions around 260 nm and its negative shoulder around 240 nm, features its turning point around 250 nm, the exact position of the first LMCT-band [151]. This behavior probably derives from interaction of the

electronic transition dipole moment of the thiolate ligands in an asymmetric environment in cadmium thiolate complexes [159]. However, since bridging thiolates experience a higher polarization [158] thereby absorbing at higher wavelengths than terminal thiolate-ligands, a certain distortion of the LMCT bands resulting in a shift to lower energy is to be expected. The chiral optical spectra of Zn_5MT1 and Cd_5MT1 reflect the general behavior reported for Cd_7GIF [117] and mammalian Zn_7MT and Cd_7MT [160]. However, a turning point at around 230 nm as seen for mammalian isoforms [158] is not observed, except for the small shoulder of the cadmium form.

7.2.7 Incremental reconstitution of apo-MT1 with Cd(II): Formation of Cd_5MT1

7.2.7.1 Electronic absorption spectra

The reconstitution of the metal-free apo-form with metal ions is a frequently performed experiment in MT research. It enables the incorporation of metal ions with lower binding affinity than Zn(II), e.g. Co(II). Nevertheless, it always needs to be verified first that the protein is in principle still able to coordinate to metal ions after the acidification step necessary to obtain the apo-form of the protein (see chapter 6). Therefore, reconstitution is normally first performed with a metal ion with known binding characteristics, e.g. Cd(II). A reconstitution experiment also has the advantage that the LMCT bands formed are only overlaid with transitions from the protein ligand but not by LMCT bands originating from other metal ions.

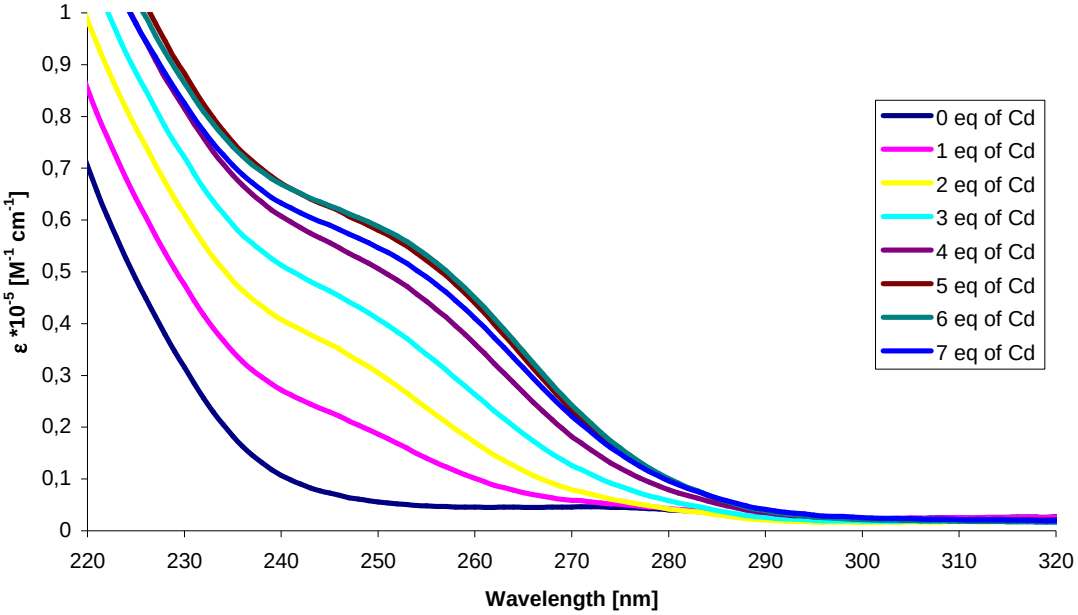

Figure 26: Incremental reconstitution of *C. arietinum* apo-MT1 with Cd(II) followed by UV absorption spectroscopy. The formation of the typical LMCT bands at 250 nm is evident. Measurements were performed in 2 mM Tris-HCl buffer pH 7.5 and 10 mM NaCl.

Figure 26 shows the effect of the incremental reconstitution of apo-MT1 with Cd(II) on the electronic absorption spectra. The absorption envelope resulting from the formation of the tetrahedral Cd-thiolate complexes increases monotonically until saturation with Cd(II) is reached. Upon addition of 5 equivalents the maximum spectral envelope is seen. Further addition of Cd(II) ions leads to a decrease of the specific LMCT band at 250 nm. The overall appearance of the electronic spectra is comparable to the behavior of mammalian isoforms [156]. Surprisingly, MT1 can bind the same amount of zinc or cadmium as MT2 from *C. arietinum*, which has 14 Cys (unpublished data X. Wan).

In the apo-form the aromatic band at 280 nm is clearly visible, but diminishes after the addition of the third equivalent due to the predominant S → Cd LMCT band. The little decrease at 250 nm for the seventh equivalent of Cd(II) could be caused by a slight "opening up" of the cluster structure. This behavior is always found in reconstitution experiments [152, 157]. The decrease depends on the equivalents added (not shown) and becomes stronger with increasing cadmium concentrations as reported before [157] and has been described to be caused by an increasing participation of chloride anions to the formed cluster.

Table 4: Comparison of molar absorptivity per equivalent of Cd(II) added to apo-MT1.

Equivalents of Cd^{2+}	ε_{250nm} *10^{-5} [M^{-1} cm^{-1}]	$\Delta\varepsilon_{250}$(n+1)-n
0	0.06	
1	0.19	0.13
2	0.30	0.12
3	0.41	0.10
4	0.51	0.10
5	0.58	0.07
6	0.59	0.01
7	0.55	-0.04

Table 4 summarizes the changes in intensity of the S → Cd(II) LMCT band for the incremental reconstitution of apo-MT1. The average increase of 0.12 is smaller than seen for mammalian MT of 0.16 [152] for the first 3 equivalents of Cd. However, they match the values seen above 3 equivalents of 0.12 [152], where clustering is seen for mammalian MT1. This coincides very well with the behavior seen for cicMT1. From MCD (7.2.7.3) and Co(II) (7.2.10) studies an unusual clustering behavior from the second equivalent on becomes obvious. On this basis the values match very well. The lower values of 0.07 seen for addition of the fifth equivalent, however, might be an indication for an unusual coordination sphere of the last equivalent.

7.2.7.2 Chiral optical spectra

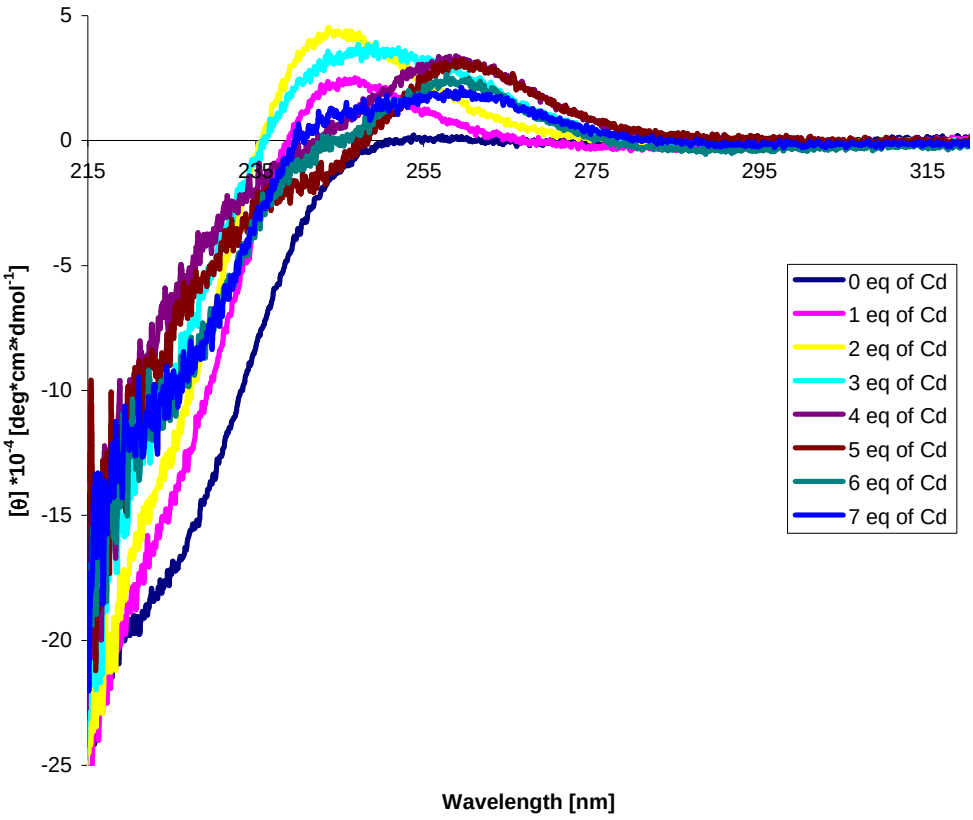

Figure 27: Incremental reconstitution of apo-MT1 with Cd(II) followed by CD spectroscopy. Measurements were performed in 2 mM Tris-HCl buffer pH 7.5 and 10 mM NaCl.

In general, circular dichroism shows the cluster formation and gives information about the cluster structure. For all MTs described so far, absorbance and CD data have revealed that optical properties in the UV-range depend mostly on the contribution of the metal-thiolate chromophores [156, 161].

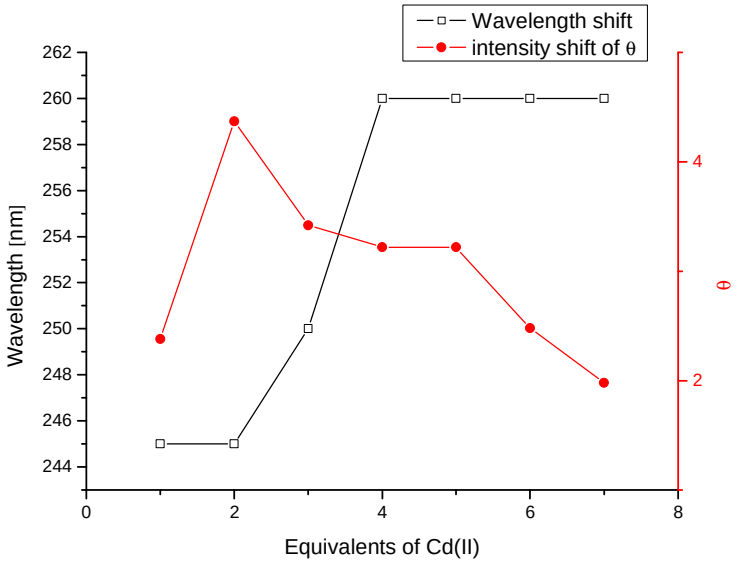

Figure 28: Plot showing the wavelength shift as well as the changes in intensity of θ during the incremental reconstitution of apo-$_5$MT1 with Cd(II) monitored by CD.

Overall, the spectra depicted in Figure 27 differ significantly from published CD-spectra for mammalian MTs [152, 155, 156]. The apo-form is almost featureless in this range and shows negative ellipticity starting at 245 nm and reaching its minimum at approximately 215 nm. However, at 224 nm contributions of secondary structural elements are causing a kink in transition. This contribution originates from the protein backbone and side-chain transitions, revealing that the polypeptide moiety only has a minor but not neglectable influence to the overall chiroptical properties in the range of LCMT bands. Addition of Cd(II) leads to a broad positive ellipticity band with a maximum at 245 nm. The intensity of this band increases upon addition of the second equivalent of cadmium. The third equivalent causes a red shift of the maximum to 250 nm and a slight decrease in intensity. Further addition leads to the final red-shift at 260 nm for equivalents 4 and 5 (Figure 28). A surplus of cadmium leads to broadening and further reduction in intensity of the signal. The general chiroptical behavior is unprecedented in the literature so far. Typically, mammalian isoforms show a positive shoulder at 260 nm (θ = 1,5*10^{-5} deg*cm^2*mol^{-1}) a negative one at around 242 nm (θ = -1*10^{-5} deg*cm^2*mol^{-1}) and another positive band around 220 nm (θ = 0,5*10^{-5} deg*cm^2*mol^{-1}) [152]. However, mammalian MTs lack aromatic amino acids and defined secondary structural elements [152, 155, 156], which can be found in cicMT1 (see 7.3). Since the metal ion binding capacity of plant MTs is smaller than that of the mammalian isoforms, the overall contribution of the metal cluster is lower compared to secondary structure elements. Probably any positive ellipticity is overlaid by the strong negative band of the

structured peptide backbone. The spectra that contain contributions both from Cd-thiolate and from the polypeptide transitions could be simplified by the subtraction of the CD spectrum of apo-MT1. However, this subtraction is only justified when the apo-protein displays only a broad and featureless negative CD shoulder [159] and when there is no indication of transitions originating from secondary structural elements, which are thought to occur in same spectral regions as metal ion binding to apo-MT1 [152, 162]. MT1 from *C. arietinum* does not meet any of these requirements (see also 7.3), therefore no difference spectra will be presented in this thesis.

7.2.7.3 Magnetic chiral optical spectra

In the magnetic circular dichroism (MCD) experiment, a magnetic field aligned with the optical path of a CD spectrometer is used to perturb the ground and excited states of the chromophore. In the simplest form, the MCD spectrum shows either (i) the Faraday A-term, a temperature independent, derivative shaped envelope in which the inflection point aligns with the band maximum of the corresponding absorption band, (ii) the Faraday B-term, a temperature independent, Gaussian shaped envelope that is centered on the position of the band maximum of the corresponding absorption band or (iii) a Faraday C-term, a temperature dependent Gaussian shaped band of either positive or negative amplitude, that resembles the band envelope in the absorption spectrum [149]. Figure 29 gives an overview about MCD contributions and terms. Generally, the MCD spectral information is divided into two regions: charge transfer transitions for all metal ions and d-d transitions for the transition metal ions. For Cd-MT forms the charge transfer bands are observed between 240–320 nm and, like the associated CD spectra, dominate the MCD spectra providing specific information on the binding of the metal ion to the thiolate ligands.

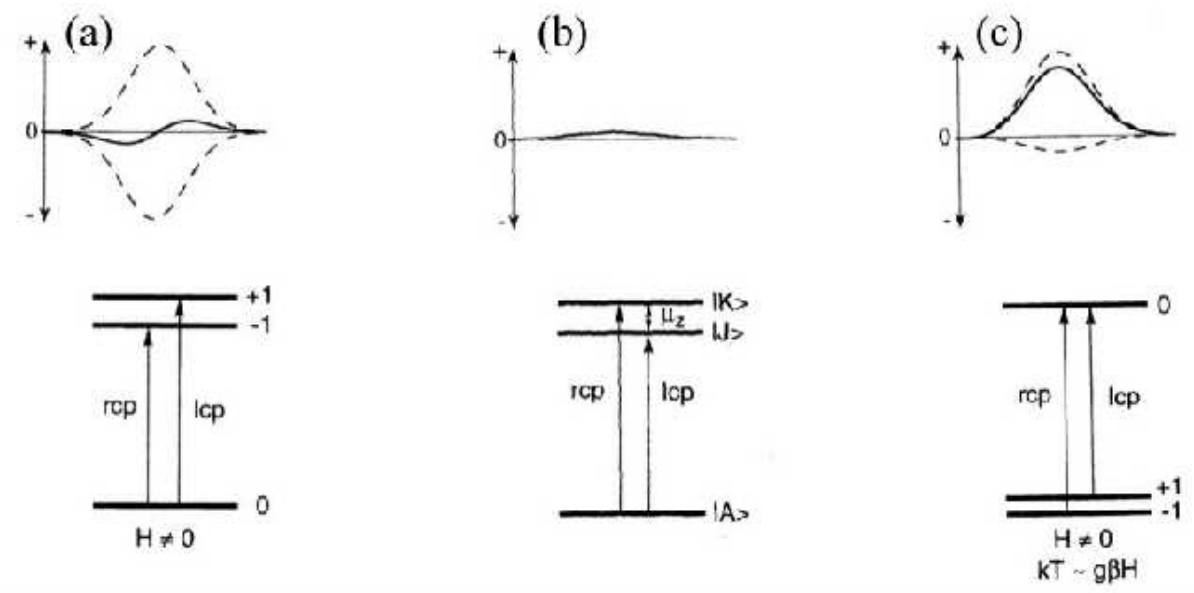

Figure 29: MCD mechanisms: (a) *A*-term, (b) *B*-term, and (c) *C*-term. Taken from [163].

MCD measurements can deliver information about electronic transitions, which are not resolved in electronic spectra. The MCD spectra of the incremental reconstitution of apo-MT1 are shown in Figure 30. For the apo-form, a small positive transition with a maximum around 223 nm (θ_m = 0.48 *10^4 deg*cm²*dmol^{-1}*T^{-1}) is observed. This is probably caused by an n→π* amide-transition of the protein [149, 160, 164]. Upon addition of one equivalent Cd(II) to apo-MT1 clearly two transitions around 250 nm, the position of the S → Cd LMCT band in the UV absorption spectra, are formed. These transitions result in a positive band at 225 nm (225(+): θ_m = 0.86 *10^4 deg*cm²*dmol^{-1}*T^{-1}) and a negative band at 255 nm (255(-): θ_m = 1.02 *10^4 deg*cm²*dmol^{-1}*T^{-1}). With increasing amounts of Cd(II) a continuous red shift to 235 nm (235(+): θ_m = 1.24 *10^4 deg*cm²*dmol^{-1}*T^{-1}) and 262 nm (262(-): θ_m = 3.0*10^4 deg*cm²*dmol^{-1}*T^{-1}) with a continuous increase of magnetic ellipticity for the negative band is observed. The positive lobe however, is overlaid by a B-term and therefore does not resemble the structural surroundings linearily [164, 165]. The biphasic band with the smaller positive and larger negative component is asymmetrically to the inflection point. In accordance with the literature this behavior is assigned to a positive A-term [155, 164, 166], because the positive lobe is to higher energy to the infliction point. The spectra (Figure 30) therefore are typical for tetrahedral distorted coordination of cadmium ions in MTs, showing that plant MT1s feature the same coordination spheres as the mammalian isoforms.

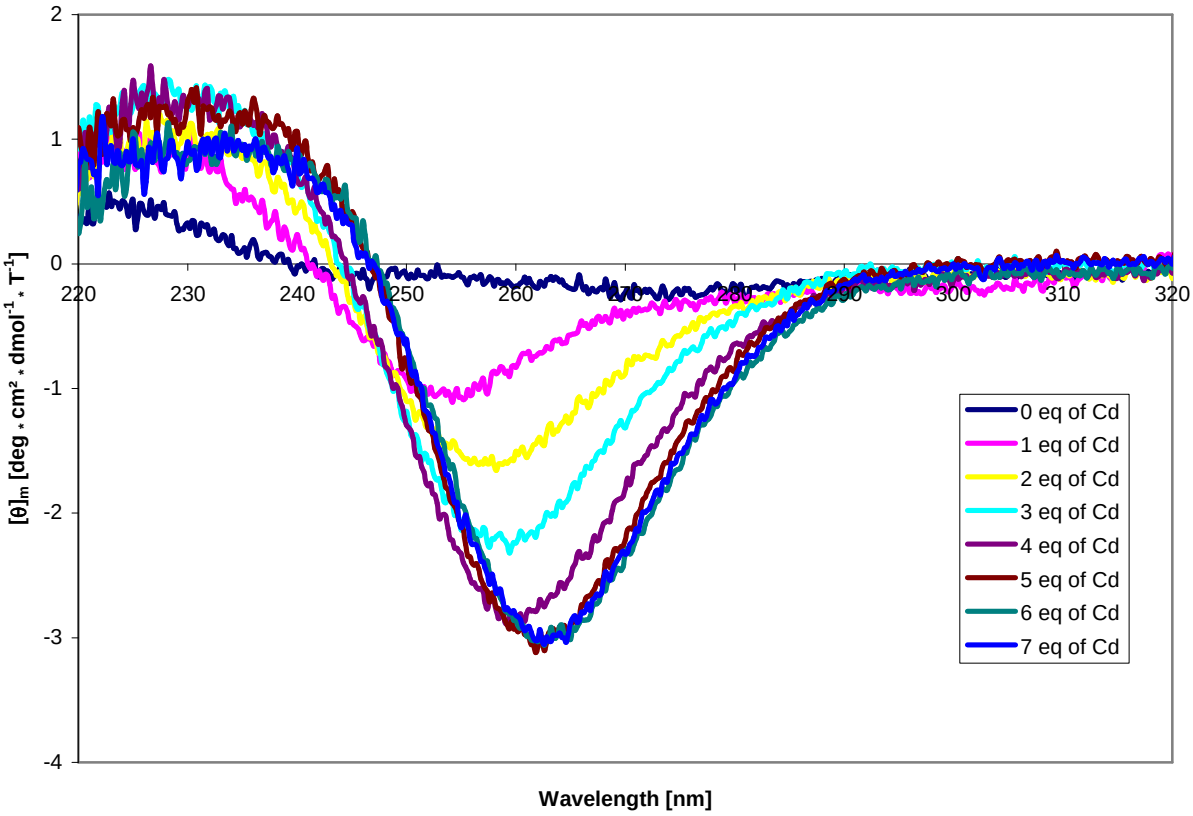

Figure 30: Effect of incremental reconstitution of apo-MT1 with Cd(II) on magneto-spectropolarimetric properties. Measurements were performed in 2 mM Tris-HCl buffer pH 7.5 and 10 mM NaCl.

Cadmium ions coordinated exclusively to terminal thiolate groups do not cause a red shift, but a stronger pronounced isoenergetic envelope [129]. Polarization of thiolate groups in the bridging mode leads to a lower energy transition, seen as red shift in the MCD. This shows that apo-MT1 from *C. arietinum* forms clusters from the second equivalent on. Additionally, it indicates cooperativity in metal ion binding to cicMT1. The direct correlation of equivalents of Cd(II) added and the shift of the minimum can be unambiguously followed in Figure 31.

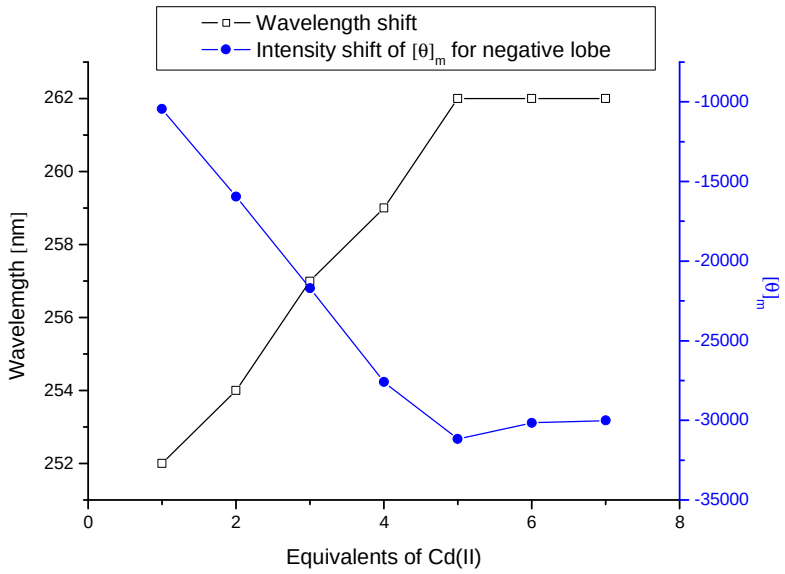

Figure 31: Plot showing the wavelength shift as well as the changes in intensity of θ_m of the negative lobe during the incremental reconstitution monitored by MCD as depicted in Figure 30.

7.2.8 Incremental reconstitution of apo-MT1 with Cd(II): Cd_4MT1

7.2.8.1 Electronic absorption spectra

As mentioned in chapter (7.1) under conditions, which were not systematically reproduceable MT1 was purified with a metal content of 4 equivalents of Zn(II). Reconstitution of the apo-form leads in ~ 60% of the experiments to a Cd_5MT1 species. AS the recombinant Zn(II)-form, also fractional reconstitution with Cd(II) occasionally leads to a Cd_4MT1 species, again in a not reproducible manner.

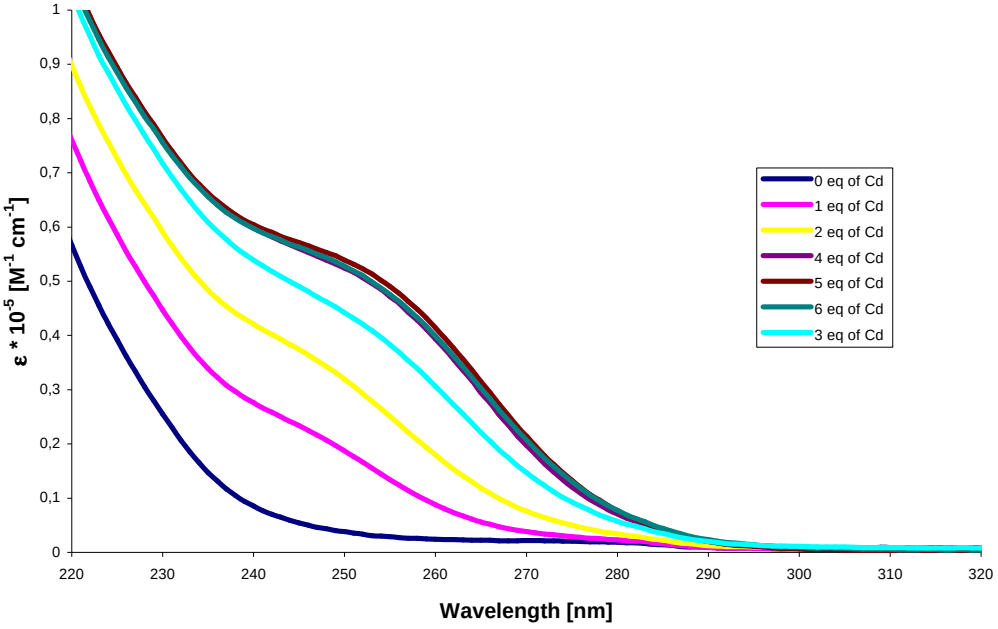

Figure 32: Effects of incremental reconstitution of apo-MT1 with Cd(II) on the development of UV absorption bands resulting in the Cd_4MT1 form. Measurements were performed in 2 mM Tris-HCl buffer pH 7.5 and 10 mM NaCl.

The UV spectra (Figure 32) of the fractional reconstitution of the apo-form sometimes showed the presence of species unable of binding a fifth equivalent of Cd(II). The electronic absorption spectra show the S → Cd LMCT band. The stepwise incorporation of the first 4 equivalents of Cd(II) into apo-MT1 cause an almost linearly increase of the absorption bands. The LMCT band faces a slight red shift from 250 nm to 254 nm (determined by the intersection point of two tangents) for equivalents 3 and 4, which probably is caused by bridging thiolates. In the apo-form the aromatic band at 280 nm is weakly observable, but becomes less evident after the addition of the third equivalent due to the predominant S → Cd LMCT band. The two UV spectra of the apo reconstitution (Figure 26 and Figure 32) look remarkably similarup to the addition of 4 equivalents of Cd(II).

Table 5: Comparison of molar absorbance of the S → Cd LMCT band for reconstituted Cd_4MT1 and Cd_5MT1.

	Cd_4MT1	Cd_5MT1
Equivalents of Cd^{2+}	ε_{250} *10^{-5} [M^{-1} cm^{-1}]	ε_{250} *10^{5} [M^{-1} cm^{-1}]
0	0.04	0.06
1	0.19	0.19
2	0.32	0.30
3	0.44	0.41
4	0.52	0.51
5	0.54	0.58
6	0.53	0.59

Table 5 summarizes the development of the S →Cd LMCT band seen in electronic spectra upon sequential addition of cadmium ions to the apo-form. Up to the fourth equivalent, values and linear increase of the molar absorbance are remarkably similar in both cases, revealing the presence of coordination sites with more or less identical properties. The additional increase of absorption upon binding of a fifth equivalent of Cd(II) indicates that thiolate ligands participate in its binding.

7.2.8.2 Chiral optical spectra

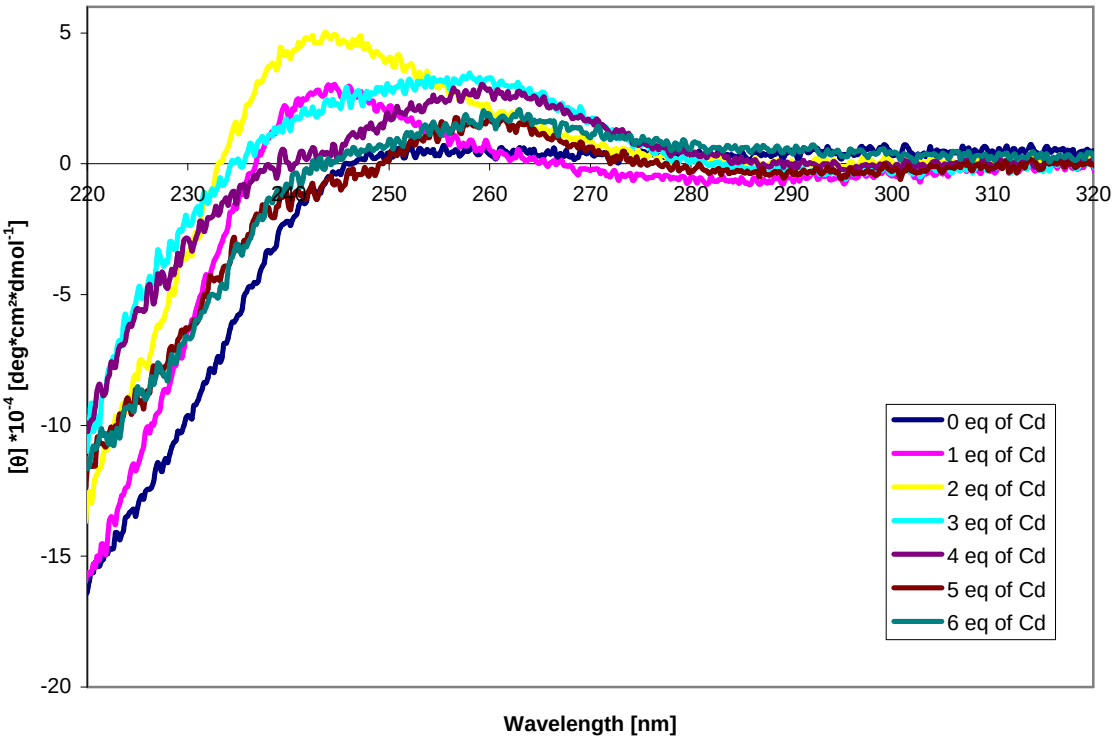

Figure 33: Effect of incremental reconstitution of apo-MT1 with Cd(II) resulting in the Cd_4MT form on spectropolarimetric properties. Measurements were performed in 2 mM Tris-HCl buffer pH 7.5 and 10 mM NaCl.

Pronounced changes upon metal-binding site occupation are displayed in the CD spectra (Figure 33). Clearly visible is the positive band around 242 nm, which increases until the second equivalent of Cd(II) has been added and defines the maximum envelope. Then a red shift to the final positive envelope around 260 nm occurs. This is different to the Cd_5MT1 titration (Figure 27) where the third equivalent of Cd(II) displays an intermediate to the final shift. At 4 equivalents added, the negative shoulder around 242 nm arises as seen before. However, further addition of Cd(II) leads to decrease and broadening of the 260 nm transitions (Figure 34). Addition of further Cd(II) results in a decrease in the overall intensity.

This lack of complete saturation of metal ion binding sites has been noted previously for human apo-MT as well, where Cd(II) binding results in a Cd_6MT rather than a Cd_7MT species [167]. Similar behavior has been reported for MT β-fragments where binding of the third equivalent to the apo-form was not achieved [155].

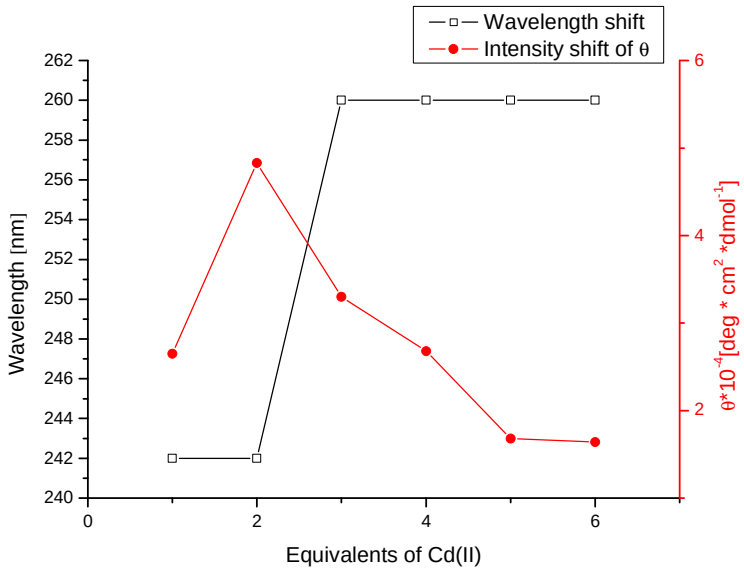

Figure 34: Plot showing the wavelength shift as well as the changes in intensity of [θ] during the incremental reconstitution of apo-MT1 with Cd(II)monitored by CD.

7.2.9 Comparison of Cd_5MT1 and Cd_4MT1

Comparing the UV and CD-data obtained for Cd_5MT1 and Cd_4MT1 helps to spot the differences in metal ion binding behavior. The UV data (Figure 35) indicate that no significant difference in absorption is seen up to 4 equivalents of cadmium. Obvious changes appear upon addition of the fifth equivalent where for the Cd_5-form an increase is observed but not for the Cd_4 -form.

CD spectra (Figure 36) show no obvious difference in position and spectropolarimetric intensity up to 2 equivalents of Cd(II). For the third equivalent the position of the spectral envelope is shifted to lower energy (260 nm) for the Cd_4-form compared to the Cd_5-form with comparable θ values. For additional equivalents the bands arise at the same wavelength and coincide for equivalent 5 of Cd_5 and 4 of Cd_4.

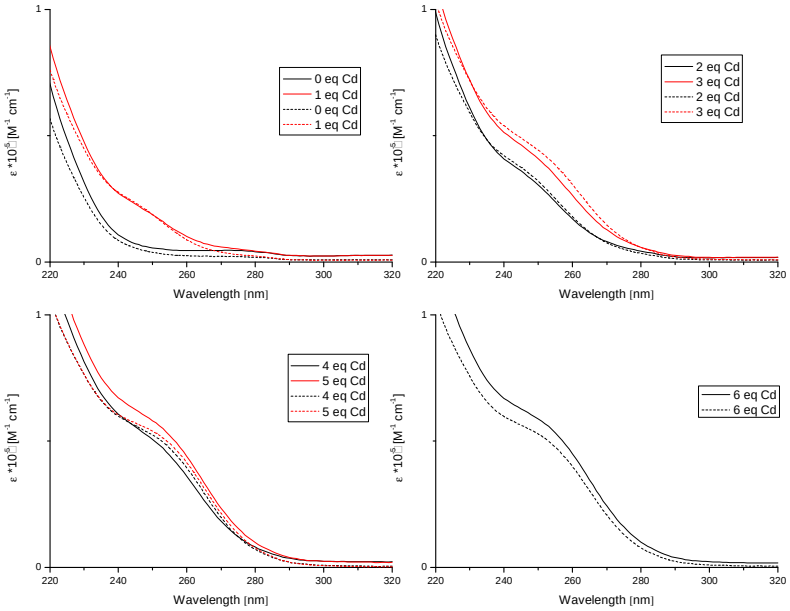

Figure 35: Comparison of the UV properties of the Cd_5MT1 species (solid lines) and the Cd_4MT1 species (dashed lines).

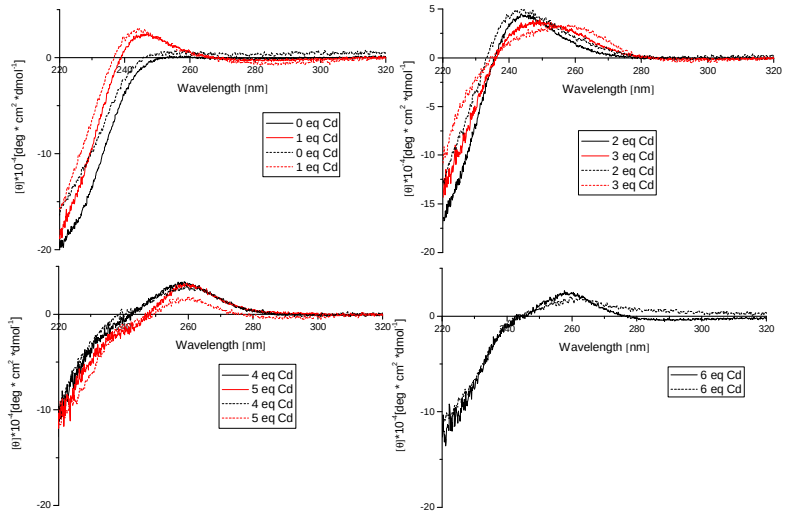

Figure 36: Comparison of the CD properties of the Cd_5MT1 species (solid lines) and the Cd_4MT1 species (dashed lines).

7.2.10 Incremental reconstitution of apo-MT1 with Co(II)

The unique properties of Co(II) which are accessible by spectrophotometric measurements have been effectively used to study cluster formation in MTs [73, 166, 168, 169].

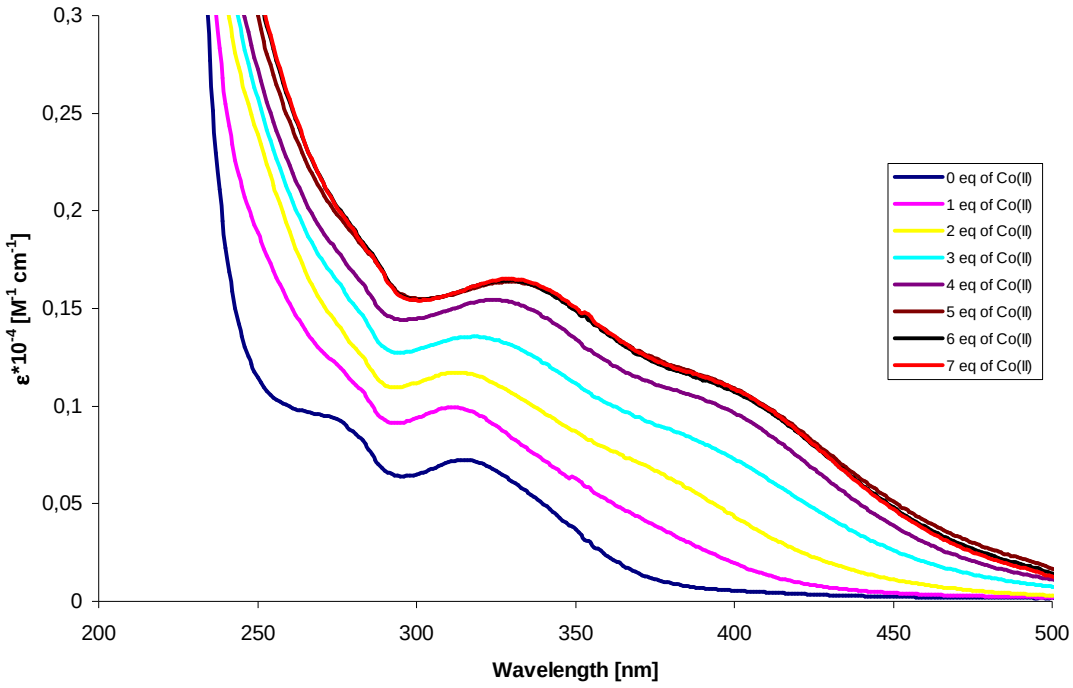

Figure 37: UV spectra of charge transfer region of the stepwise reconstitution of apo-MT1 with Co(II).

The LMCT region of the fractional reconstitution of apo-MT1 with Co(II) is shown in Figure 37. An overall increase in absorbance can be observed up to addition of the 5th equivalent of Co(II) and is thus in agreement with the reconstitution of apo-MT1 with Cd(II) resulting in Cd_5MT1 (Figure 26). The spectra are characterized by a minimum at around 291-296 nm and a maximum at 310-330 nm originating from S → Co(II) charge transfer transitions and a shoulder around 408 nm seen after the addition of the third equivalent of Co(II). After the addition of one equivalent of Co(II) to apo-MT1 a gradual bathochromic shift of the S → Co(II) LMCT band (310-330 nm) occurs until cluster formation is complete at 5 equivalents. Figure 38 illustrates the red shift of the S → Co LMCT band at 310-330 nm.

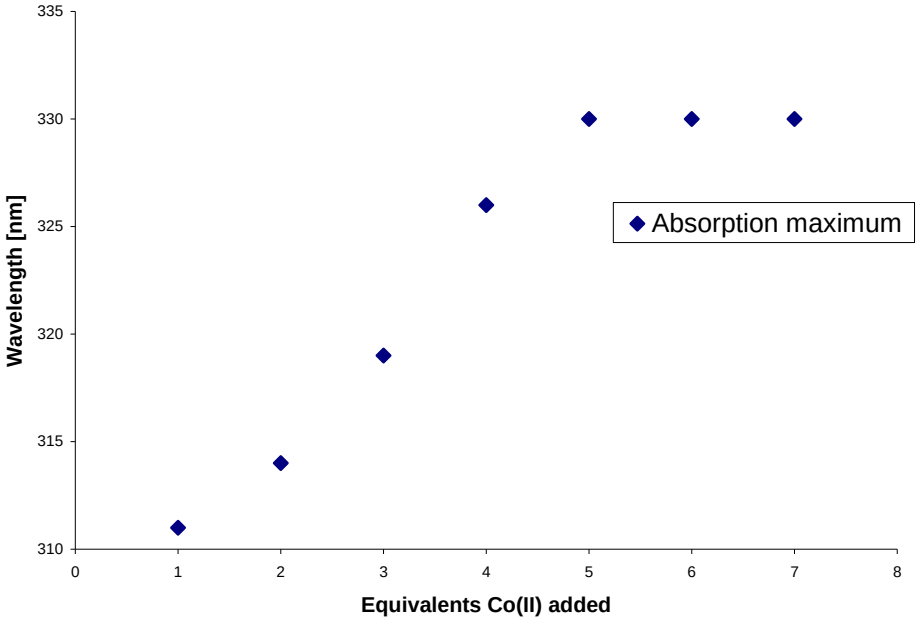

Figure 38: Plot of the wavelength shift in the high energy region with increasing Co(II) concentrations.

The appearance of the bathochromic shift is indicative of cluster formation, i.e. the transition from solely coordination of metal ions by terminal thiolate ligands to bridging thiolates [169]. The red shift observed in conjunction with thiolate cluster formation might be interpreted as an indication of a reduction of the optical electronegativity difference by coordination of the thiolate ligand to an additional electron-donating metal ion [130].

The intensity of the bands in the lower energy region of the spectrum (Figure 39) (above 500 nm) accounts to approximately 10% of the absorptivity for the transitions in the LMCT region. The absorption envelope originates from d-d transitions and is formed by three gaussian shaped bands with maxima at 592, 695 and 749 nm and molar absorptivities of 95, 131 and 109 M^{-1} cm^{-1}, respectively, for the Co_5MT1 species. The splitting into three absorption bands originates form spin-orbit coupling and has been assigned to tetrahedral tetrathiolate Co(II) coordination [166, 169]. These features of Co_5MT1 resemble those reported forcrab *Cancer pagurus* [166] and vary slightly from values for wheat E_c-1 [73].

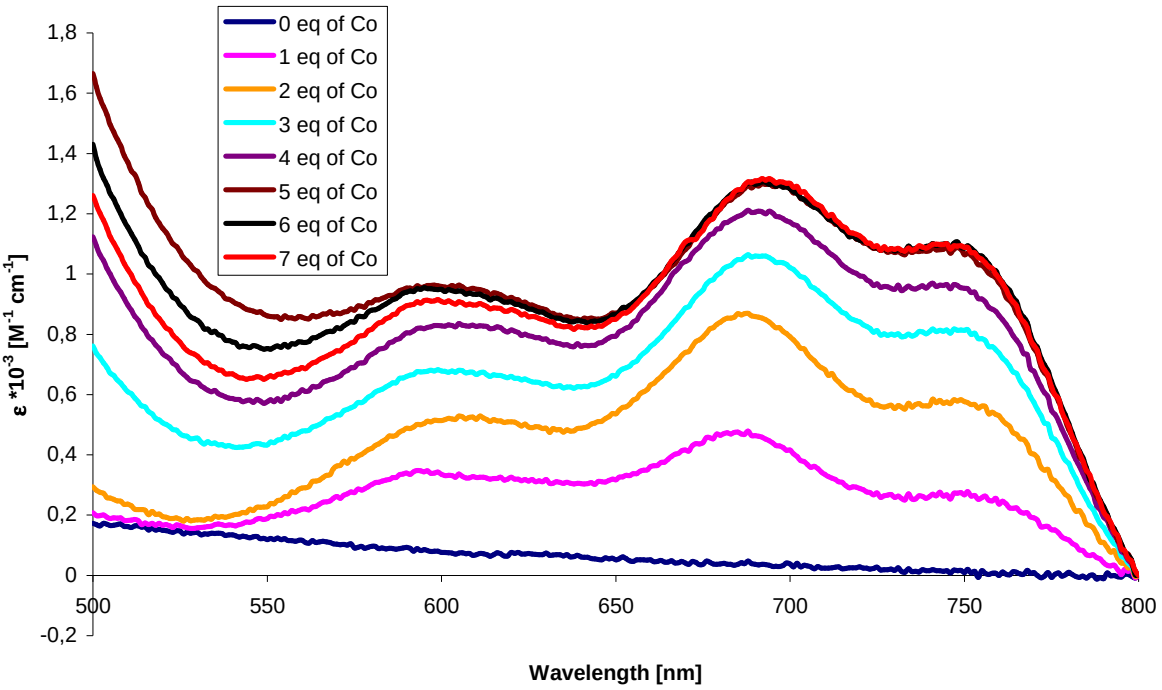

Figure 39: UV-Vis spectra of the *d-d* transition region for the incremental reconstitution of apo-MT1 with Co(II).

The central band starts to shift bathochromicaly already after the addition of the first equivalent of Co(II) (see Figure 40). Additionally, the higher energy (592 nm) and lower energy (749 nm) bands in the visible region shows a slight hypsochromic shift with increasing molar concentrations of Co(II) as it's the case for rabbit liver MT [168].

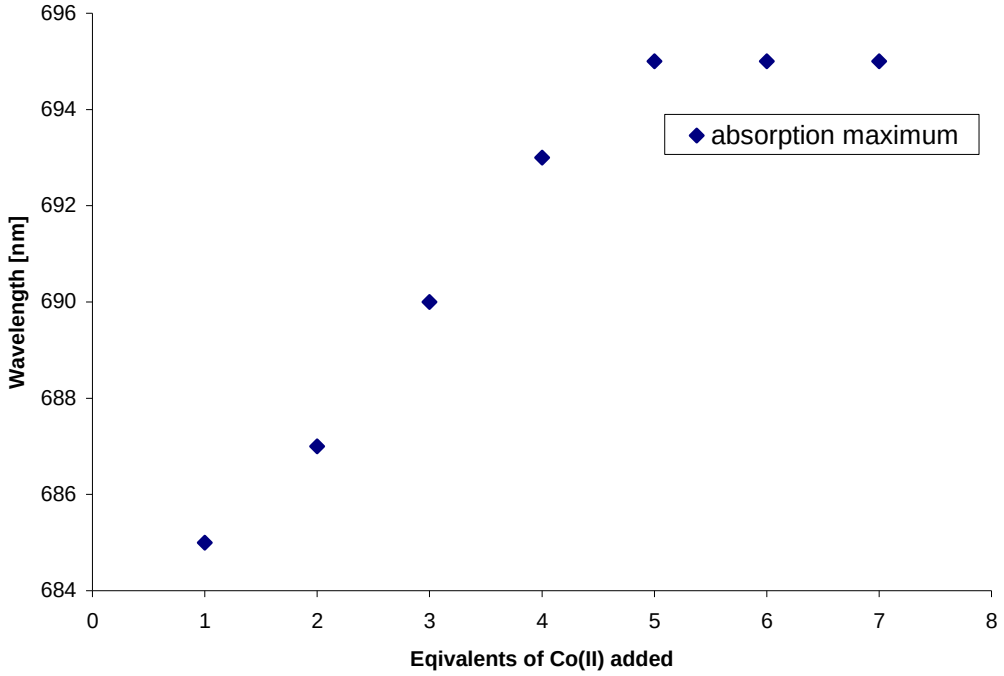

Figure 40: Plot of bathochromic shift of the maximum around 690 nm.

It is worthwhile to note that high and low energy parts of the spectrum give the same information for cicMT1, however, discrepancies in form of a further increase of the *d-d* transitions compared to LMCT transitions have been reported [166].

7.2.11 Cu(I) binding to apo-MT1

Spectrometric titrations were carried out to assess the potential Cu(I) binding capacity of cicMT1. So far, only estimated data for plant MTs are available, e.g. 6.2 Cu(I) ions per protein molecule for a plant MT1 from *P. sativum*, $PSMT_A$ [85].This is even more surprising as certain classes of plant MT1 are available at the moment, and additionally plant MTs are believed to play a role in copper homeostasis [105].

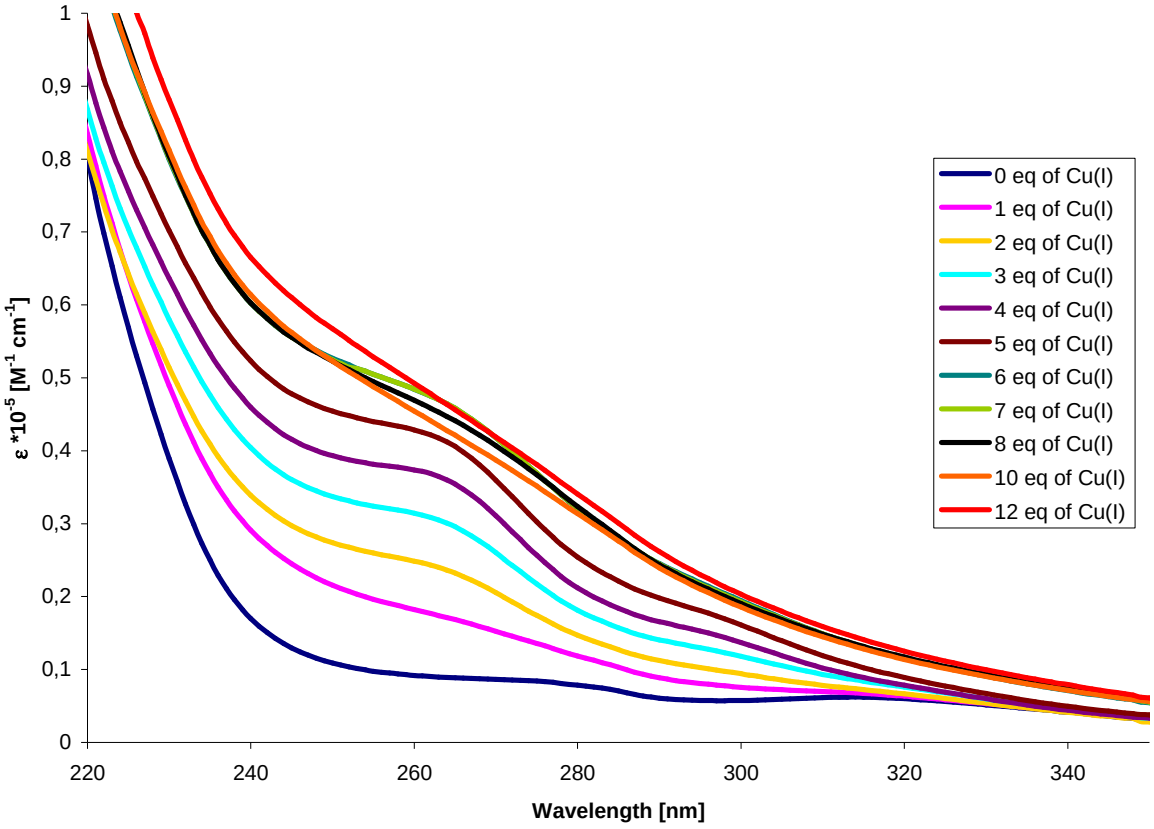

Figure 41: UV spectra of incremental reconstitution of apo-MT1 with Cu(I).

Figure 41 shows the UV spectra of the addition of Cu(I) to the apo-form of cic-MT1. Titrations were performed under anaerobic conditions using the tetraacteonitrilcopper(I) complex, $[Cu^{I}(NCCH_3)_4]^+$ [138], as Cu(I) source. The apo-form (0 eq of Cu(I)) shows the typical featureless UV spectrum with absorptions originating only from the peptide backbone and the aromatic amino acids as described in chapter 6.2.1. Increasing concentrations of Cu(I) lead to the formation of spectra with a clear shoulder 260 nm and a minor one around 295 nm. The shoulder at 260 nm shows a small red shift reaching its final position at 262 nm after the addition of 6 equivalents Cu(I), which also marks the point of saturation of MT1 with metal ions. At this point the molar absorptivity accounts to $\varepsilon_{262nm} = 4.75*10^{-4}$ M^{-1} cm^{-1}. A similar red shift has been reported for rabbit liver MT [127].

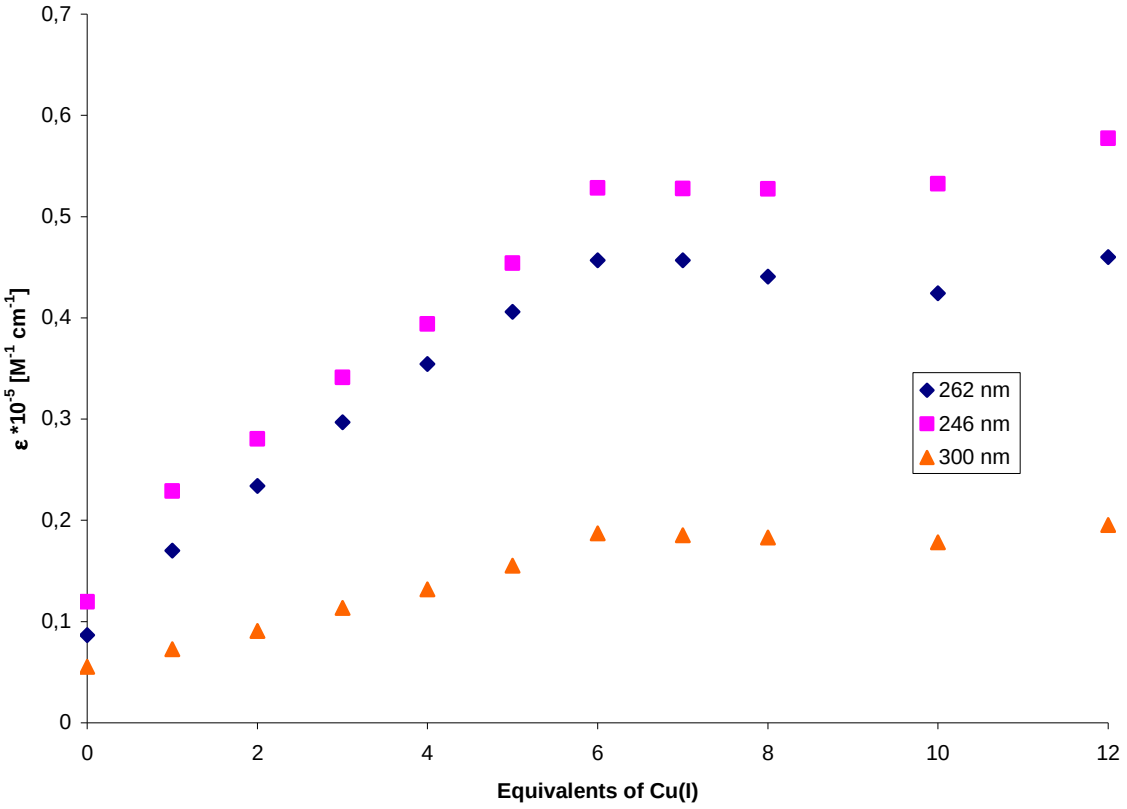

Figure 42: Plot of molar absorptivity 262 nm against molar equivalents of Cu(I) added to apo-MT1.

Additionally absorptions around 280-350 nm raise and become predominant after addition of the sixth equivalent of Cu(I), leading to a featureless spectrum. Similar behavior has been reported for rabbit liver MT [170]. Further increase in Cu(I) concentration leads to a decrease of the Cys-Cu(I) LMCT transition at 262 nm up to the addition of 10 equivalents of metal accompanied by the disappearance of the clear shoulder. The 12th molar equivalent of Cu(I) leads to an additional increase of this band, probably caused by an overlay of electronically weak cluster centered (CC) transitions [127]. However, electronic absorption spectra are quiet featureless compared to chiroptical spectra. Figure 43 shows the CD spectra of the incremental reconstitution of the apo-form with Cu(I). All chiroptical changes take place above 240 nm and are consequently mostly influenced by changes that occur within the metal-thiolate binding core(s).

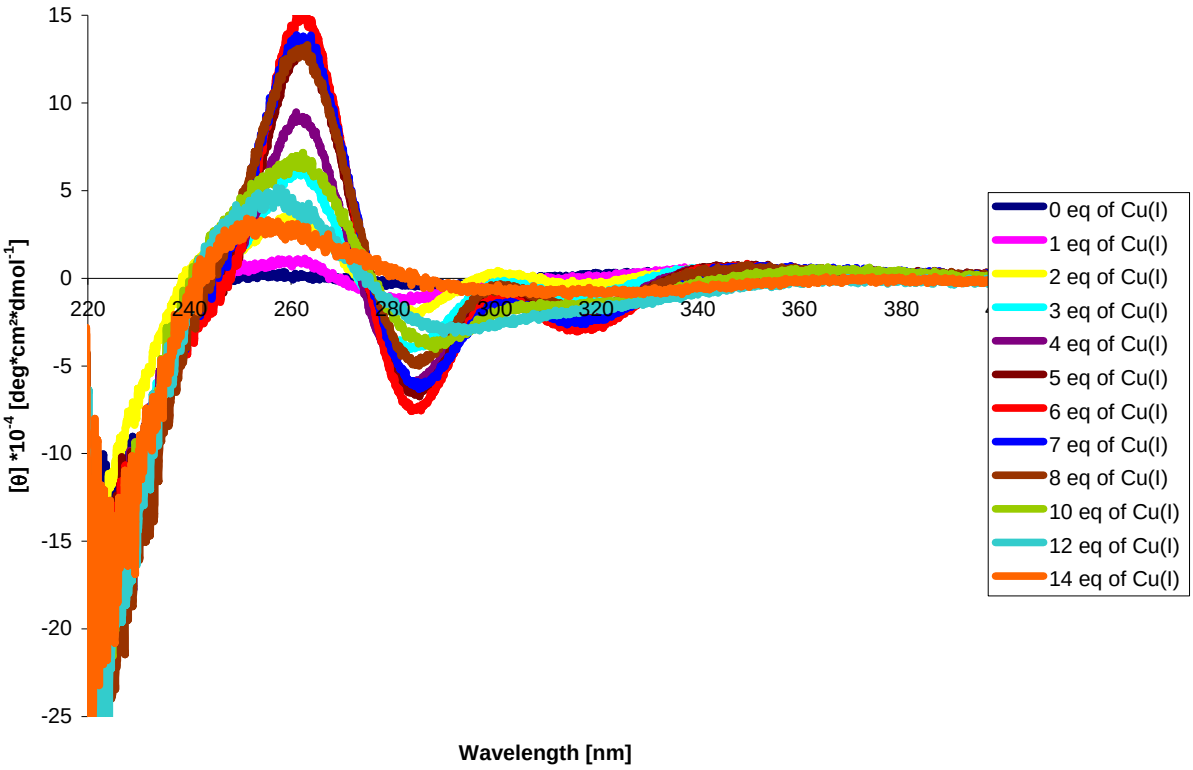

Figure 43: CD spectra of incremental reconstitution of apo-MT1 with Cu(I).

Apo-MT1 shows negative ellipticity below 240 nm, originating from the peptide backbone. At lower energies (> 350 nm) the protein is absolutely featureless. Addition of the first molar equivalent of Cu(I) leads to the formation of two transitions, a positive at 262 nm and a negative at 283 nm. The absolute intensity values of both ellipticities are increasing until the maximum is reached at 6 molar equivalents of Cu(I). The second equivalent of Cu(I) introduces a second negative ellipticity band at 320 nm that also finds its maximum at 6 equivalents. The plot given in Figure 44 illustrates the observed, almost linear increase of the three bands. The slight decrease at equivalent 7 and increase at 8 equivalents shows that there is still a certain level of unsaturation in the protein at 6 equivalents of copper added, probably leading to a rearrangement of the cluster. A continuous decrease would signify a brakeup of the formed cluster structure [149, 171].

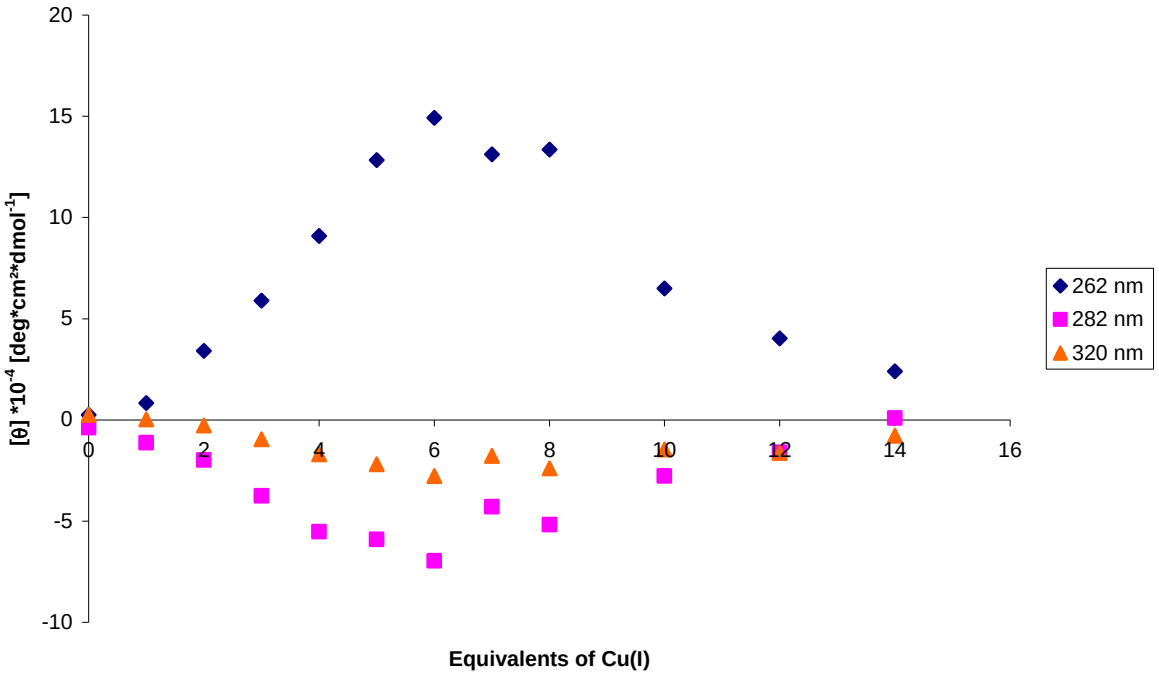

Figure 44: Plot of molar ellipticity at different wavelengths against Cu(I) equivalents added to apo-MT1.

Upon addition of 10 equivalents or more the CD signal loses its characteristic features with broadening of the ellipticity bands and additional merging of the two bands at 282 and 320 nm, accompanied by decreasing intensities. A brake up of the formed cluster structure can be assumed at the end of the titration (14 equivalents of Cu(I)) as the spectra become completely featureless above 250 nm.

7.2.12 Cu(I) binding to Zn_5-MT1

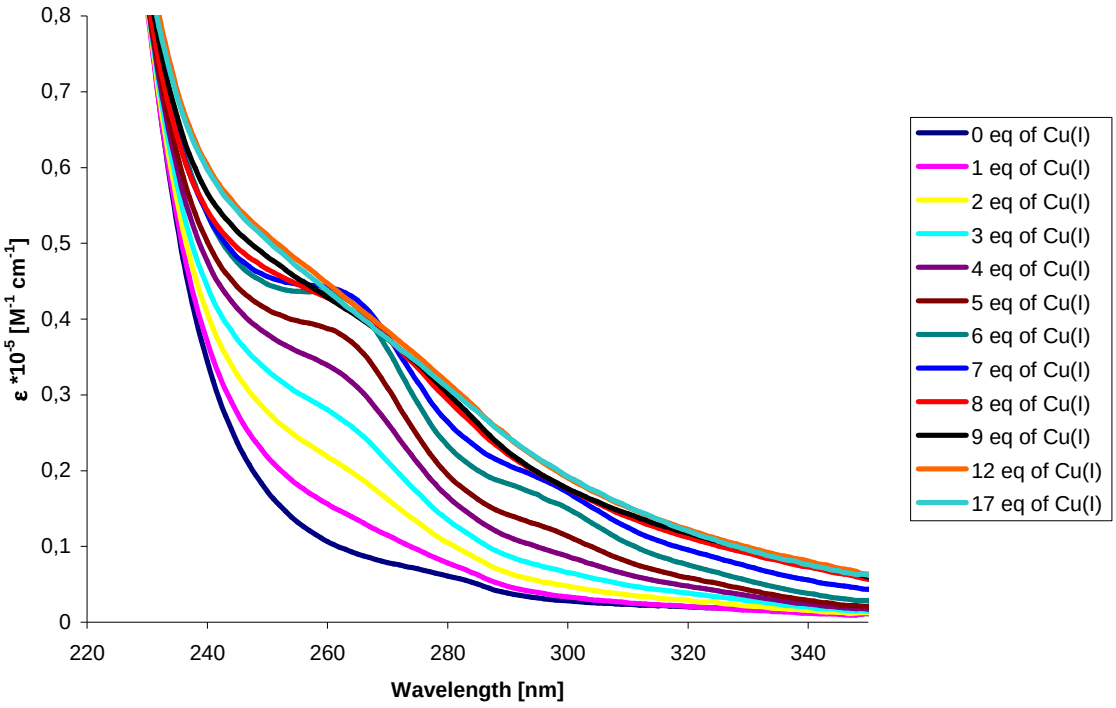

Figure 45: UV spectra of the fractional titration of Zn_5-MT1 by Cu(I)

Substitution of Zn(II) by Cu(I) (Figure 45) leads to slightly different electronic spectra than seen with the apo-form (Figure 41). The maximum at 262 nm is reached with six equivalents of Cu(I) added to Zn_5MT1. The slight increase in the UV spectrum at the seventh equivalent lies within the error of the experiment. CD spectra (Figure 47) clearly reveal the maximum of 6 equivalents. Further addition of Cu(I) results in a featureless UV spectrum.

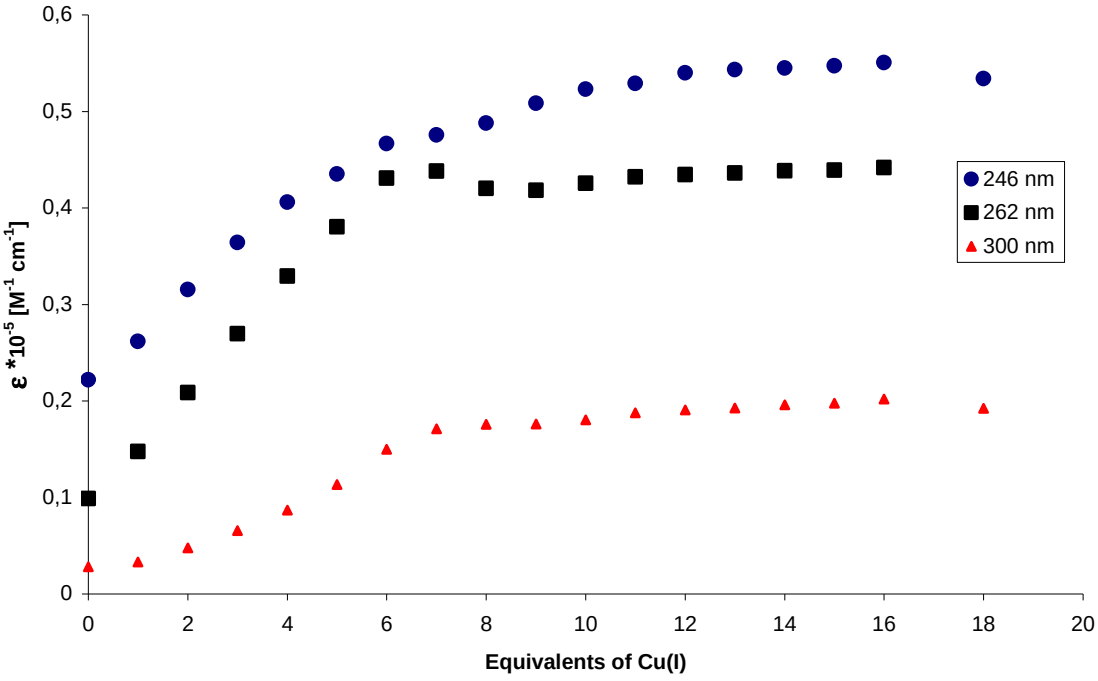

Figure 46: Plot of molar absorptivity at 246, 262 and 300 nm against equivalents of Cu(I) added to Zn_5MT1.

Following the substitution of Zn(II) by Cu(I) in cicMT1 with CD spectroscopy (Figure 47) gives a more detailed picture of the structural changes in the protein and its metal cluster. Intense dichroic bands develop in the CD spectra of Cu(I)-MT1, which at 262 nm, the position of the S → Cu(I) LMCT band, parallel the behavior of the absorption spectra (Figure 45) by showing a constant increase in intensity until addition of 6 molar equivalents of Cu(I). A continuous red shift from 255 to 262 nm, along with the development of a minimum at 282 nm is observed upon replacement of Zn(II) by Cu(I).

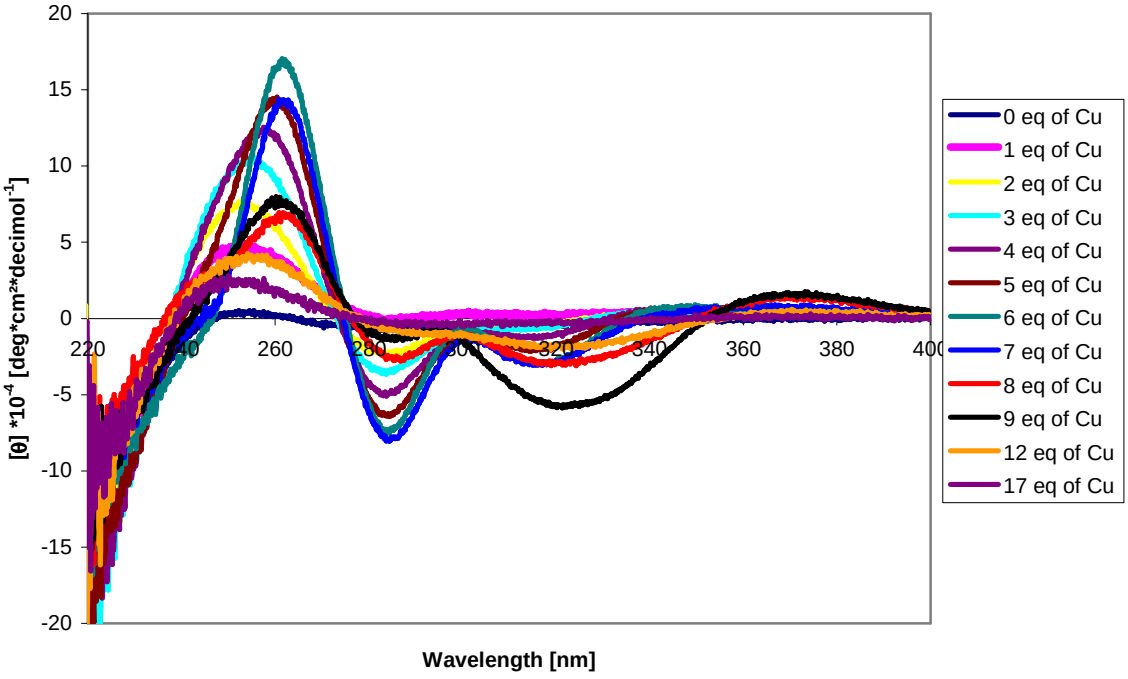

Figure 47: CD spectra of Cu(I) titration of Zn_5MT1in NH_4OAc pH 7.5.

The CD spectrum of $Cu(I)_6$MT1 is similar to previously reported spectra for mammalian MTs [172-174]. However, the positive band seen at 335 nm for rabbit liver MT [127, 174] is not observed. The band at 320 nm (-) finds its maximum at 9 molar equivalents of Cu(I). As d^{10} Cu(I) ion has a fully occupied valence shell, this band cannot originate from metal-centered *d-d* electronic transitions (300-340 nm). Consequently, the major optical transitions observed are LMCT bands originating from the Cu(I)-thiolate clusters formed between Cu(I) and the MT [127] as depicted in Figure 47. However, it has been demonstrated that metal cluster-centered (CC) *d-s* transitions are possible for Cu(I)-ligand clusters depending on symmetry effects (320 nm) [175, 176]. These transitions occur at slightly lower energies than the LMCT transitions. Figure 48 demonstrates the shifts of the maxima at different wavelengths of the CD spectrum. The maximum of the CC transitions at 9 equivalents is also reflected at 262 nm as after a sharp decrease from the 6th to the 8th equivalent again a small increase for the next equivalent of Cu(I) is observed. Further Cu(I) additions lead to a continuous disappearance of observable structural elements.

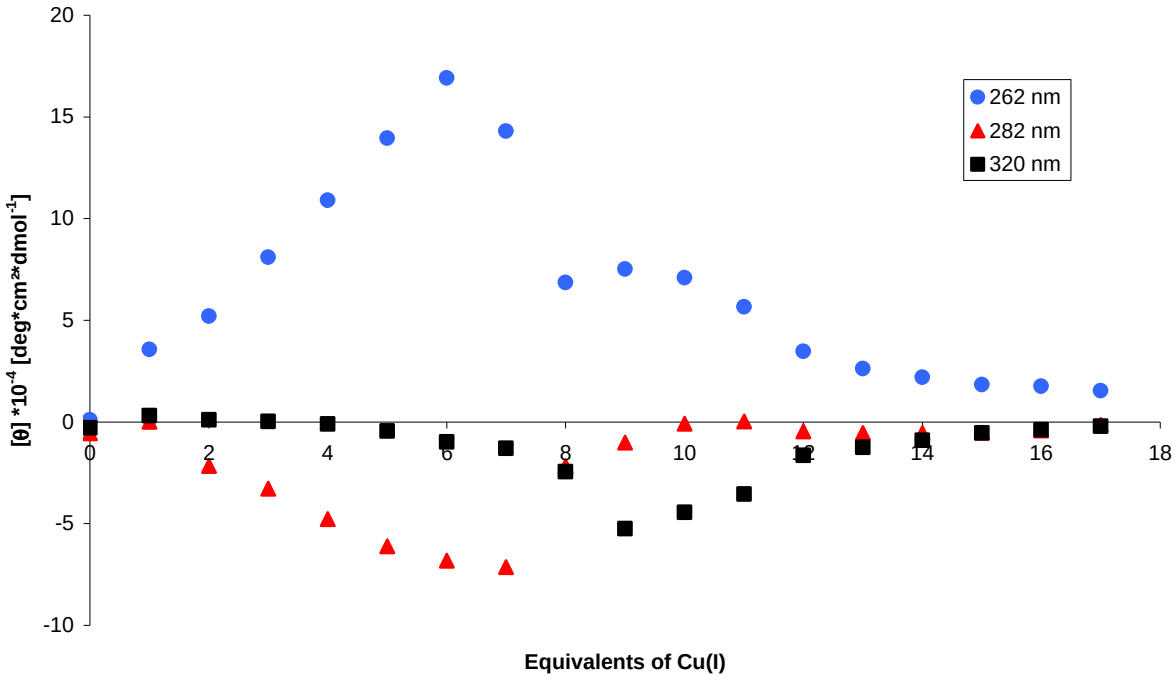

Figure 48: Plot of molar ellipticities at different wavelengths against Cu(I) equivalents added to Zn_5MT1.

Figure 48 clearly indicates the presence of two different species formed during the replacement of Zn(II) by Cu(I): The first one at 6 equivalents of Cu(I), as evident by the maximum value for the Cys → Cu(I) LMCT transition at 262 nm, and the second one manifests at 9 equivalents of Cu(I) by showing a maximum of the electronically weak but pronounced CD signals of the CC transitions at 320 nm.

7.2.13 Addition of Hg(II) to Zn_5MT1 at pH 7.5

Unlike reactions of Cd(II) with cicMT1, which are completed basically immediately after addition of Cd(II) to the protein solution, reactions between Hg(II) and MT1 need approximately 20 min at room temperature until a stable UV spectrum is reached. Therefore each spectrum of a (Hg(II) titration) reported in this thesis was recorded after giving the reaction sufficient time to reach a thermodynamic equilibrium. Figure 49 shows the titration of Zn_5MT1 with molar equivalents of Hg(II). These spectra reveal the more complex coordination chemistry of Hg(II) with thiolate ligands. The spectrum is dominated by band at 254 nm and the S → Hg LMCT band at 303 nm together forming a long tailing shoulder.

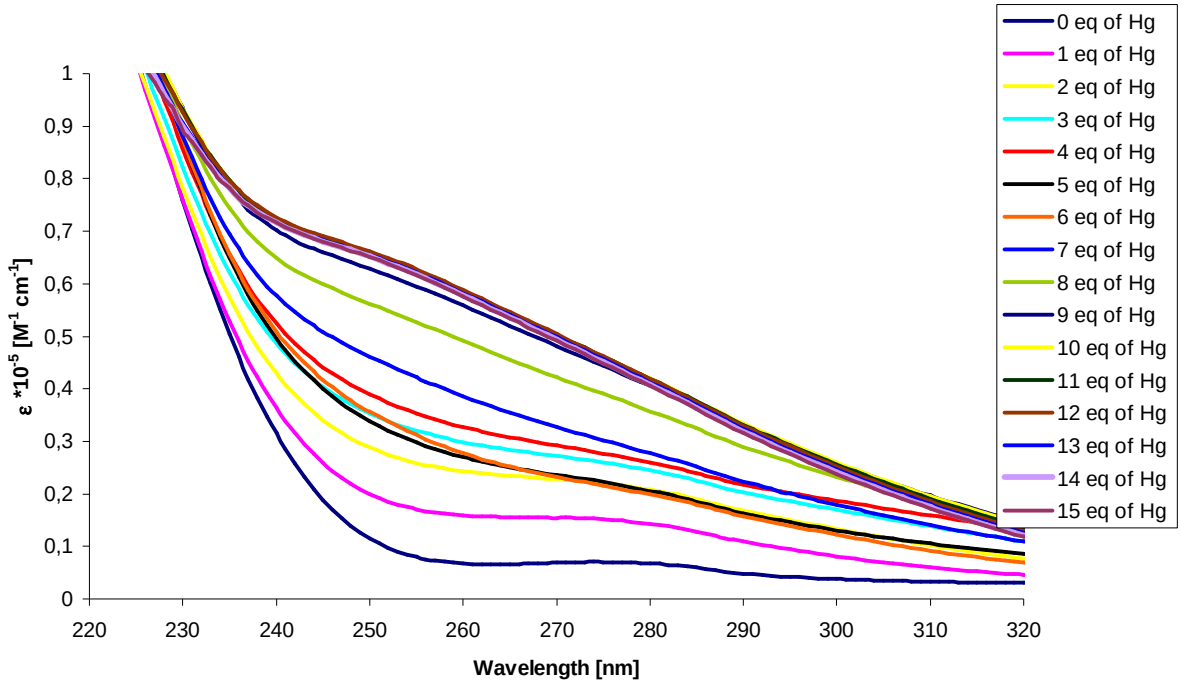

Figure 49: Electronic spectra of the incremental substitution of Zn(II) by Hg(II) in MT1 at pH 7.5.

The spectra can be divided in into 3 different parts: from 0-4, 5-6 and 7 or more equivalents of Hg(II). This behavior is very well illustrated in Figure 50. Up to 4 equivalents a linear increase of the LMCT bands is observed followed by a decrease for equivalents 5 and 6. This spectral behavior (Figure 49) suggests that at a Hg:MT ratio > 4 the cluster structure "opens" and a new complex with a different coordination pattern begins to form until a maximum ratio of Hg:MT = 6. Further addition of Hg(II) results in drastic increase of the S→ Hg(II) LMCT bands up to the addition of 10 equivalents of Hg(II). Translation of the spectral behavior into Hg Cys coordination leads to the assumption, that Hg firstly is tetrahedral coordinated until 4 equivalents are added. Upon further addition of Hg and due to its high thiofilicity adoption of a linear geometry is enforced.

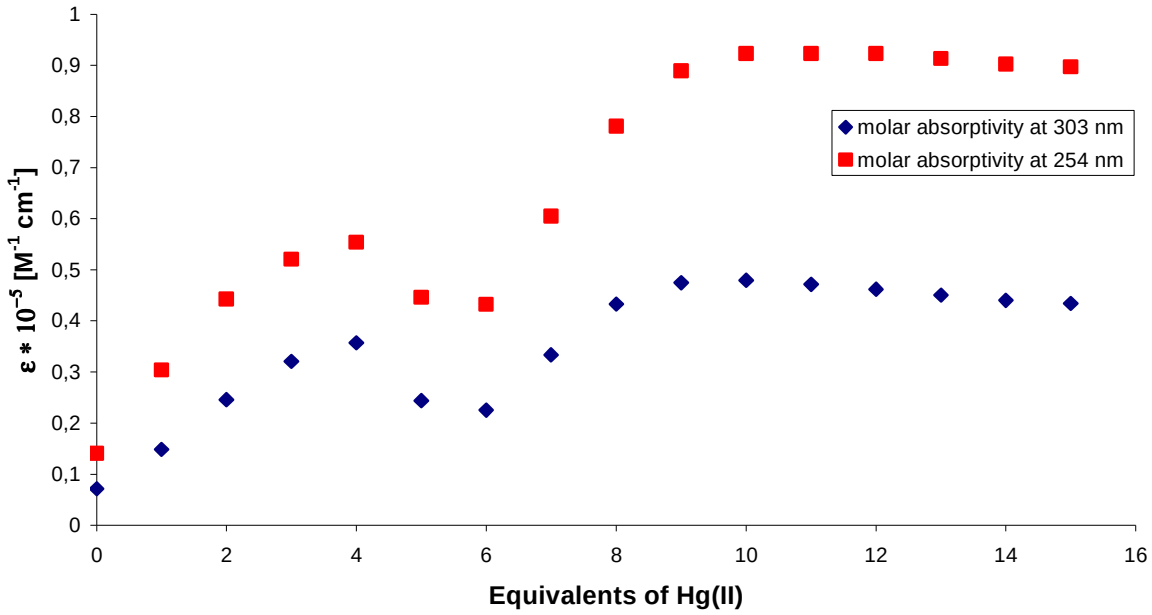

Figure 50: Plot of molar equivalents of Hg(II) against molar absorptivity at 254 and 303 nm.

Additional mercury ions do not further affect the UV spectrum and therefore indicate saturation of the protein with metal ions.

7.2.14 Addition of Hg(II) to apo-MT1 at pH 2

A completely different trend is observed when the Hg(II) titration is performed at pH 2. At this pH value Zn(II) ions are no longer able to compete with the protons for the binding sites and the protein can be considered to be practically devoid from the protein. Nevertheless, Hg(II) is able to bind to the protein underlining its extraordinary thiophilicity.

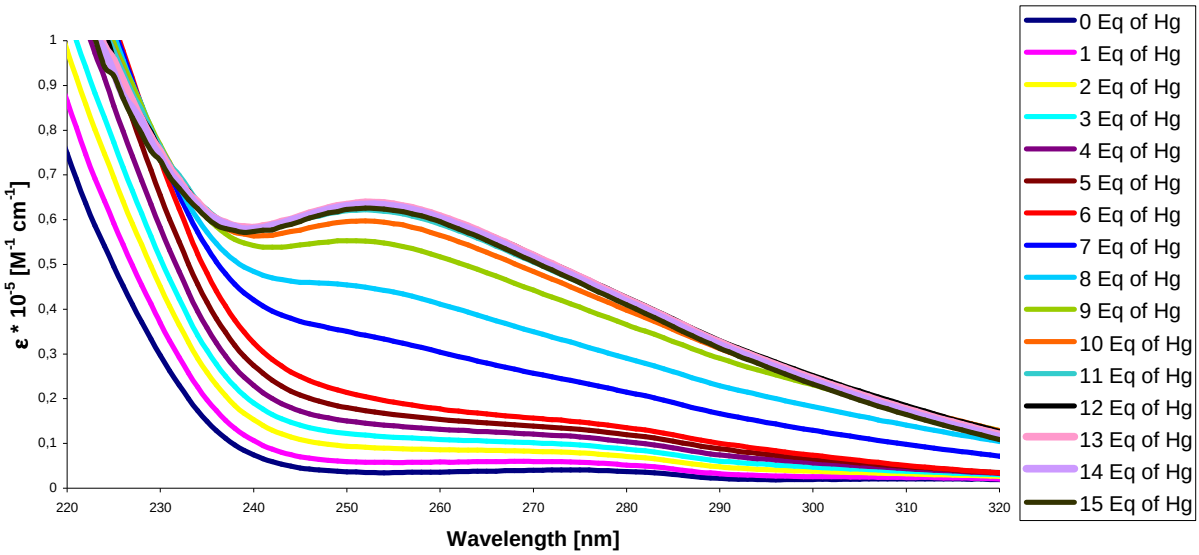

Figure 51: Electronic spectra of the incremental reconstitution of apo-MT1 with Hg(II) at pH 2.

The UV spectra given in Figure 51 show that Hg(II) binds to apo-MT1 in two different stages. From 0 to 6 equivalents a slight linear increase of the LMCT bands occurs. After binding of the 7th equivalent the slope increases steeply up to the addition of the 12th equivalent of Hg(II). A decrease as seen during the titration of Zn_5MT1 (Figure 49) upon addition of 5 and 6 equivalents of Hg(II) does not occur, indicating that under these experimental conditions no structural preset for Hg(II) coordination is given. This enables the mercury ions to coordinate in a linear fashion from the first equivalent on. The overall behavior is illustrated in the plot of molar equivalents of Hg(II) against the molar absorptivity at different wavelengths (Figure 52).

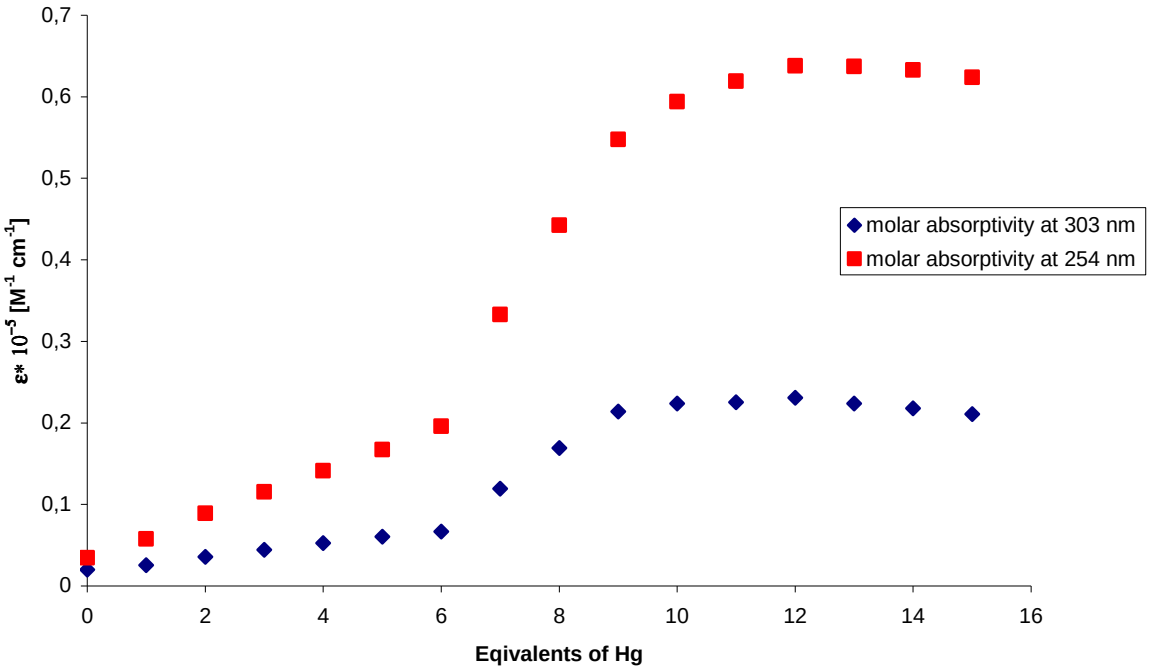

Figure 52: Plot of molar equivalents of Hg(II) against molar absorptivity of apo-MT1 at 254 and 303 nm (pH 2).

7.3 Secondary structure determination of Cd_5MT1

There is an appealing lack of structural information about plant MTs. In contrast to the vertebrate isoforms, neither X-ray nor NMR structural informations are available [2, 38, 177]. Consequently, hardly any information exists about the contribution of their Cys-rich domains and the spacer region to the final MT conformation. Attempts to propose a general fold for plant MTs of subfamilies p1–3, have led to two models: Formation of two separate metal-thiolate clusters with a dumbbell shaped structural arrangement similar to mammalian MTs [178, 179] or a hairpin model in which the two Cys-rich domains are connected by a single metal-thiolate cluster of unique structure [72, 74]. FTIR- and CD-spectroscopy are both powerful techniques to estimate the nature as well as the content of secondary structure elements formed by the protein backbone [141, 142, 180]. The peptide group, the structural repeat unit of proteins, gives up to 9 characteristic bands in the IR-spectrum named amide A, B, I, II ... VII [142, 181, 182]. The amide A (about 3500 cm^{-1}) and the amide B bands (about 3100 cm^{-1}) originate from a Fermi resonance between the first overtone of the amide II and the N-H stretching vibration. Amide I and amide II bands are the two most intense bands of the protein infrared spectrum. The amide I band (between 1600 and 1700 cm^{-1}) is mainly

associated with the C=O stretching vibration (70-85%) and is directly related to the backbone conformation. The amide II band results from the N-H bending (40-60%), the C-N stretching (18-40%) as well as the C-C (about 10%) stretching vibrations [142]. This band is conformational sensitive. Amide III (1300-1450 cm^{-1}) and IV (900-1000 cm^{-1}) are very complex bands resulting from a mixture of several coordinate displacements. The out-of-plane motions are reflected in the amide V, VI, and VII bands.

The CD spectrum of the amide region (180-240 nm) provides information about the backbone conformation and is therefore used to characterize the secondary structure of a protein and changes thereof. In particular, the α-helix displays a strong and characteristic negative ellipticity in the CD spectrum in the UV region [180]. The spectral contributions of the other secondary structural elements are less well defined, such as β-sheets and random coils [180].

7.3.1 Secondary structure determination of Cd_5MT1 using FTIR spectroscopy

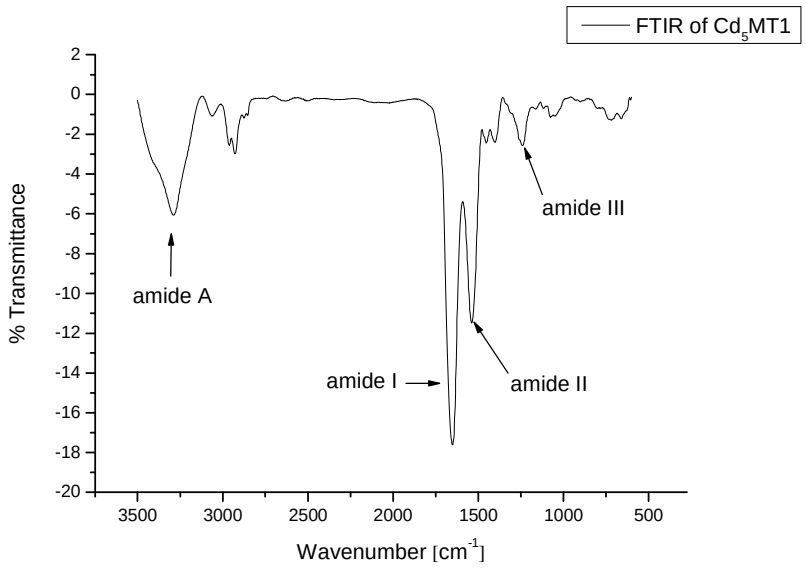

Figure 53: FTIR spectrum of Cd_5MT1 in KBr pellet.

As expected, the FTIR spectrum (Figure 53) is dominated by the different amide bands of the peptide backbone with the amide I band showing the largest transmittance. Also the amide bands A, I, II, and III become clearly visible. The maximum of the amide A band is centered at 3294 cm^{-1}, of the amide I band at 1649 cm^{-1} and of the amide band II at 1543 cm^{-1}. Only very limited secondary structural information can be obtained directly from the original FTIR

spectrum shown in Figure 53. Detailed structure assignment is mainly performed by deconvolution and gaussian fitting of the amide I band [142, 143] (Figure 54).

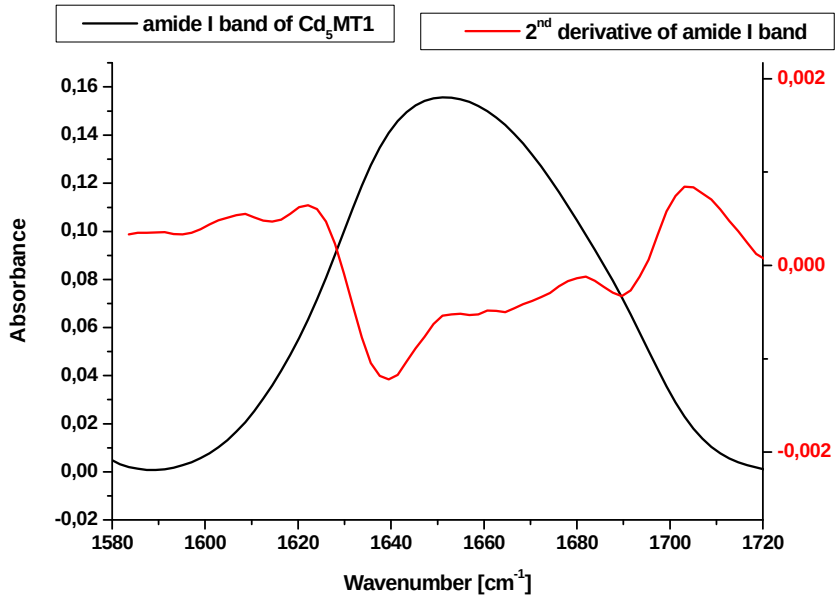

Figure 54: Plot of the truncated, baseline corrected FTIR spectrum of Cd_5MT1 depicted in Figure 53 showing the amide I band and its second derivative. Calculations were performed with Origin®.

First, the full range FTIR spectrum has to be truncated to show only the amide band I. Apodization by a Happ Genzel function [142] to smooth the discontinuities at the beginning and end of the spectrum results in a protein confirm spectrum [142]. Fourier self-deconvolution was performed with an enhancement factor of 2.5 and a half bandwidth of 20 cm^{-1}. The second derivative of the deconvoluted amide I band was then used to assign the contributing overlapping vibrations [140].

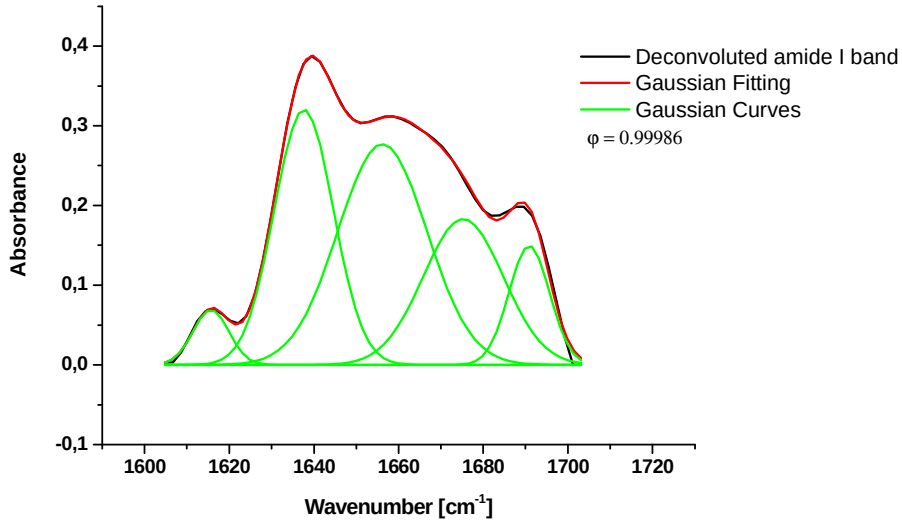

Figure 55: Deconvoluted amide I band of Cd_5MT1 and gaussian fitting to the number of components seen in the second derivative (Figure 54). Fitting performed with Origin®

Figure 55 shows the deconvoluted amide I band of Cd_5MT1. A gaussian fitting method based on a least square fit revealed the contribution of five major vibrations, which where assigned according to published procedures [140, 142].

Integration of each gaussian peak allows determining its quantitative contribution to the total amide I absorbance. The results for Cd_5MT1 are summarized in Table 6: Position, % area and secondary structural assignment of the five gaussian peaks used to fit the deconvoluted amide I band of Cd_5MT1 as depicted in Figure 55. It has been reported that KBr/protein mixtures show only slight differences compared to aqueous solutions [183, 184].

Table 6: Position, % area and secondary structural assignment of the five gaussian peaks used to fit the deconvoluted amide I band of Cd_5MT1 as depicted in Figure 55.

Peak [cm^{-1}]	% Area	Secondary structure [140, 142]
1616	3.7	aggregated strands
1638	28.4	β-sheets
1656	36.9	random coil
1675	21.9	β-turns
1691	9.1	β-turns

As can be seen from the data in Table 6 random coil and β-turn regions dominate the secondary structure of the protein. This is a typical property of metallothioneins as the

formation of the metal-thiolate cluster is dominant over the formation of regular secondary structural elements such as β-sheets and α-helices, forcing the surrounding amino acids to concede the steric strains [162, 185]. A β-sheet content of 28.4 % is outstanding for metallothioneins and has never been reported before. According to secondary structure predictions done by Jnet for *C. arietinum* MT1 these β-sheets are formed by the linker region between the Cys-rich domains [186].

7.3.2 Secondary structure determination of apo-MT1 using FTIR spectroscopy

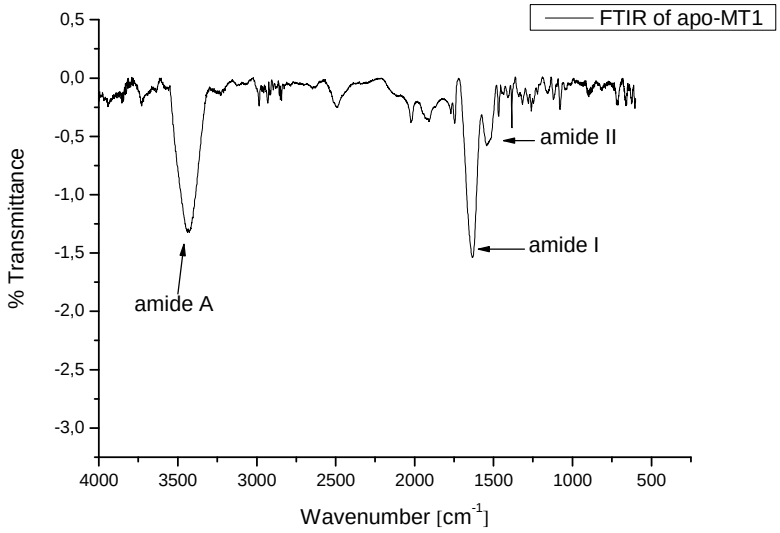

Figure 56: FTIR spectrum of apo-MT1 measured in KBr pellet.

The apo-form of MT1 shows a slightly different FTIR spectrum compared to Cd_5MT1 (Figure 53). It is dominated by the amide I band as well, but additionally shows a very strong amide A band centered at 3437 cm^{-1}. The amide A band does not depend on the backbone conformation but is very sensitive to the strength of hydrogen bonding [181]. An increased ratio of transmittance for amide A band compared to amide I band is a typical indication for a protein in the denatured state [187]. The amide band I centered at 1632 cm^{-1} shows the largest transmittance, being typical for any protein in the native or denaturated state [187]. The amide band II at 1539 cm^{-1} is less pronounced than in the cadmium form. A less pronounced amide band II has been reported for several apo-metalloproteins [188-190], and is seen as an indication for metal depletetion in proteins [141].

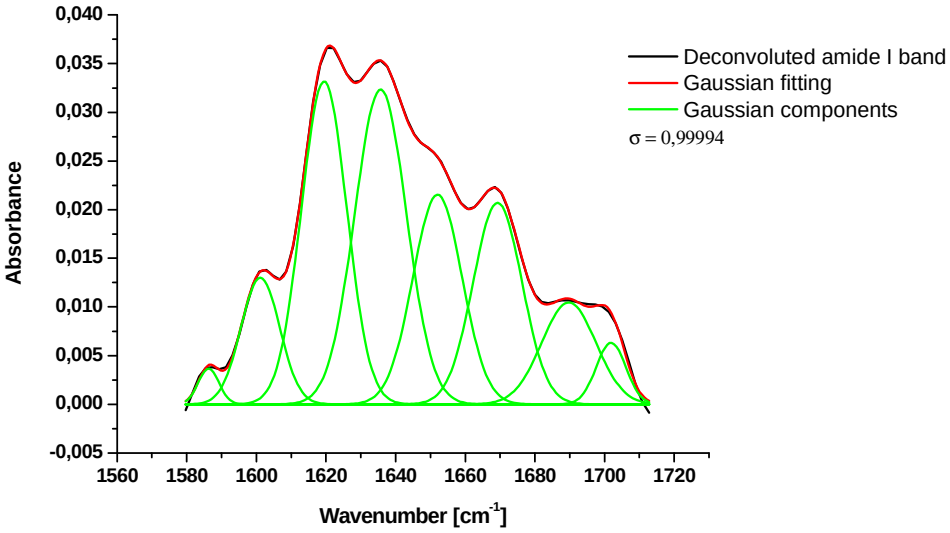

Figure 57: Deconvoluted amide I band of apo-MT1 and gaussian fitting to 8 components.

The FTIR spectrum (Figure 56) was again truncated to the amide I band and Fourier self-deconvolution was performed with an enhancement factor of 2.7 and a half bandwidth of 20 cm^{-1}. After apodization, Gaussian fitting according to known procedures leads to eight components, which were assigned to their corresponding secondary structural elements [140, 187], as summarized in Table 7.

Table 7: Position, % area and secondary structural assignment of the five gaussian peaks used to fit the deconvoluted amide I band of apo-MT1 as depicted in Figure 57: Deconvoluted amide I band of apo-MT1 and gaussian fitting to 8

Peak [cm^{-1}]	% Area	Secondary structure [140, 142]
1586	1.2	Not assigned
1601	7.7	aggregated strands
1619	22.9	aggregated strands
1635	25.4	□-sheets
1652	16.1	□-helix
1669	15.4	random coil
1689	8.6	turns
1701	2.8	Not assigned

Interestingly, the amount of β-sheets found in the apo-form is remarkably similar to the one found for Cd_5MT1. This is in accordance with calculations done for mammalian apo-metallothioneins [126], showing that the apo-form still retains a significant amount of secondary structural elements. This indicates that the formation of β-sheets is not depended on the formation of the metal-thiolate cluster, underlining the secondary structure prediction

performed with the Jnet sever, which showed that the β-sheets are formed by the residues of the linker region. The amount of random coil elements has decreased, most likely due to the absence of the metal cluster, which acts as a structural template for the MT. The appearance of α-helical structural elements might be due to the same reasons. The loss of the structural preset through the metal-thiolate cluster enables the amino acids to adopt the energetically most favorable structure, which might in some parts be α-helical.

7.3.3 Determination of secondary structural elements in Cd_5MT1 by ATR-FTIR spectroscopy in aqueous solutions.

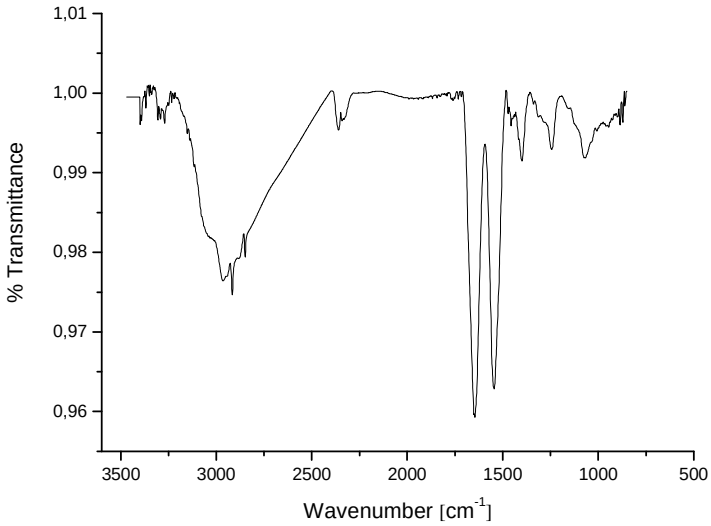

Figure 58: FTIR-ATR spectrum of Cd_5MT1 in aqueous solution.

Since differences (e.g. wavenumber shifs) of FTIR spectra in the solid state compared to the solution state are known [142, 184] e.g. for lysozyme a solution FTIR was performed for Cd_5MT1 to confirm the solid state data obtained in a KBr pellet. Figure 58 shows the attenuated total reflection (ATR)-FTIR spectrum of a 2 mM aqueous solution of Cd_5MT1. The amide A band appears at 2974 cm^{-1}, the amide I band is centered at 1644 cm^{-1} and the amide II band at 1545 cm^{-1}. The amide band A is shifted to higher energy compared to solid-state data. Moreover, ATR spectra of proteins in H_2O are not directly comparable to transmission spectra due to the anomalous dispersion effect [191], requiring cautious comparison between the two methods. However, since the amide A band is not used for secondary structure analysis, changes do not effect the overall results. Similar behavior of shifts for amide A, I, II bands has been reported for lysozyme [184]. The amide I and II bands

of MT1 are centered remarkably close to the values found with the KBr pellets, indicating that the effects on the secondary structure in the solid state vary only slightly from the situation in solution.

Table 8: Secondary structure content of Cd_5MT1 measured by aqueous ATR-FTIR and evaluated with OPUS® software.

Secondary structure	Content (%)
α-helix	7.6
β-sheet	27.4
random coil/ turns	65

The content of secondary structural elements listed in Table 8 was calculated with the OPUS® software directly. Results compare very well with values obtained for Cd_5MT1 measured in KBr pellets. The appearance of α-helical structures calculated by the OPUS® software, is a direct consequence of the algorithm used, which is based on "normal" proteins, which do not show any or only little conformational influence of a metal ion bound. However, MTs are dominated by the metal-thiolate cluster leading to exceptional tertiary structures, being difficult to calculate by standard algorithms [162].

7.3.4 Secondary structure determination of Cd_5MT1 by CD spectroscopy

CD bands of proteins appear mainly in the far-UV or amide region (170-250 nm), dominated by contributions of the peptide bonds. Bonds in this region are able to provide informations on the secondary structure of the protein [180]. In metalloproteins this region might be superimposed by LMCT bands depending on the metal ion present, resulting in potentially inaccurate results [162]. In an α-helical protein, a negative band near 228 nm is observed due to the strong hydrogen-bonding environment of this conformation [180]. This transition is relatively independent of the length of the helix. The CD spectra of β-sheet containing proteins display a negative band near 216 nm, a positive band between 195 and 200 nm and another negative band near 175 nm. However, the position and magnitude of these bands is variable, resulting in less accurate predictions for β-structures than for α-helices by CD [192]. In order to get optimal results only buffer or excipients without absorption in the UV (190-240 nm) should be used. Chloride salts must be strictly avoided as they absorb in the far UV region [192].

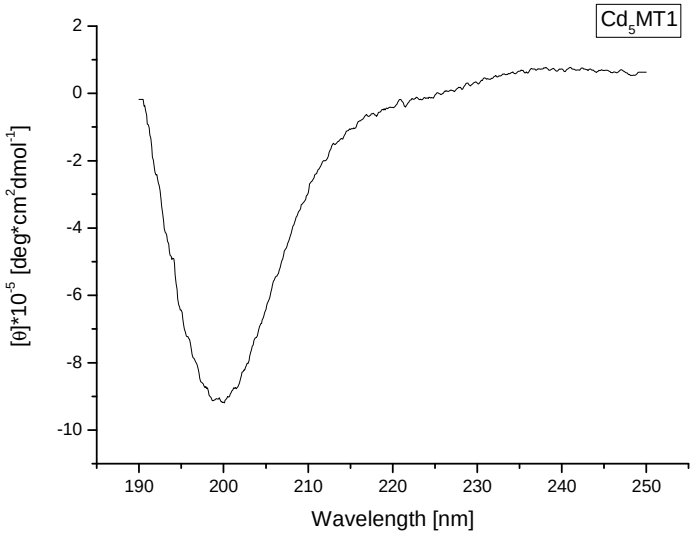

Figure 59: CD spectrum of 1 µM Cd_5MT1 in 3 mM phosphate buffer pH 7.5.

The CD spectrum of Cd_5MT1 (Figure 59) shows only a minimum at 200 nm and thus the clear absence of α-helical elements. A minimum being located around 200 nm indicates a random coil dominated structure [180]. To calculate the secondary structure content the molar ellipticity was normalized to the amount of amino acids by dividing the molar ellipticity with the number of amino acids of MT1 and processed using the k2D server [193-195].

Table 9: Secondary structure content of Cd_5MT1 calculated with the k2D server from normalized CD-spectral data.

Secondary structure	Computed values [%]
α-helix	10
β-sheet	32
random coil	58

The data obtained from the CD measurement correlate well with values obtained from FTIR studies. Given the uncertainties evaluating correct amounts of β-sheets by CD [192], the values become even more satisfactory. However, the amount of α-helical elements has to be considered with caution, since calculations are done based on non-metalloproteins, and thus without a metal-thiolate cluster dominated tertiary structure.

8 Discussion

8.1 MT1 pH titration

UV spectra confirm that Zn(II) and Cd(II) are bound to the thiolate groups of cysteine residues, as indicated by the characteristic LMCT bands. The effects of progressive acidification differ from the well known UV spectra of mammalian Cd_7MT [155] or the plant metallothionein E_c-1 from *T. aestivum* [73]. In contrast, pH titrations of Zn_5MT1 (Figure 12) and Cd_5MT1 (Figure 15) closer resemble spectra reported for plant MT3 from *M. aicuminata* [137] and also show similarity to spectra reported for the Cd-MT2 from the earthworm *Lumbricus rubellus* [196]. However, a plateau of ε_{250}at pH values above 7, as described in E_c-1 from *T. aestivum* [73] or MT3 from *M. acuminata* [137] could not be observed. Instead, a continuous decrease of the thiolate-metal LMCT band is observed from the start value of 8.5 on (Figure 16 and Figure 19). The continuous pH dependent decrease of the sulfur-zinc band could also indicate a conformationally strained cluster, where, on a speculative basis, zinc ions could be released easily due to small local pH changes in the cell. Again, this could point to a possible function of MT1 in *in vivo* zinc delivery [2]. However, the possibility of just one binding site with a lower affinity cannot be neglected. The steady decrease of the LMCT band is also observed in the pH titration of Cd_5MT1, but due to the higher affinity of Cd(II) to thiolate groups the decrease of the according LMCT band is slower and stretched over a longer pH range. Maybe also the larger size of the Cd(II) ion compared to Zn(II) leads also to a conformationally less strained cluster, explaining the slower absorption decrease.

In both cases, Zn- and Cd-forms, the slope of the curve at the second pK_a is much steeper than at the first one suggesting an overlay of several individual apparent pK_a values of very similar dimensions. Fitting multiple pK_a curves could show this behavior (Figure 13 and Figure 16). Consequently, addition of multiple protons, and release of multiple metal ions seem to be governed by a certain amount of cooperativity around the apparent pK_a. The two-steps behavior could be a distinct sign for the breakup of the proposed $M(II)_5Cys_{12}$ cluster after depletion of one metal ion into two more or less identical clusters. This would match very well with the cysteine residues distribution pattern of six cysteines at the C- and N-terminus, respectively. Proteolytic digestion followed by a size exclusion chromatography (or dynamic light scattering (DLS) measurements) at two different pH values should then show one or two

clusters. The general behavior of shifted pK_a values comparing zinc- and cadmium-forms by approximately one pH unit is typical for Zn-S and Cd-S cluster [73, 137].

Interestingly, the half-dissociation value of 3.9 for Cd_5MT1 is almost identical to the one from *P. sativum* MT1 of 3.95 [85], and similar to values for the plant MT2 from *Fucus vesiculosus* of 4.1 [197] and MT3 from *M. acuminata* of 4.2 [137], but differs clearly from values for equine MT1 of 3.0 [85] and wheat E_c-1 3.33 [73]. These values show that cadmium binding in plant MT1 is weaker than in the mammalian isoforms. On a speculative basis this could implement that the plant MT1 species are not primarily functioning in cadmium detoxification in plants, unlike PCs [33]. However, MT1 knockout mutants of *A. thaliana* did indicate an involvement in cadmium detoxification [84].

CicZn_5MT1, has a half-dissociation value of 4.9 which is identical to banana MT3 (4.9) [137], deviates slightly from pea MT1 with 5.25 [85] and differs clearly from equine MT 4.6 and wheat E_c-1 4.25. These data show that release of zinc from plant MT1s is easier facilitated than from plant MTs of the pec subfamily, underlining their different potential functions in nature. Nevertheless, pec MTs are believed to be involved in Zn(II) distribution [48], but Zn(II) depletion *in vivo* is facilitated through redox control [53, 198].

8.2 Metal ion substitution titrations

Recombinantly produced MT1 from *C. arietinum*, has been characterized for the first time. From its homology to the absorption spectra of tetrahedral halide complexes of Cd(II) it has been previously inferred that the characteristic and intense absorption shoulder of Cd-MT forms near 250 nm is a manifestation of tetrahedral coordination [169]. The spectrophotometric titration experiments with Cd(II) performed in this thesis indicate that the overall features of tetrahedral coordination are maintained at all stages of reconstitution of the apo-protein. However, the distinct red shift, developing upon addition of more than 2 equivalents of Cd(II) to the apo-form seen in CD spectra (Figure 27) does not find a direct correlation in the absorption spectra (Figure 26) where a constant small red shift is observed. Nonetheless, despite the differences in the intensity mechanisms between the absorption, CD and MCD techniques, in general each technique detects bands originating from the same LMCT states, so that the band center and width should coincide in spectra recorded with the three techniques.

As the Cys residues of the primary amino acid sequence of plant MTs from subfamily p1 are found exclusively in the N-and C-terminal regions separated by a 42 amino acid long Cys-free

linker, it was initially expected, that *C. arietinum* MT1 forms two separate metal-thiolate clusters with $M(II)_2Cys_6$ stoichiometry each. This hypothesis correlates very well with results obtained from experiments leading to a $M(II)_4$MT1 form (Figure 32, Figure 33). Such $M(II)_2Cys_6$ clusters are known from inorganic coordination compounds [114] and from transcriptional activators proteins [199, 200]. Their existence was recently also proposed for the first time to exist in the wheat E_c-1 [73]. Additionally, a ZnS_2Cys_4 cluster was speculated to be present in the plant MT2 from *Quercus suber* (Corkoak) [201]. However, in a recent the linker in plant MTs has been proposed to be crucial for the direct interaction of the two cysteine rich domains rather then facilitating their separation [72]. Further, as MT1 has been shown to be able to coordinate up to five divalent metal ions, assumption of two separated M_2Cys_6 clusters is certainly not feasible. To explain the extraordinary ability to bind up to 5 equivalents of Zn(II) or Cd(II) via only 12 cysteine residues a new cluster for metallothioneins is proposed in this work (Figure 22). Up to now a Cd_5Cys_{12} cluster has not been described for any metalloprotein and is also not known from inorganic coordination compounds. Nonetheless, an inorganic structural analogs in form of tetrahedral coordinated mercury(II) ions in the $[Hg_5(SePh)_{12}]^{2-}$ complex [202] is known and underlines the possible existence of such a coordination pattern. The larger atomic radii of Hg and Se compared to those of Cd and S might explain, why an inorganic Cd_5S_{12} cluster has not been reported so far. This could underline that formation of this cluster by its self might not be favorable, indicating the need of a three-dimensional scaffold as given by the peptide backbone of MT1 from *C. arietinum*. Furthermore, although proteolytic cleavage of the linker region for a plant MT1 from the garden pea [74, 85] and an insect MT from *Orchesella cincta* (springtail) [203] has been shown, the separated domains still seemed to be connected by a common cluster. Thus also the existence of one homogenous cluster seems to be possible in *C. arietinum* MT1. Evidence to underline the existence of the M_5Cys_{12} cluster is derived from absorption spectra of the substitution of zinc by cadmium ions (Figure 20, Figure 23) as well as from the incremental reconstitution experiment (Figure 26, Figure 32). The molar absorption coefficient for Cd_5MT1 is 5.8 $*10^4$ M^{-1} cm^{-1} and for Cd_4MT1 5.2 $*10^4$ M^{-1} cm^{-1}, respectively. These data clearly indicate that the fifth equivalent of cadmium is coordinated via bridging thiolate groups. Furthermore, the molar absorption coefficient can be taken as a direct measure of the number of Cys ligands engaged in Cd(II) binding to the metalloprotein. Thus, from the average absorbance of one Cd-bound Cys at 250 nm of 0.5 $*10^4$ M^{-1} cm^{-1} taken from the spectra of structurally characterized mammalian Cd_7MT2 [161] and sea urchin Cd_7MTA [204] it follows that in fully Cd(II) occupied *C. arietinum* MT1 (5.8 $*10^4$ M^{-1} cm^{-1}) all 12

cysteine side chains are involved in the coordination of the 5 Cd(II) ions. However, a contribution of the His residue to the cluster structure at this point cannot be excluded. Additionally, Co(II) titrations of apo-MT1 (see chapter 7.2.10) did not give any indication in this way.

Interestingly, the metal ion content of the recombinantly obtained protein (4 or 5 equivalents per MT1) had no influence on the metal ion binding capacities of the respective apo-MT1. The reason for these different binding capacities might be found in the procedure required for the apo-protein preparation and reconstitution. To obtain metal ion depleted apo-MT1 a purification steps at low pH is necessary, leading to a complete denaturation of the protein (see Experimental section) including the loss of the majority of secondary structure elements. Since formation of the M_5Cys_{12} cluster requires close proximity of the C- and N-terminal Cys-rich regions and the linker region was found to features a significant amount of secondary structural elements, a proper reconstitution of these elements by an instant raise of the pH from 2 to 7.5 might not always be given. Moreover, metal ion coordination only occurs at pH values above 4 and therefore cannot facilitate the formation of a single cluster by itsself, since secondary structural elements such as α helices and β-sheets are usually formed at pH values between 2 and 3 [205]. This means that protein folding occurs before metal ion clustering and therefore provides a structural manifold for metal ion clustering.

Apart from the UV spectra also the CD data presented in this thesis (Figure 27 and Figure 33) indicate that MT1 can bind a maximum of 5 equivalents of Cd(II), as evident from the formation of a shoulder derived from a positive transition around 220 nm usually seen during cluster formation of Cd(II) in metallothioneins without significant secondary structure elements [151, 155, 156]. In *C. arietinum* MT1 this transition is clearly dominated by the negative ellipticity caused by random coil, α-helix and β-sheet structures and therefore not seen in the Cd spectra. Difference CD spectra obtained by subtraction of the apo-form spectrum from all other CD spectra are not applicable for plant MT1, as valid for mammalian MTs. These are only justified in the absence of secondary structural elements, since their spectral overlap will result in false and non comparable difference spectra [152, 159, 162]. The maximum binding of 5 mol equivalent divalent d^{10} metal ions seen in the UV spectra is not reflected in the CD measurements. The radical change in the CD profile that sets in when bridging thiolate ligands make their appearance has no easily recognizable correlate in the absorption spectrum. Moreover, these changes are difficult to explain on the basis of the configurational asymmetry of the cysteine ligands alone judging from the preservation of the absorption profile neither the coordination geometry nor the physical character of the Cd-

thiolate transitions is altered clearly with additionally Cd(II) incorporation. This kind of change must be induced by the overall cluster geometry and induce a kind of new coordinational dissymmetry [158]. Such new symmetry can be either generated through the greater framework of the cluster or through chromophoric ligands within the coordination sphere of a single metal ion [159]. Similar behavior has been described for snail MT [156]
Interestingly, the negative band below 240 nm featuring secondary structure information of the backbone is shifted to higher energies with increasing equivalents of Cd(II). Beyond 3 equivalents bound, a new CD profile emerges resulting in a truncated biphasic signal usually found for cadmium containing MTs [152, 156]. Furthermore the maximum of 5 equivalents seen in the absorption spectra of reconstituted apo-MT1 does not show in the CD, instead upon addition of 3 equivalents a red shift occurs, clearly indicating clustering, due to stronger polarization at the bridging sulfurs [158].

$$I \sim \left[A_1 \left(\frac{-\partial f(E)}{\partial E} \right) + \left(B_0 + \frac{C_0}{kT} \right) f(E) \right]$$

Equation 2: Composition of the total MCD intensity [163]

Compared to the CD data (Figure 27), the MCD data (Figure 30) are less detailed but underline the existence of the postulated M_5Cys_{12} cluster. The characteristic positive Faraday *A*-term signals (Equation 2) are reflections of the relatively high symmetry of the responsible chromophores. *A*-terms are most distinctive in room temperature spectra because the derivate-shaped band is usually much more intense than *B*- or *C*-term. The derivative-shaped feature of *A* terms is observed when the ground state is nondegenerate and the exited state is orbitally degenerated. The red shift can be attributed to a decrease in distortion of the metal complexes when they are joined to clusters [206].

8.3 Co(II) titrations

The Co(II) titration followed by UV-Vis-spectroscopy (Figure 37 and Figure 39) reveals interesting properties of cicMT1 and are consistent with results obtained from MCD measurements of the reconstitution of apo-MT1 with Cd(II) (Figure 30). Theoretically, enough terminal thiolate residues in apo-cicMT1 are available to accommodate at least 2 if not 3 nonclustered Co(II) ions. However, both spectral parts of the titration show the unexpected cluster formation from the 2nd added equivalent of divalent metal ion on.

Clustering can be unambiguously followed using the sensitivity of the S → Co(II) LMCT bands as well as the *d-d* transitions to the participation of bridging thiolates. This behavior provides instant information of the geometrical surrounding of the coordinated Co(II) ions [169]. The suitability of Co(II) as a paramagnetic probe for Zn(II) containing proteins has been shown [166, 168] and discussed before [149]. Thus, it is important to note that Co(II) generally shows no cooperative behavior and binds to terminal thiolate ligands first [149, 168, 169]. It is thus somewhat contradictory, that the Co(II) titration experiment of cicMT1 reveals the presence of bridging thiolates already from the second equivalent on and that the cluster formation process is only completed after complete saturation of the protein with 5 metal ions is achieved. The later underlines the findings of Domenech et al. [72], that the two Cys rich domains are not independent but mutually dependent when binding to Zn(II). Additionally, *d-d* transitions of Co(II) titrations of reveal no clear indication for His binding to the metal ions as seen for E_c-1. In the case of wheat E_c-1 an increased absorption of the band at 592 nm compared to the one at 749 was observed. Inversion of the two absorption maxima of the highest *d-d* transitions would be indicative for His contribution to the overall cluster [207-209]. Further indication that the coordination of divalent metal ions in cicMT1 solely occurs via thiolate groups, is given by the Cys molar absorption coefficient of $1.2*10^4$ M^{-1} cm^{-1} at 250 nm for Cd_5MT1, which compares well to values for the His-devoid mammalian MTs of $1.1*10^4$ M^{-1} cm^{-1}[154].

8.4 Cu(I) titrations

Copper is an essential element to life, necessary for almost all living organisms. In plants it shows a huge variety of possible functions [14], e. g. a major role in electron transfer reactions [149] and enzymatic reactions such as present in the superoxide dismutase [210].
Both, UV and CD spectra of the fractional addition of Cu(I) to the apo-form (Figure 41 and Figure 43) as well as to the Zn_5-form (Figure 45 and Figure 47) show a maximum of the Cys → Cu(I) LMCT band at 6 equivalents of Cu(I). This finding underlines that there is a defined structure existing at this point. The maxima observed in the two respective UV spectra even have the same value of $\varepsilon_{262} \approx 45000$ M^{-1} cm^{-1}, regardless whether the 6 Cu(I) ions were added to apo- or Zn_5-form. Thus the molar absorptivity per cysteine residue amounts to approximately 3950 M^{-1} cm^{-1} which is similar to values reported for human MT3 [115]. This is also an indication that all 12 cysteine residues of cicMT1 are involved in Cu(I) binding. However, a certain level of unsaturation remains within the protein, which is evident by

emerging CC transitions upon further addition of Cu(I) ions. Even more structural information can be obtained by CD spectroscopy. Based on previous studies on MTs [131, 172] it has been proposed, that the strongest CD intensity is observed for metal-thiolate stoichiometries which result in stable metal-thiolate structures where all metal binding sites are filled, and in which the metal coordination geometry is the same throughout the structure [127]. While bands in the high-energy region (below 280 nm) originate predominantly from Cys → Cu(I) LMCT transitions, the features in the low-energy region (300-350 nm) with very weak molar absorptivities, but rather strong CD bands, originate from formally spin forbidden 3d→4s CC transitions brought about by Cu(I)-Cu(I) interactions in polynuclear Cu(I) complexes [115]. It is proposed that these bands indicate the transition of the Cu(I) coordination mode from trigonal to linear as the protein accommodates the additional Cu(I) ions to yield a second stable three dimensional structure [127]. With the addition of the 10^{th} equivalent of Cu(I) to the Zn-form also this second structure collapses. This behavior is significantly different to the one observed during titration of the apo-form where no intensification of CC transitions is detected above 6 molar equivalents of Cu(I). Based on the titration experiments done in this thesis, defined structures at 6 and 8 equivalents for apo-MT1 and 9 equivalents of Cu(I) for the Zn_5-MT1 form have been observed, respectively. Different binding abilities of Cu(I) to MTs depending on the starting material (Zn(II)-or apo-form) have been already reported [171, 211] suggesting that Zn(II) binding is needed as a structural preset of the protein backbone [121]. Furthermore, native Zn_7MT expressed by mammals exposed to metal ions such as Cu(I) always yielded mixed metal clusters that contained Zn(II) ions [212, 213]. However, a preferred binding to one domain as demonstrated for mammalian MTs [71, 214, 215] is not seen for cicMT1 as evident from constant increase at the Cys → Cu(I) LMCT band (Figure 48) and the continuous decrease of the CD band at 280 nm.

The absorption (Figure 41 and Figure 45) and CD spectra (Figure 43 and Figure 47) show similar behavior to reported spectra of diverse MTs [115, 174, 211]. However, an additional positive band around 220 as shown for rabbit liver [127], yeast [128] and *N. crassa* MT [216] is not detected. One reason for this might be the masking of this band by the strong negative ellipticity of the secondary structural elements present in cicMT1 from (see chapter 7.3).

Even though a $Cu(I)_6Cys_{11}$ [127] or a $Cu(I)_7Cys_{10}$ [217] cluster has already been reported, the coordination of 6 Cu(I) to 12 Cys would be a completely new finding. One might also envision that the 6 Cu(I) ions are evenly distributed between the two cys-rich domains resulting into two $Cu(I)_3Cys_6$ clusters. Also such clusters would be inprecedented in the

literature. There is only reference to a $Cu(I)_4Cys_{6-7}$ cluster [174]. The only three dimensional structures available today for a copper containing MT is the solution structure from the fungus *N. crassa* showing a $Cu(I)_6Cys_7$ cluster [121] as well as the yeast $Cu(I)_7Cys_{10}$ [120] and $Cu(I)_8Cys_{10}$ cluster [122]. Based on the increase of the S → Cu(I) LMCT bands in the UV and CD spectra, all published Cu(I)-Cys clusters show larger Cu(I)/Cys ratios then found for MT1 from *C. arietinum*. Since molar absorptivity related to the Cys content reveals an involvement of all 12 Cys residues in Cu(I) coordination it is tempting to speculate that cicMT1 from *C. arietinum* features a unique cluster structure among MTs. A trinuclear Cu(I) compound in form of the $[(Cu_3(SCH_2CH_2S)_3]^{3-}$ complex has already been described [114]. Additionally, isobestic points give an indication, that the $Cu(I)_6Cys_{12}$ cluster is homogenous formed [127].

8.5 Hg(II) titrations

Hg(II) is known to activate the PC synthase in various different plant species [218, 219]. In mammalians Hg(II) is detoxified by MTs via cysteine complexation and sequestration [220]. Up to date, optical spectroscopy has been used to study mercury-binding properties of mammalian MTs, for which several Hg-MT stoichiometries (Hg_7-MT and Hg_{18}MT are the most frequent ones) have been reported [149].

The electronic spectra observed during the titration of the Zn-holo form (Figure 49) are comparable to spectra reported for rabbit liver MT [221]. The electronic absorption band for Hg-MT1 lies between values reported for Hg(II)-rubredoxin [222] and Hg_7MT [221] of 257 and 251 nm, respectively. Initially, Hg(II) replaces Zn(II), in tetrahedral coordination geometry by analogy work of Vasák et al. [151]. The drastic change in absorption upon addition of the 5th and 6th equivalent of Hg(II) resulting in a decrease of absorption has been interpreted as a change in coordination geometry from distorted tetrahedral to trigonal [221, 223]. The increase of the S → Hg(II) LMCT bands upon further Hg(II) addition is caused by linear coordinated Hg(II). This behavior has also been discribed as the "Zinc family paradoxon" [223]. Tetrahedral coordination for Zn(II) and Cd(II) is described simply assuming sp^3 hybridization of the empty *s* and *p* orbitals of the metal ions and expansion of the coordination sphere. The unusual linear coordination chemistry of Hg(II) has been attributed to a large 6s-6p orbital separation scheme favoring *s-p* linear hybrids over tetrahedral sp^3 hybrids [224].

Titration behavior of the apo-form at pH 2 is different from the Zn-form at pH 7.5, resulting in a slightly higher binding capacity of apo-MT1 towards Hg(II). This is in agreement with results obtained for mammalian MT [225]. Furthermore, the different absorption patterns for the apo- and Zn-forms indicate different coordination geometries of Hg(II) at equivalent Hg:MT1 stoichiometries. Thus, it can be concluded, that the presence of structural preorganisation, which can be influenced by the reaction conditions have a larger effect on the structural properties of Hg(II) binding than the stoichiometry of the Hg-MT species.

8.6 Secondary structure determination

FTIR and CD spectra of Cd_5MT1 and apo-MT1 indicate the presence of secondary structural elements. The high amount of almost 30% β-sheets is unusual for MTs. However, if one considers that structural information about MTs is predominantly focused on proteins being devoid of larger Cys-free amino acid stretches, the high β-sheet content of a plant MT from subfamily p1 becomes less surprising. Until now, only one publication is available dealing with the determination of secondary structural elements from plant MTs [201]. It shows that MT2 from *Q. suber* seems to contain even 55 or 58% of β-strands according to FTIR measurements of the Zn_5- or Cd_5-form, respectively. Computational studies based on the primary sequence of cicMT1 using the neuronal network prediction server Jnet [186] revealed that the structural elements are situated mainly in the Cys devoid linker region. The whole spacer region of MT1 constitutes to 55% of the primary structure and therefore is a good candidate to adopt a β-sheet fold, that would not be distorted by metal ion coordination, especially if one considers that β-strands are not self sustainable and need a parallel or anti-parallel strand or structure stabilization [182] in contrast to α-helical structures [226]. The small content of α-structures in MT1 only observed with ATR-FTIR and CD spectroscopy might be even an artefact, since the data sets, on which the general calculation procedures are based, do not include the unusual secondary structural arrangement of MTs [162]. On the other hand α-helical contents of 10 % in mammalian MT3 have been reported as well. However, this helix is located around the metal ion cluster and not in the Cys-devoid linker region [227]. β-turns accounting to 31% in Cd_5cicMT1 confirm the folding of the Cys-rich region around the metal ion cluster [201] and are in agreement with the amount amino acids in the primary sequence of MT1. Overall the distribution of secondary structural elements, especially β-turns and random coils, found in cicMT1 fit well to reported values for

prokaryotic and mammalian MTs of around 30%, respectively [177, 201, 227]. The ability of FTIR spectroscopy to detect small changes in protein structure introduced, for instance, by site-directed mutagenesis [228, 229] or by Ca(II) binding to apo-forms of Ca(II)-binding proteins [190] has been demonstrated. Moreover, using the vibrational bands of metal-coordinating COO^- groups (not affecting amide I band) in parvalbumin, differences in coordination of Ca(II), Mg(II) and Mn(II) have been shown [230]. Importantly, the FTIR analysis of both Fe- [231] and Cd-rubredoxin [232] are closely similar and fit reasonably well to the crystal structure of apo- rubredoxin [233]. This clearly showed that the amide I band region is not affected by the nature of the bound metal. Thus, FTIR is the method of choice for establishing isostructural metal ion replacement in metalloproteins [233].

The CD spectra (Figure 59) features its minimum at 200 nm. α-helical parts, which are dominant in CD spectra [180] and usually appear around 228 nm, are not obviously appearing for cicMT1. CD analysis confirms the overall secondary structure of Cd_5MT1 obtained by FTIR measurements, although LMCT contributions are overlapping with the amide backbone transitions and have been shown to give error prone results for mammalian MTs [162]. However, mammalian and prokaryotic MTs seldomly feature considerable amounts of secondary structural elements such as α-helices and β-sheets [162, 177, 185] unlike plant MTs [201]. The use of CD spectroscopy has clearly been shown not to be appropriate for secondary structural analysis of mammalian MTs [233]. In particular the presence of intense CD features between 210 and 250 nm for the Cys-Cd(II) chromophores and between 235 and 210 nm for the Cys-Zn(II) chromphore are well documented. The influence of such optically active chromophores to the overall CD signal will be much less significant in larger proteins, where the metal ion to protein ratio is significantly lower than for mammalian MTs. From CD spectra of cicMT1 (Figure 25) it becomes obvious that contributions of the amide backbone are dominant and therefore allow the evaluation of secondary structural elements for MT1. However, a minor contribution of LMCT bands in the range of 210 to 240 nm may not be neglected. The extraordinary agreement of FITR data with CD analysis of Cd_5MT1 confirms, that CD spectroscopic contributions of the protein backbone experience only neglectable interferences by thiolate –metal ion LMCT bands.

The apo-protein shows a β-sheet content of 25.4% and 16.1% α-helices. Since the apo-form lacks the structural preorganization of a metal-cluster, different secondary structural element contents could be expected. The Cys-rich domains in the apo-form are in principle able to form non-sequence specific secondary structures. This could explain the appearance of α-helical structures. However, due to the extraordinary sensitivity of the free cysteinyl groups to

oxidation, the formation of disulfide bonds during KBr pellet processing [184] is likely. In combination with lyophilization [184] this could explain the larger content of aggregated strands seen in the FTIR for apo-MT1 (Table 7) [142]. Nonetheless, the content of secondary structural elements in the apo- and holo-form remain remarkably similar. This behavior has been reported for mammalian MT2 and MT3 as well [227], indicating that structural preorganization *in vivo* might be required to ensure proper cellular functionality of cicMT1, like providing a frame where metal ion binding is directed to result in the final M_5MT1 form.

9 Literature

1. Callahan, D.L., Baker, A.J.M., Kolev, S.D., and Wedd, A.G., *Metal ion ligands in hyperaccumulating plants.* J. Biol. Inorg. Chem., 2006. **11**(1): p. 2-12.
2. Rauser, W.E., *Structure and function of metal chelators produced by plants - The case for organic acids, amino acids, phytin, and metallothioneins.* Cell Biochem. Biophys., 1999. **31**(1): p. 19-48.
3. Ernst, W.H.O., J.A.C., V., and Schat, H., *Metal tolerance in plants.* Acta. Bot. Neerl., 1992. **41**: p. 229-248.
4. Vanassche, F. and Clijsters, H., *Effects of metals on enzyme-activity in plants.* Plant Cell. Environ., 1990. **13**(3): p. 195-206.
5. Lane, T.W. and Morel, F.M., *A biological function for cadmium in marine diatoms.* Proc. Natl. Acad. Sci. USA, 2000. **97**(9): p. 4627-4631.
6. Küpper, H., Mijovilovich, A., Meyer-Klaucke, W., and Kroneck, P.M., *Tissue- and age-dependent differences in the complexation of cadmium and zinc in the cadmium/zinc hyperaccumulator Thlaspi caerulescens (Ganges ecotype) revealed by x-ray absorption spectroscopy.* Plant. Physiol., 2004. **134**(2): p. 748-757.
7. Nieboer, E. and Richardson, D.H.S., *The replacement of the non-descript term heavy-metals by a biologically and chemically significant classification of metal-ions.* Environ. Pollut. B, 1980. **1**(1): p. 3-26.
8. Laity, J.H. and Andrews, G.K., *Understanding the mechanisms of zinc-sensing by metal-response element binding transcription factor-1 (MTF-1).* Arch. Biochem. Biophys., 2007.
9. Guilfoyle, T., *Plant biology: sticking with auxin.* Nature, 2007. **446**(7136): p. 621-622.
10. Durzan, D.J., *Free amino acids as indicators of little leaf in zinc deficiency in the pistachio (Pistacia vera L. cultivar 'Kerman').* SCI HORTIC-AMSTERDAM, 1995. **60**(3): p. 221-233.
11. Yang, G., Inoue, A., Takasaki, H., Kaku, H., Akao, S., and Komatsu, S., *A proteomic approach to analyze auxin- and zinc-responsive protein in rice.* J. Proteome. Res., 2005. **4**(2): p. 456-463.
12. Dietz, K.-J., Baie, r.M., and Krämer, U., *Free radicals and reactive oxygen sepcies as mediators of heavy metal toxicity in plants*. Heavy metal stress in plants: from molecules to ecosystems., ed. Prasad, M. and Hagemeyer, J. 1999, Berlin: Springer-Verlag. 73-97.
13. Valko, M., Morris, H., and Cronin, M.T., *Metals, toxicity and oxidative stress.* Curr. Med. Chem., 2005. **12**(10): p. 1161-1208.
14. Grotz, N. and Guerinot, M.L., *Molecular aspects of Cu, Fe and Zn homeostasis in plants.* Biochim. Biophys. Acta, 2006. **1763**(7): p. 595-608.
15. Hirayama, T., Kieber, J.J., Hirayama, N., Kogan, M., Guzman, P., Nourizadeh, S., Alonso, J.M., Dailey, W.P., Dancis, A., and Ecker, J.R., *Responsive to antagonist1, a Menkes/Wilson disease-related copper transporter, is required for ethylene signaling in Arabidopsis.* Cell, 1999. **97**(3): p. 383-393.
16. Southron, J.L., Basu, U., and Taylor, G.J., *Complementation of Saccharomyces cerevisiae ccc2 mutant by a putative P1B-ATPase from Brassica napus supports a copper-transporting function.* FEBS Lett., 2004. **566**(1-3): p. 218-222.
17. Wagner, G.J., *Accumulation of cadmium in crop plants and its consequences to human health.* Adv. Agron., 1993. **51**: p. 173-212.
18. Reeves, P.G., Chaney, R.L., Simmons, R.W., and Cherian, M.G., *Metallothionein indiction is not involved in cadmium accumulation in the duodenum of mice and rats*

fed diets containing high-cadmium rice or sunflower kernels and a marginal supply of zinc, iron, and calcium. . J. Nutr., 2005. **135**(4): p. 966-966.
19. Hall, J.L., *Cellular mechanisms for heavy metal detoxification and tolerance.* J. Exp. Bot., 2002. **53**(366): p. 1-11.
20. Silver, S., *Bacterial resistances to toxic metal ions--a review.* Gene, 1996. **179**(1): p. 9-19.
21. Williams, L.E., Pittman, J.K., and Hall, J.L., *Emerging mechanisms for heavy metal transport in plants.* Biochim. Biophys. Acta, 2000. **1465**(1-2): p. 104-126.
22. Quartacci, M.F., Cosi, E., and Navari-Izzo, F., *Lipids and NADPH-dependent superoxide production in plasma membrane vesicles from roots of wheat grown under copper deficiency or excess.* J. Exp. Bot., 2001. **52**(354): p. 77-84.
23. Meharg, J.V., McGowan-Jordan, J., Charles, A., Parmelee, J.T., Cutaia, M.V., and Rounds, S., *Hydrogen peroxide stimulates sodium-potassium pump activity in cultured pulmonary arterial endothelial cells.* Am. J. Physiol., 1993. **265**(6 Pt 1): p. L613-621.
24. Ros, R.O.C., Cooke, D.T., Burden, R.S., and James, C.S., *Effects of the herbicide MCPA and the heavy metals, cadmium and nickel on the lipid composition, Mg^{2+}-ATPase activity and fluidity of plasma membranes from rice, Oryza sativa (cv. Bahia) shoots.* J. Exp. Bot., 1990. **41**: p. 457-462.
25. Hernandez, L.E. and Cooke, D.T., *Modification of the root plasma membrane lipid composition of cadmium treated Pisum sativum.* J. Exp. Bot., 1997. **48**: p. 1375-1381.
26. Fodor, E., Szabonagy, A., and Erdei, L., *The effects of cadmium on the fluidity and H^{+}-ATPase activity of plasma-membrane from sunflower and wheat roots.* J. Plant. Physiol., 1995. **147**(1): p. 87-92.
27. Demidchik, V., Sokolik, A., and Yurin, V., *The effect of Cu^{2+} on ion transport systems of the plant cell plasmalemma.* Plant. Physiol., 1997. **114**(4): p. 1313-1325.
28. Cakmak, I., *Possible roles of zinc in protecting plant cells from damage of reactive oxygen species.* New. Phytol., 2000. **146**: p. 185-205.
29. Salt, D.E., Smith, R.D., and Raskin, I., *Phytoremediation.* Annu. Rev. Plant Physiol. Plant Mol. Biol., 1998. **49**: p. 643-668.
30. Lewis, S., Donkin, M.E., Cordi, B., Billingshurst, Z., and Depledge, M.H., *Stress proteins (HSPs): methods of detection and their use as an environmental biomarker.* Ecotoxicology, 1999. **8**: p. 351-368.
31. Vierling, E., *The roles of heat shock proteins in plants.* Annu. Rev. Plant Phys., 1991. **42**: p. 579-620.
32. Neumann, D., Lichtenberger, O., Gunther, D., Tschiersch, K., and Nover, L., *Heat-shock proteins induce heavy-metal tolerance in higher-plants.* Planta, 1994. **194**(3): p. 360-367.
33. Rauser, W.E., *Phytochelatins and related peptides. Structure, biosynthesis, and function.* Plant Physiol., 1995. **109**(4): p. 1141-1149.
34. Haag-Kerwer, A., Schäfer, H.J., Heiss, S., Walter, C., and Rausch, T., *Cadmium exposure in Brassica juncea causes a decline in transpiration rate and leaf expansion without effect on photosynthesis.* J. Exp. Bot., 1999. **50**: p. 1827-1835.
35. Clemens, S., Kim, E.J., Neumann, D., and Schroeder, J.I., *Tolerance to toxic metals by a gene family of phytochelatin synthases from plants and yeast.* Embo J., 1999. **18**(12): p. 3325-3333.
36. Vatamaniuk, O.K., Mari, S., Lu, Y.P., and Rea, P.A., *AtPCS1, a phytochelatin synthase from Arabidopsis: Isolation and in vitro reconstitution.* P. Natl. Acad. Sci. USA, 1999. **96**(12): p. 7110-7115.
37. Ha, S.B., Smith, A.P., Howden, R., Dietrich, W.M., Bugg, S., O'Connell, M.J., Goldsbrough, P.B., and Cobbett, C.S., *Phytochelatin synthase genes from Arabidopsis and the yeast Schizosaccharomyces pombe.* Plant Cell, 1999. **11**(6): p. 1153-1164.

38. Cobbett, C. and Goldsbrough, P., *Phytochelatins and metallothioneins: Roles in heavy metal detoxification and homeostasis.* Annu. Rev. Plant. Biol., 2002. **53**: p. 159-182.
39. Schat, H., Llugany, M., and Bernhard, R., *Metal-specific patterns of tolerance, uptake and transport of heavy metals in hyperaccumulating and nonhyperaccumulating metallophytes*. Phytoremdeiation of contaminated soil and water, ed. Terry, N. and Banuelos, G. 2000: CRC Press LLC. 171-188.
40. Salt, D.E. and Rauser, W.E., *Mgatp-dependent transport of phytochelatins across the tonoplast of oat roots.* Plant Physiol., 1995. **107**(4): p. 1293-1301.
41. Ortiz, D.F., Kreppel, L., Speiser, D.M., Scheel, G., McDonald, G., and Ow, D.W., *Heavy metal tolerance in the fission yeast requires an ATP-binding cassette-type vacuolar membrane transporter.* Embo J., 1992. **11**(10): p. 3491-3499.
42. Rea, P.A., Li, Z.S., Lu, Y.P., Drozdowicz, Y.M., and Martinoia, E., *From vacuolar Gs-X pumps to multispecific Abc transporters.* Annu. Rev. Plant Physiol. Plant Mol. Biol., 1998. **49**: p. 727-760.
43. Murphy, A. and Taiz, L., *Comparison of metallothionein gene expression and nonprotein thiols in ten Arabidopsis ecotypes. Correlation with copper tolerance.* Plant. Physiol., 1995. **109**(3): p. 945-954.
44. Margoshes, M. and Vallee, B.L., *A cadmium protein from equine kidney cortex.* J. Am. Chem. Soc., 1957. **79**(17): p. 4813-4814.
45. Cherian, M.G. and Kang, Y.J., *Metallothionein and liver cell regeneration.* Exp. Biol. Med., 2006. **231**(2): p. 138-144.
46. Brouwer, M., Winge, D.R., and Gray, W.R., *Structural and functional diversity of copper-metallothioneins from the american lobster Homarus-americanus.* J. Inorg. Biochem., 1989. **35**(4): p. 289-303.
47. Roesijadi, G., *Metallothionein and its role in toxic metal regulation.* Comp. Biochem. Phys. C, 1996. **113**(2): p. 117-123.
48. Kawashima, I., Kennedy, T.D., Chino, M., and Lane, B.G., *Wheat Ec metallothionein genes - like mammalian Zn^{2+} metallothionein genes, wheat Zn^{2+} metallothionein genes are conspicuously expressed during embryogenesis.* Eur. J. Biochem., 1992. **209**(3): p. 971-976.
49. Reynolds, T.L. and Crawford, R.L., *Changes in abundance of an abscisic acid-responsive, early cysteine-labeled metallothionein transcript during pollen embryogenesis in bread wheat (Triticum aestivum).* Plant Mol. Biol., 1996. **32**(5): p. 823-829.
50. Hsieh, H.M., Liu, W.K., and Huang, P.C., *A novel stress-inducible metallothionein-like gene from rice.* Plant Mol. Biol., 1995. **28**(3): p. 381-389.
51. Zhou, J. and Goldsbrough, P.B., *Functional homologs of fungal metallothionein genes from Arabidopsis.* Plant. Cell., 1994. **6**(6): p. 875-884.
52. Zhou, J. and Goldsbrough, P.B., *Structure, organization and expression of the metallothionein gene family in Arabidopsis.* Mol. Gen. Genet., 1995. **248**(3): p. 318-328.
53. Kang, Y.J., *Metallothionein redox cycle and function.* Exp. Biol. Med. , 2006. **231**(9): p. 1459-1467.
54. Jacob, C., Maret, W., and Vallee, B.L., *Control of zinc transfer between thionein, metallothionein, and zinc proteins.* Proc. Natl. Acad. Sci. USA, 1998. **95**(7): p. 3489-3494.
55. St Croix, C.M., Stoyanovsky, D., Stitt, M.S., Leelavanichkul, K., Wasserloos, K.J., Watkins, S.C., and Pitt, B.R., *Nitric oxide (NO) induced modification of protein thiolate clusters as determined by fluorescence resonance energy transfer (FRET) in live pulmonary endothelial cells.* Faseb J., 2003. **17**(5): p. A1249.

56. Feng, W., Cai, J., Pierce, W.M., Franklin, R.B., Maret, W., Benz, F.W., and Kang, Y.J., *Metallothionein transfers zinc to mitochondrial aconitase through a direct interaction in mouse hearts.* Biochem. Biophys. Res. Commun., 2005. **332**(3): p. 853-858.
57. Hathout, Y., Fabris, D., and Fenselau, C., *Stoichiometry in zinc ion transfer from metallothionein to zinc finger peptides.* Int. J. Mass. Spectrom., 2001. **204**(1-3): p. 1-6.
58. Kojima, Y., Binz, P.-A., and Kägi, J.H.R., *Nomenclature of metallothionein: proposal for a revision.*, in *Metallothionein IV*, C., K., Editor. 1999, Birkhäuser: Basel. p. 3-6.
59. Kägi, J.H.R., *http://www.expasy.ch/cgi-bin/lists?metallo.txt*. 2007, Expasy.
60. Binz, P.-A., *Metallothioneins: studies on molecular evolution and on the structural and chiroptical features of their metal thiolate clusters.*, in *Biochemistry*. 1996, University of Zürich: Zürich.
61. Binz, P.-A. and Kägi, J.H.R., *Metallothionein: molecular evolution and classification.*, in *Metallothionein IV*, C., K., Editor. 1999, Birkhäuser: Basel. p. 7-13.
62. Blindauer, C.A., Harrison, M.D., Robinson, A.K., Parkinson, J.A., Bowness, P.W., Sadler, P.J., and Robinson, N.J., *Multiple bacteria encode metallothioneins and SmtA-like zinc fingers.* Mol. Microbiol., 2002. **45**(5): p. 1421-1432.
63. Munoz, A., Petering, D.H., and Shaw, C.F., 3rd, *Structure-reactivity relationships among metallothionein three-metal domains: role of non-cysteine amino acid residues in lobster metallothionein and human metallothionein-3.* Inorg. Chem., 2000. **39**(26): p. 6114-6123.
64. Domenech, J., *MT research project*, in *http://es.geocities.com/MetallothioneinResearch/MTresearchproject.htm#spurpuratus*.
65. Capasso, C., Carginale, V., Crescenzi, O., Di Maro, D., Parisi, E., Spadaccini, R., and Temussi, P.A., *Solution structure of MT_nc, a novel metallothionein from the Antarctic fish Notothenia coriiceps.* Structure, 2003. **11**(4): p. 435-443.
66. Valls, M., Bofill, R., Gonzalez-Duarte, R., Gonzalez-Duarte, P., Capdevila, M., and Atrian, S., *A new insight into metallothionein (MT) classification and evolution. The in vivo and in vitro metal binding features of Homarus americanus recombinant MT.* J. Biol. Chem., 2001. **276**(35): p. 32835-32843.
67. Peterson, C.W., Narula, S.S., and Armitage, I.M., *3D solution structure of copper and silver-substituted yeast metallothioneins.* FEBS Lett., 1996. **379**(1): p. 85-93.
68. Riek, R., Precheur, B., Wang, Y., Mackay, E.A., Wider, G., Guntert, P., Liu, A., Kägi, J.H., and Wüthrich, K., *NMR structure of the sea urchin (Strongylocentrotus purpuratus) metallothionein MTA.* J. Mol. Biol., 1999. **291**(2): p. 417-428.
69. Wang, H., Zhang, Q., Cai, B., Li, H., Sze, K.H., Huang, Z.X., Wu, H.M., and Sun, H., *Solution structure and dynamics of human metallothionein-3 (MT-3).* FEBS Lett., 2006. **580**(3): p. 795-800.
70. Zhu, C., Lü, T., Zhang, R., Zhao, N., and Liu, J., *Modeling of kiwi fruit metallothionein kiwi503.* Chin. Sci. Bull., 2000. **45**: p. 1413-1417.
71. Nielson, K.B. and Winge, D.R., *Independence of the domains of metallothionein in metal binding.* J. Biol. Chem., 1985. **260**(15): p. 8698-8701.
72. Domenech, J., Mir, G., Huguet, G., Capdevila, M., Molinas, M., and Atrian, S., *Plant metallothionein domains: functional insight into physiological metal binding and protein folding.* Biochimie, 2006. **88**(6): p. 583-593.
73. Peroza, E.A. and Freisinger, E., *Metal ion binding properties of Triticum aestivum Ec-1 metallothionein: evidence supporting two separate metal thiolate clusters.* J. Biol. Inorg. Chem., 2007. **12**(3): p. 377-391.
74. Kille, P., Winge, D.R., Harwood, J.L., and Kay, J., *A plant metallothionein produced in E. coli.* FEBS Lett., 1991. **295**(1-3): p. 171-175.

75. Blindauer, C.A., Harrison, M.D., Parkinson, J.A., Robinson, A.K., Cavet, J.S., Robinson, N.J., and Sadler, P.J., *A metallothionein containing a zinc finger within a four-metal cluster protects a bacterium from zinc toxicity.* Proc. Natl. Acad. Sci. USA, 2001. **98**(17): p. 9593-9598.
76. Palumaa, P. and Vasak, M., *Binding of inorganic phosphate to the cadmium-induced dimeric form of metallothionein from rabbit liver.* Eur. J. Biochem., 1992. **205**(3): p. 1131-1135.
77. Zangger, K. and Armitage, I.M., *Dynamics of interdomain and intermolecular interactions in mammalian metallothioneins.* J. Inorg. Biochem., 2002. **88**(2): p. 135-143.
78. Feng, W., Benz, F.W., Cai, J., Pierce, W.M., and Kang, Y.J., *Metallothionein disulfides are present in metallothionein-overexpressing transgenic mouse heart and increase under conditions of oxidative stress.* J. Biol. Chem., 2006. **281**(2): p. 681-687.
79. Y. Kojima, P.-A.B., J.H.R. Kägi, *Nomenclature of metallothionein:proposal for a revision in:* . Metallothionein IV, ed. Klaassen, C. 1999, Basel: Birkhäuser Verlag.
80. Hanley-Bowdoin, L. and Lane, B.G., *A novel protein programmed by the mRNA conserved in dry wheat embryos. The principal site of cysteine incorporation during early germination.* Eur. J. Biochem., 1983. **135**(1): p. 9-15.
81. Hofmann, T., Kells, D.I.C., and Lane, B.G., *Partial amino-acid-sequence of the wheat-germ Ec-protein - comparison with another protein very rich in half-cystine and glycine - wheat-germ-Agglutinin.* Can. J. Biochem. Cell B, 1984. **62**(9): p. 908-913.
82. Lane, B.G., Kajioka, R., and Kennedy, T.D., *The wheat germ Ec protein is a zinc containing metallothionein.* Cell. Biol., 1987. **65**: p. 1001-1005.
83. Guo, W.J., Bundithya, W., and Goldsbrough, P.B., *Characterization of the Arabidopsis metallothionein gene family: tissue-specific expression and induction during senescence and in response to copper.* New Phytol., 2003. **159**(2): p. 369-381.
84. Zimeri, A.M., Dhankher, O.P., McCaig, B., and Meagher, R.B., *The plant MT1 metallothioneins are stabilized by binding cadmiums and are required for cadmium tolerance and accumulation.* Plant. Mol. Biol., 2005. **58**(6): p. 839-855.
85. Tommey, A.M., Shi, J.G., Lindsay, W.P., Urwin, P.E., and Robinson, N.J., *Expression of the pea gene Psmta in Escherichia-coli - metal-binding properties of the expressed protein.* Febs Lett., 1991. **292**(1-2): p. 48-52.
86. Lucca, P., Hurrell, R., and Potrykus, I., *Genetic engineering approaches to improve the bioavailability and the level of iron in rice grains.* Theor. Appl. Genet., 2001. **102**(2-3): p. 392-397.
87. James, B.R., *The challenge of remedeating chromium contaminated soils.* Eviron. Sci. Tech., 1996. **30**: p. 248-251.
88. Chaney, R.L., Malik, M., Li, Y.M., Brown, S.L., Brewer, E.P., Angle, J.S., and Baker, A.J., *Phytoremediation of soil metals.* Curr. Opin. Biotechnol., 1997. **8**(3): p. 279-284.
89. Ruby, M.V., Davis, A., and Nicholson, A., *In situ formation of lead phosphates in soils as a method to immobilize lead.* Environ. Sci. Technol., 1994. **28**: p. 646-654.
90. Vogeli-Lange, R. and Wagner, G.J., *Subcellular localization of cadmium and cadmium-binding peptides in tobacco leaves : implication of a transport function for cadmium-binding peptides.* Plant Physiol., 1990. **92**(4): p. 1086-1093.
91. Robinson, N.J., Tommey, A.M., Kuske, C., and Jackson, P.J., *Plant Metallothioneins.* Biochem. J., 1993. **295**: p. 1-10.
92. Brandle, J.E., Labbe, H., Hattori, J., and Miki, B.L., *Field performance and heavy metal concentrations of transgenic flue-cured tobacco expressing a mammalian metallothionein-beta-glucuronidase gene fusion.* Genome, 1993. **36**(2): p. 255-260.

93. Elmayan, T. and Tepfer, M., *Synthesis of a bifunctional metallothionein/beta-glucuronidase fusion protein in transgenic tobacco plants as a means of reducing leaf cadmium levels.* Plant. J., 1994. **6**(3): p. 433-440.
94. Pan, A., Tie, F., Duau, Z., Yang, M., Wang, Z., Li, L., Chen, Z., and Ru, B., *Alpha-domain of human metallothionein IA can bind to metals in transgenic tobacco plants.* Mol. Gen. Genet., 1994. **242**(6): p. 666-674.
95. Yeargan, R., Maiti, I.B., Nielsen, M.T., Hunt, A.G., and Wagner, G.J., *Tissue partitioning of cadmium in transgenic tobacco seedlings and field grown plants expressing the mouse metallothionein I gene.* Transgenic. Res., 1992. **1**(6): p. 261-267.
96. Evans, K.M., Gatehouse, J.A., Lindsay, W.P., Shi, J., Tommey, A.M., and Robinson, N.J., *Expression of the pea metallothionein-like gene Psmta in Escherichia-coli and Arabidopsis-thaliana and analysis of trace-metal ion accumulation - implications for Psmta function.* Plant Mol. Biol., 1992. **20**(6): p. 1019-1028.
97. Eapen, S. and D'Souza, S.F., *Prospects of genetic engineering of plants for phytoremediation of toxic metals.* Biotechnol. Adv., 2005. **23**(2): p. 97-114.
98. de Miranda, J.R., Thomas, M.A., Thurman, D.A., and Tomsett, A.B., *Metallothionein genes from the flowering plant Mimulus guttatus.* FEBS Lett., 1990. **260**(2): p. 277-280.
99. Zambryski, P. and Crawford, K., *Plasmodesmata: gatekeepers for cell-to-cell transport of developmental signals in plants.* Annu. Rev. Cell. Dev. Biol., 2000. **16**: p. 393-421.
100. Foley, R.C. and Singh, K.B., *Isolation of a Vicia faba metallothionein-like gene: expression in folair trichomes.* Plant. Mol. Biol., 1994. **26**: p. 435-444.
101. Garcia-Hernandez, M., Murphy, A., and Taiz, L., *Metallothioneins 1 and 2 have distinct but overlapping expression patterns in Arabidopsis.* Plant Physiol., 1998. **118**(2): p. 387-397.
102. Salt, D.E., Prince, R.C., Pickering, I.J., and Raskin, I., *Mechanisms of cadmium mobility and accumulation in indian mustard.* Plant Physiol., 1995. **109**(4): p. 1427-1433.
103. Buhtz, A., Kolasa, A., Arlt, K., Walz, C., and Kehr, J., *Xylem sap protein composition is conserved among different plant species.* Planta, 2004. **219**(4): p. 610-618.
104. Buchanan-Wollaston, V., *Isolation of cDNA clones for genes that are expressed during leaf senescence in Brassica napus. Identification of a gene encoding a senescence-specific metallothionein-like protein.* Plant Physiol., 1994. **105**(3): p. 839-846.
105. Pena, M.M., Lee, J., and Thiele, D.J., *A delicate balance: homeostatic control of copper uptake and distribution.* J. Nutr., 1999. **129**(7): p. 1251-1260.
106. Rae, T.D., Schmidt, P.J., Pufahl, R.A., Culotta, V.C., and O'Halloran, T.V., *Undetectable intracellular free copper: the requirement of a copper chaperone for superoxide dismutase.* Science, 1999. **284**(5415): p. 805-808.
107. Coupe, S.A., Taylor, J.E., and Roberts, J.A., *Characterization of an messenger-RNA encoding a metallothionein-like protein that accumulates during ethylene-promoted abscission of Sambucus-Nigra L leaflets.* Planta, 1995. **197**(3): p. 442-447.
108. Butt, A., Mousley, C., Morris, K., Beynon, J., Can, C., Holub, E., Greenberg, J.T., and Buchanan-Wollaston, V., *Differential expression of a senescence-enhanced metallothionein gene in Arabidopsis in response to isolates of Peronospora parasitica and Pseudomonas syringae.* Plant. Journal., 1998. **16**(2): p. 209-221.
109. Choi, D., Kim, H.M., Yun, H.K., Park, J.A., Kim, W.T., and Bok, S.H., *Molecular cloning of a metallothionein-like gene from Nicotiana glutinosa L. and its induction by wounding and tobacco mosaic virus infection.* Plant. Physiol., 1996. **112**(1): p. 353-359.

110. Snowden, K.C., Richards, K.D., and Gardner, R.C., *Aluminum-induced genes (induction by toxic metals, low calcium, and wounding and pattern of expression in root tips).* Plant Physiol., 1995. **107**(2): p. 341-348.
111. Robbins, A.H., McRee, D.E., Williamson, M., Collett, S.A., Xuong, N.H., Furey, W.F., Wang, B.C., and Stout, C.D., *Refined crystal structure of Cd, Zn metallothionein at 2.0 A resolution.* J. Mol. Biol., 1991. **221**(4): p. 1269-1293.
112. Wüthrich, K., *Protein structure determination in solution by nuclear magnetic resonance spectroscopy.* Science, 1989. **243**(4887): p. 45-50.
113. Braun, W., Vasak, M., Robbins, A.H., Stout, C.D., Wagner, G., Kägi, J.H., and Wüthrich, K., *Comparison of the NMR solution structure and the x-ray crystal structure of rat metallothionein-2.* Proc. Natl. Acad. Sci. USA, 1992. **89**(21): p. 10124-10128.
114. Henkel, G. and Krebs, B., *Metallothioneins: zinc, cadmium, mercury, and copper thiolates and selenolates mimicking protein active site features--structural aspects and biological implications.* Chem. Rev., 2004. **104**(2): p. 801-824.
115. Roschitzki, B. and Vasak, M., *A distinct Cu(4)-thiolate cluster of human metallothionein-3 is located in the N-terminal domain.* J. Biol. Inorg. Chem., 2002. **7**(6): p. 611-616.
116. Bogumil, R., Faller, P., Binz, P.A., Vasak, M., Charnock, J.M., and Garner, C.D., *Structural characterization of Cu(I) and Zn(II) sites in neuronal-growth-inhibitory factor by extended X-ray absorption fine structure (EXAFS).* Eur. J. Biochem., 1998. **255**(1): p. 172-177.
117. Bogumil, R., Faller, P., Pountney, D.L., and Vasak, M., *Evidence for Cu(I) clusters and Zn(II) clusters in neuronal growth-inhibitory factor isolated from bovine brain.* Eur. J. Biochem., 1996. **238**(3): p. 698-705.
118. Narula, S.S., Brouwer, M., Hua, Y., and Armitage, I.M., *Three-dimensional solution structure of Callinectes sapidus metallothionein-1 determined by homonuclear and heteronuclear magnetic resonance spectroscopy.* Biochem., 1995. **34**(2): p. 620-631.
119. Zhu, Z., DeRose, E.F., Mullen, G.P., Petering, D.H., and Shaw, C.F., 3rd, *Sequential proton resonance assignments and metal cluster topology of lobster metallothionein-1.* Biochem., 1994. **33**(30): p. 8858-8865.
120. Bertini, I., Hartmann, H.J., Klein, T., Liu, G., Luchinat, C., and Weser, U., *High resolution solution structure of the protein part of Cu7 metallothionein.* Eur. J. Biochem., 2000. **267**(4): p. 1008-1018.
121. Cobine, P.A., McKay, R.T., Zangger, K., Dameron, C.T., and Armitage, I.M., *Solution structure of Cu6 metallothionein from the fungus Neurospora crassa.* Eur. J. Biochem., 2004. **271**(21): p. 4213-4221.
122. Calderone, V., Dolderer, B., Hartmann, H.J., Echner, H., Luchinat, C., Del Bianco, C., Mangani, S., and Weser, U., *The crystal structure of yeast copper thionein: the solution of a long-lasting enigma.* Proc. Natl. Acad. Sci. USA, 2005. **102**(1): p. 51-56.
123. George, G.N., Byrd, J., and Winge, D.R., *X-ray absorption studies of yeast copper metallothionein.* J. Biol. Chem., 1988. **263**(17): p. 8199-8203.
124. Luchinat, C., Dolderer, B., Del Bianco, C., Echner, H., Hartmann, H.J., Voelter, W., and Weser, U., *The Cu(I)(7) cluster in yeast copper thionein survives major shortening of the polypeptide backbone as deduced from electronic absorption, circular dichroism, luminescence and (1)H NMR.* J. Biol. Inorg. Chem., 2003. **8**(3): p. 353-359.
125. Gui, Z., Green, A.R., Kasrai, M., Bancroft, G.M., and Stillman, M.J., *Sulfur K-Edge EXAFS studies of cadmium-, zinc-, copper-, and silver-rabbit liver metallothioneins.* Inorg. Chem., 1996. **35**(22): p. 6520-6529.

126. Rigby, K.E. and Stillman, M.J., *Structural studies of metal-free metallothionein.* Biochem. Biophys. Res. Commun., 2004. **325**(4): p. 1271-1278.
127. Presta, A. and Stillman, M.J., *Chiral copper(I)-thiolate clusters in metallothionein and glutathione.* Chirality, 1994. **6**(7): p. 521-530.
128. Presta, A. and Stillman, M.J., *Incorporation of copper into the yeast Saccharomyces cerevisiae. Identification of Cu(I)--metallothionein in intact yeast cells.* J. Inorg. Biochem., 1997. **66**(4): p. 231-240.
129. Stillman, M.J., *Optical spectroscopy of metallothioneins*, in *Mteallothioneins*, Stillman, M.J., Shaw, C.F., and Suzuki, K.T., Editors. 1992, VCH publishers: New York. p. 55-127.
130. Willner, H., Bernhard, W.R., and Kägi, J.H.R., *Optical properties of metallothioneins.*, in *Metallothioneins*, Stillman, M.J., Shaw, C.F., and Suzuki, K.T., Editors. 1992, VCH Publishers: New York. p. 128-143.
131. Zelaozowski, A.J. and Stillman, M.J., *Silver binding to rabbit liver zinc metallothionein and α and β fragments.* Inorg. Chem., 1992. **31**: p. 3363-3370.
132. Shipper, P.E. and Rodger, A., *Symmetry rules for the determinations of the intercalation geometry of host/guest systems using circular dichroism: a symmetry-adapted coupled-oscillator model.* J. Am. Chem., 1983. **32**: p. 4541-4550.
133. Schägger, H., Aquila, H., and Vonjagow, G., *Coomassie blue Sodium dodecyl-sulfate polyacrylamide-gel electrophoresis for direct visualization of polypeptides during electrophoresis.* Anal. Biochem., 1988. **173**(1): p. 201-205.
134. Meloni, G., Knipp, M., and Vasak, M., *Detection of neuronal growth inhibitory factor (metallothionein-3) in polyacrylamide gels and by Western blot analysis.* J. Biochem. Bioph. Meth., 2005. **64**(1): p. 76-81.
135. The_plant_MT_group, *Coomassie staining; http://www.aci.uzh.ch/MT/pdf/Coomassie_stain.pdf.*
136. The_plant_MT_group, *Silver staining; http://www.aci.uzh.ch/MT/pdf/Silver_stain.pdf.*
137. Freisinger, E., *Spectroscopic characterization of a fruit-specific metallothionein: M-acuminata MT3.* Inorg. Chim. Acta., 2007. **360**(1): p. 369-380.
138. Dietrich-Buchecker, C. and Sauvage, J.I., *locked macrocyclic ligands, the catenands*, in *Gmelin Handbook of Anorganic and Organometallic Chemistry*
Institut, G., Editor. 1990: Frankfurt Main. p. 1462.
139. Dong, A., Huang, P., and Caughey, W.S., *Protein secondary structures in water from 2^{nd}-derivative amide-I infrared-spectra.* Biochem., 1990. **29**(13): p. 3303-3308.
140. Susi, H. and Byler, D.M., *Resolution-enhanced Fourier transform infrared spectroscopy of enzymes.* Methods Enzymol., 1986. **130**: p. 290-311.
141. Haris, P.I. and Severcan, F., *FTIR spectroscopic characterization of protein structure in aqueous and non-aqueous media.* J. Mol. Catal. B-Enzym., 1999. **7**(1-4): p. 207-221.
142. Jackson, M. and Mantsch, H.H., *The use and misuse of FTIR spectroscopy in the determination of protein-structure.* Crit. Rev. Biochem. Mol., 1995. **30**(2): p. 95-120.
143. Surewicz, W.K. and Mantsch, H.H., *New insight into protein secondary structure from resolution-enhanced infrared spectra.* Biochim. Biophys. Acta, 1988. **952**(2): p. 115-130.
144. Pitt-Rivers, R. and Impiomba, F.S.A., Biochem. J., 1968. **109**: p. 825-830.
145. Valenzuela, J.G., Francischetti, I.M., Pham, V.M., Garfield, M.K., Mather, T.N., and Ribeiro, J.M., *Exploring the sialome of the tick Ixodes scapularis.* J. Exp. Biol., 2002. **205**(Pt 18): p. 2843-2864.
146. Oakley, B.R., Kirsch, D.R., and Morris, N.R., *A simplified ultrasensitive silver stain for detecting proteins in polyacrylamide gels.* Anal. Biochem., 1980. **105**(2): p. 361-3.

147. Bird, G.H. and Shin, J.A., *MALDI-TOF mass spectrometry characterization of recombinant hydrophobic mutants containing the GCN4 basic region/leucine zipper motif.* Biochim. Biophys. Acta, 2002. **1597**(2): p. 252-259.
148. Link, A.J., Robinson, K., and Church, G.M., *Comparing the predicted and observed properties of proteins encoded in the genome of Escherichia coli K-12.* Electrophoresis, 1997. **18**(8): p. 1259-1313.
149. Stillman, M.J., *Metallothioneins.* Coordin. Chem. Rev., 1995. **144**: p. 461-511.
150. Kägi, J.H. and Vallee, B.L., *Metallothionein: a cadmium and zinc-containign protein from equine renal cortex. II. Physico-chemical properties.* J. Biol. Chem., 1961. **236**: p. 2435-2442.
151. Vasak, M., Kägi, J.H., and Hill, H.A., *Zinc(II), cadmium(II), and mercury(II) thiolate transitions in metallothionein.* Biochem., 1981. **20**(10): p. 2852-2856.
152. Willner, H., Vasak, M., and Kagi, J.H.R., *Cadmium-Thiolate Clusters in Metallothionein - Spectrophotometric and Spectropolarimetric Features.* Biochem., 1987. **26**(19): p. 6287-6292.
153. Jorgensen, C.K., Prog. Inorg. Chem., 1970. **12**: p. 101.
154. Nordberg, M. and Kojima, Y., in *Metallothionein*, Kägi, J.H.R. and Nordberg, M., Editors. 1979, Birkhäuser Verlag: Basel. p. 41.
155. Stillman, M.J., Cai, W., and Zelazowski, A.J., *Cadmium binding to metallothioneins - domain specificity in reactions of alpha-fragment and beta-fragment, apometallothionein, and zinc metallothionein with* Cd^{2+}. J. Biol. Chem., 1987. **262**(10): p. 4538-4548.
156. Dallinger, R., Wang, Y.J., Berger, B., Mackay, E.A., and Kagl, J.H.R., *Spectroscopic characterization of metallothionein from the terrestrial snail, Helix pomatia.* Eur. J. Biochem., 2001. **268**(15): p. 4126-4133.
157. Villarreal, L., Tio, L., Atrian, S., and Capdevila, M., *Influence of chloride ligands on the structure of Zn- and Cd-metallothionein species.* Arch. Biochem. Biophys., 2005. **435**(2): p. 331-335.
158. Willner, H., Vasak, M., and Kägi, J.H.R., *Spectroscopic evidence for metal thiolate clusters in complexes of Cd(II) with dithiol hexapeptides and in Cd-metallothionein.* Inorg. Chim. a-Bioinor., 1983. **79**(1-6): p. 106-107.
159. Bühler, R.H.O. and Kägi, J.H.R., *Metallothionein.* 1979: p. 211.
160. Vasak, M. and Kägi, J.H.R., *Spectroscopic properties of metallothionein.* Met. Ions Biol. Syst., 1983. **15**: p. 213-273.
161. Gilg, D.E.O., *Strukturuntersuchungen an Metallothionein aus Pferde- und Kanninchenleber*, in *Biochemistry*. 1985, University of Zürich, Switzerland: Zürich.
162. Pande, J., Pande, C., Gilg, D., Vasak, M., Callender, R., and Kagi, J.H., *Raman, infrared, and circular dichroism spectroscopic studies on metallothionein: a predominantly "turn"-containing protein.* Biochem., 1986. **25**(19): p. 5526-5532.
163. Solomon, E.I., Pavel, E.G., Loeb, K.E., and Campochiaro, C., Coord. Chem. Rev., 1995. **144**: p. 369-460.
164. Law, A.Y.C. and Stillman, M.J., *Characterization of the cadmium(II) binding-site in Cd, Zn-metallothionein by magnetic circular-dichroism spectroscopy.* Biochem. Bioph. Res. Co., 1981. **102**(1): p. 397-402.
165. Szymanska, J.A., Zelazowski, A.J., and Stillman, M.J., *Spectroscopic characterization of rat kidney Hg,Cu-metallothionein.* Biochem. Biophys. Res. Commun., 1983. **115**(1): p. 167-173.
166. Overnell, J., Good, M., and Vasak, M., *Spectroscopic studies on cadmium(II)-substituted and cobalt(Ii)-substituted metallothionein from the crab cancer-pagurus - evidence for one additional low-affinity metal-binding site.* Eur. J. Biochem., 1988. **172**(1): p. 171-177.

167. Avdeef, A., Zelazowski, A.J., and Garvey, J.S., *Cadmium binding by biological ligands .3. 5-cadmium and 7-cadmium binding in metallothionein - a detailed thermodynamic study.* Inorg. Chem., 1985. **24**(12): p. 1928-1933.
168. Vasak, M., Kägi, J.H., Holmquist, B., and Vallee, B.L., *Spectral studies of cobalt (II)- and Nickel (II)-metallothionein.* Biochem., 1981. **20**(23): p. 6659-6664.
169. Vasak, M. and Kägi, J.H.R., *Metal thiolate clusters in cobalt(II)-metallothionein.* P. Natl. Acad. Sci-Biol., 1981. **78**(11): p. 6709-6713.
170. Chen, P., Munoz, A., Nettesheim, D., Shaw, C.F., 3rd, and Petering, D.H., *Stoichiometry and cluster specificity of copper binding to metallothionein: homogeneous metal clusters.* Biochem. J., 1996. **317 (Pt 2)**: p. 395-402.
171. Presta, A., Green, A.R., Zelazowski, A., and Stillman, M.J., *Copper binding to rabbit liver metallothionein. Formation of a continuum of copper(I)-thiolate stoichiometric species.* Eur. J. Biochem., 1995. **227**(1-2): p. 226-240.
172. Li, Y.J. and Weser, U., *Circular dichroism, luminescence, and electronic absorption of copper binding sites in metallothionein and its chemically synthezied α and β domains.* Inorg. Chem., 1992. **31**: p. 5526-5533.
173. Rupp, H. and Weser, U., *Circular dichroism of metallothioneins. A structural approach.* Biochim. Biophys. Acta., 1978. **533**(1): p. 209-226.
174. Pountney, D.L., Schauwecker, I., Zarn, J., and Vasak, M., *Formation of mammalian Cu8-metallothionein in vitro: evidence for the existence of two Cu(I)4-thiolate clusters.* Biochemistry, 1994. **33**(32): p. 9699-9705.
175. Sabin, F., Ryu, C.K., Ford, P.C., and Vogler, A., *Photophysical properties of hexanuclear copper(I) and silver (I) clusters.* Inorg. Chem., 1992. **31**: p. 1941-1945.
176. Ryu, C.K., Vitale, M., and Ford, P.C., *Photoluminescence properties of the structurally analogous tetranuclear copper(I) clusters Cu4X4(dpmp)4 (X = I, Br, Cl; dpmp = 2-(diphenylmethyl)pyridine).* Inorg. Chem., 1993. **32**: p. 869-874.
177. Blindauer, C.A. and Sadler, P.J., *How to hide zinc in a small protein.* Acc. Chem. Res., 2005. **38**(1): p. 62-69.
178. Abdullah, S.N.A., Cheah, S.C., and Murphy, D.J., *Isolation and charachterisation of two divergent type 3 metallothoneins from oil palm, Elaeis guineensis.* Plant Physiol. Bioch., 2002. **40**: p. 255-263.
179. White, C.N. and Rivin, C.J., *Characterization and expression of a cDNA encoding seed specific metallothionein in maize.* Plant Physiol., 1995. **108**: p. 831-832.
180. Schmid, F.X., *Optical spectroscopy to characterize protein conformation and conformational changes*, in *Protein Structure: A Practical Approach*, Creighton, T.E., Editor. 1997, IRL PRess: Oxford. p. 261-297.
181. Jabs, A., *Determination of secondary structure in proteins by fourier transform infrared spectroscopy (FTIR)*, http://www.imb-jena.de/ImgLibDoc/ftir/IMAGE_FTIR.html#head, Editor.
182. Chou, K.C., Pottle, M., Nemethy, G., Ueda, Y., and Scheraga, H.A., *Structure of beta-sheets - origin of the right-handed twist and of the increased stability of antiparallel over parallel sheets.* J. Mol. Biol., 1982. **162**(1): p. 89-112.
183. Forato, L.A., Bernardes-Filho, R., and Colnago, L.A., *Protein structure in KBr pellets by infrared spectroscopy.* Anal. Biochem., 1998. **259**(1): p. 136-141.
184. Meyer, J.D., Manning, M.C., and Carpenter, J.F., *Effects of potassium bromide disk formation on the infrared spectra of dried model proteins.* J. Pharm. Sci., 2004. **93**(2): p. 496-506.
185. Shi, Y.B., Fang, J.L., Liu, X.Y., Du, L., and Tang, W.X., *Fourier transform IR and Fourier transform Raman spectroscopy studies of metallothionein-III: amide I band assignments and secondary structural comparison with metallothioneins-I and -II.* Biopolymers, 2002. **65**(2): p. 81-88.

186. Cuff, J.A. and Barton, G.J., *Application of multiple sequence alignment profiles to improve protein secondary structure prediction.* Proteins, 2000. **40**(3): p. 502-511.
187. Arrondo, J.L., Muga, A., Castresana, J., and Goni, F.M., *Quantitative studies of the structure of proteins in solution by Fourier-transform infrared spectroscopy.* Prog. Biophys. Mol. Biol., 1993. **59**(1): p. 23-56.
188. Alvarez, J., Haris, P.I., Lee, D.C., and Chapman, D., *Conformational changes in concanavalin A associated with demetallization and alpha-methylmannose binding studied by Fourier transform infrared spectroscopy.* Biochim. Biophys. Acta, 1987. **916**(1): p. 5-12.
189. Hadden, J.M., Bloemendal, M., Haris, P.I., Srai, S.K., and Chapman, D., *Fourier transform infrared spectroscopy and differential scanning calorimetry of transferrins: human serum transferrin, rabbit serum transferrin and human lactoferrin.* Biochim. Biophys. Acta, 1994. **1205**(1): p. 59-67.
190. Jackson, M., Haris, P.I., and Chapman, D., *Fourier transform infrared spectroscopic studies of Ca(2+)-binding proteins.* Biochem., 1991. **30**(40): p. 9681-9686.
191. van de Weert, M., Haris, P.I., Hennink, W.E., and Crommelin, D.J., *Fourier transform infrared spectrometric analysis of protein conformation: effect of sampling method and stress factors.* Anal. Biochem., 2001. **297**(2): p. 160-169.
192. Pelton, J.T. and McLean, L.R., *Spectroscopic methods for analysis of protein secondary structure.* Anal. Biochem., 2000. **277**(2): p. 167-176.
193. EMBL, *Prediction of percentages of protein secondary structure from CD spectra*, http://www.embl-heidelberg.de/~andrade/k2d/.
194. Unneberg, P., Merelo, J.J., Chacon, P., and Moran, F., *SOMCD: Method for evaluating protein secondary structure from UV circular dichroism spectra.* Proteins, 2001. **42**(4): p. 460-470.
195. Farnsworth, P.N., GrothVasselli, B., Greenfield, N.J., and Singh, K., *Effects of temperature and concentration on bovine lens alpha-crystallin secondary structure: A circular dichroism spectroscopic study.* Int. J. Biol. Macromol., 1997. **20**(4): p. 283-291.
196. Ngu, T.T., Sturzenbaum, S.R., and Stillman, M.J., *Cadmium binding studies to the earthworm Lumbricus rubellus metallothionein by electrospray mass spectrometry and circular dichroism spectroscopy.* Biochem. Bioph. Res. Co., 2006. **351**(1): p. 229-233.
197. Morris, C.A., Nicolaus, B., Sampson, V., Harwood, J.L., and Kille, P., *Identification and characterization of a recombinant metallothionein protein from a marine alga, Fucus vesiculosus.* Biochem. J., 1999. **338**: p. 553-560.
198. Maret, W. and Vallee, B.L., *Thiolate ligands in metallothionein confer redox activity on zinc clusters.* Proc. Natl. Acad. Sci. USA, 1998. **95**(7): p. 3478-3482.
199. Marmorstein, R., Carey, M., Ptashne, M., and Harrison, S.C., *DNA recognition by GAL4: structure of a protein-DNA complex.* Nature, 1992. **356**(6368): p. 408-414.
200. Marmorstein, R. and Harrison, S.C., *Crystal structure of a PPR1-DNA complex: DNA recognition by proteins containing a Zn2Cys6 binuclear cluster.* Genes Dev., 1994. **8**(20): p. 2504-2512.
201. Domenech, J., Tinti, A., Capdevila, M., Atrian, S., and Torreggiani, A., *Structural study of the zinc and cadmium complexes of a type 2 plant (Quercus suber) metallothionein: Insights by vibrational spectroscopy.* Biopolymers, 2007.
202. Beradini, M., Emge, T.J., and Brennan, J.G., Inorg. Chem., 1995. **34**: p. 5327.
203. Hensbergen, P.J., Donker, M.H., Hunziker, P.E., van der Schors, R.C., and van Straalen, N.M., *Two metal-binding peptides from the insect Orchesella cincta (Collembola) as a result of metallothionein cleavage.* Insect Biochem. Molec., 2001. **31**(11): p. 1105-1114.

204. Wang, Y., Hess, D., Hunziker, P.E., and Kägi, J.H., *Separation and characterization of the metal-thiolate-cluster domains of recombinant sea urchin metallothionein.* Eur. J. Biochem., 1996. **241**(3): p. 835-839.
205. Cabrita, L.D. and Bottomley, S.P., *Protein expression and refolding--a practical guide to getting the most out of inclusion bodies.* Biotechnol. Annu. Rev., 2004. **10**: p. 31-50.
206. Carson, G.K., Dean, P.A.W., and Stillman, M.J., *A multi-nuclear (H-1, C-13, Cd-113) nuclear magnetic-resonance and magnetic circular-dichroism spectroscopic study of thiolate complexes of cadmium.* Inorg. Chim. Acta, 1981. **56**(3): p. 59-71.
207. Green, L.M. and Berg, J.M., *A retroviral Cys-Xaa2-Cys-Xaa4-His-Xaa4-Cys peptide binds metal ions: spectroscopic studies and a proposed three-dimensional structure.* Proc. Natl. Acad. Sci. USA, 1989. **86**(11): p. 4047-4051.
208. Sytkowski, A.J. and Vallee, B.L., *Chemical reactivities of catalytic and noncatalytic zinc or cobalt atoms of horse liver alcohol dehydrogenase: differentiation by their thermodynamic and kinetic properties.* Proc. Nat.l Acad. Sci. USA, 1976. **73**(2): p. 344-348.
209. Winge, D.R., *Copper coordination in metallothionein.* Experientia Suppl., 1987. **52**: p. 213-218.
210. Liochev, S.I. and Fridovich, I., *The effects of superoxide dismutase on H2O2 formation.* Free Radic. Biol. Med., 2007. **42**(10): p. 1465-1469.
211. Bofill, R., Palacios, O., Capdevila, M., Cols, N., Gonzalez-Duarte, R., Atrian, S., and Gonzalez-Duarte, P., *A new insight into the Ag^{+} and Cu^{+} binding sites in the metallothionein beta domain.* J. Inorg. Biochem., 1999. **73**(1-2): p. 57-64.
212. Bremner, I. and Young, B.W., *Isolation of (copper, zinc)-thioneins from the livers of copper-injected rats.* Biochem. J., 1976. **157**(2): p. 517-520.
213. Briggs, R.W. and Armitage, I.M., *Evidence for site-selective metal binding in calf liver metallothionein.* J. Biol. Chem., 1982. **257**(3): p. 1259-1262.
214. Nielson, K.B. and Winge, D.R., *Order of metal binding in metallothionein.* J. Biol. Chem., 1983. **258**(21): p. 13063-13069.
215. Winge, D.R. and Miklossy, K.A., *Domain nature of metallothionein.* J. Biol. Chem., 1982. **257**(7): p. 3471-3476.
216. Beltramini, M. and Lerch, K., *Spectroscopic studies on Neurospora copper metallothionein.* Biochem., 1983. **22**(9): p. 2043-2048.
217. Narula, S.S., Winge, D.R., and Armitage, I.M., *Copper- and silver-substituted yeast metallothioneins: sequential 1H NMR assignments reflecting conformational heterogeneity at the C terminus.* Biochem., 1993. **32**(26): p. 6773-6787.
218. Ahner, B.A. and Morel, *Phytochelatin production in marine algae. 2. Induction by various metals.* Limnol. Oceanogr., 1995. **40**: p. 658-665.
219. Steffens, J.C., *The Heavy Metal-Binding Peptides of Plants.* Annu. Rev. Plant Physiol. Plant Mol. Biol., 1990. **41**: p. 553-575.
220. Satoh, M., N., N., Kanayama, Y., Naganuma, A., Suzuki, T., and Tohyama, C., *Enhanced renal toxicity by inorganic mercury in metallothionein-null mice.* J. Pharmacol. Exp. Ther, 1997. **283**: p. 1529-1533.
221. Lu, W. and Stillman, M., *Mercury-thiolate clusters in metallothionein. Analysis of circular dichroism spectra of complexes formed between α-metallothionein, apometallothionein, zinc metallothionein, and cadmium metallothionein and Hg^{2+}.* J. Am. Chem. Soc., 1992. **1993**: p. 3291-3299.
222. Faller, P., Ctortecka, B., Troger, W., Butz, T., and Vasak, M., *Optical and TDPAC spectroscopy of Hg(II)-rubredoxin: model for a mononuclear tetrahedral [Hg(CysS)4]2- center. ISOLDE Collaboration.* J. Biol. Inorg. Chem., 2000. **5**(3): p. 393-401.

223. Wright, J.G., Natan, M.J., MacDonnell, F.M., Ralston, D.M., and O´Halloran, T.V., *Mercury(II)-thiolate chemistry and the mechanism of the heavy metal biosensor MerR.* Progress in Inroganic Chemistry: Bioinorganic Chemistry, ed. Lippard, S.J. Vol. 38. 1990: John Wiley & Sons, Inc.
224. Nyholm, R.S., Proc. Chem. Soc. London, 1961: p. 273.
225. Leiva-Presa, A., Capdevila, M., and Gonzalez-Duarte, P., *Mercury(II) binding to metallothioneins. Variables governing the formation and structural features of the mammalian Hg-MT species.* Eur. J. Biochem., 2004. **271**(23-24): p. 4872-4880.
226. Saito, N., *Principles of protein architecture.* Adv. Biophys., 1989. **25**: p. 95-132.
227. Palumaa, P., Tammiste, I., Kruusel, K., Kangur, L., Jornvall, H., and Sillard, R., *Metal binding of metallothionein-3 versus metallothionein-2: lower affinity and higher plasticity.* Biochim. Biophys. Acta., 2005. **1747**(2): p. 205-211.
228. Bowler, B.E., May, K., Zaragoza, T., York, P., Dong, A., and Caughey, W.S., *Destabilizing effects of replacing a surface lysine of cytochrome c with aromatic amino acids: implications for the denatured state.* Biochem., 1993. **32**(1): p. 183-190.
229. Haris, P.I. and Chapman, D., *Does fourier-transform infrared spectroscopy provide useful information on protein structures?* Trends Biochem. Sci., 1992. **17**(9): p. 328-333.
230. Nara, M., Tasumi, M., Tanokura, M., Hiraoki, T., Yazawa, M., and Tsutsumi, A., *Infrared studies of interaction between metal ions and Ca(2+)-binding proteins. Marker bands for identifying the types of coordination of the side-chain COO- groups to metal ions in pike parvalbumin (pI = 4.10).* FEBS Lett., 1994. **349**(1): p. 84-88.
231. Frey, M., Sieker, L., Payan, F., Haser, R., Bruschi, M., Pepe, G., and LeGall, J., *Rubredoxin from Desulfovibrio gigas. A molecular model of the oxidized form at 1.4 A resolution.* J. Mol. Biol., 1987. **197**(3): p. 525-541.
232. Henehan, C.J., Pountney, D.L., Zerbe, O., and Vasak, M., *Identification of cysteine ligands in metalloproteins using optical and NMR spectroscopy: cadmium-substituted rubredoxin as a model [Cd(CysS)4]2- center.* Protein Sci., 1993. **2**(10): p. 1756-1764.
233. Pountney, D.L., Henehan, C.J., and Vasak, M., *Establishing isostructural metal substitution in metalloproteins using 1H NMR, circular dichroism, and Fourier transform infrared spectroscopy.* Protein Sci., 1995. **4**(8): p. 1571-1576.

10 Appendices

10.1 Quantification of SH groups with 2,2'-Dithio-dipyridine (2-PDS)

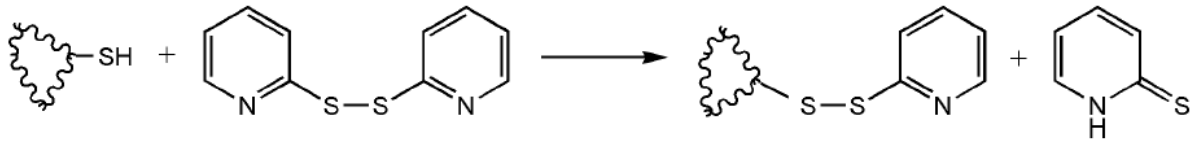

2,2'-Dithio-dipyridine
(ε_{281} 9730 M^{-1} cm^{-1})

2-Thiopyridinone
(ε_{343} 7600 M^{-1} cm^{-1})

For each SH-group one molecule of 2-Thiopyridinone is formed.
The latter can be quantified via its absorption maximum at 343nm.
Required stock solutions:
ca. 1mM 2-PDS in 0.2M NaOAc (pH 4.0)
1M NaOAc (pH 4.0)

- start the Cary WinUV program "Scan" and let the UV-lamp warm up
- select scan range 380-250nm
- prepare the following samples

	blind	**sample**
Solution containing SH groups	0 µL	x µL
1mM 2-PDS	12.5 µL	12.5 µL
1M NaOAc (pH 4.0)	22.5 µL	22.5 µL
ddH2O	90 µL	90-x µL
	125 µL	125 µL

10.2 Quantification of Proteins via A_{280}

--> *This method only works with proteins containing aromatic residues*

- start the Cary WinUV program "Simple Reads" (or "Scan") and let the UV-lamp warm up
- dilute protein solution (if necessary) in ddH_2O (or buffer) and mix gently (100µL total)
- blank UV spec. against ddH_2O (or buffer)
- measure A_{280} (make sure that A_{280} reading is between 0.1 and 1.0!!!) (or scan 250-290nm)

A_{280} x (dilution factor) : $\varepsilon_{protein}$ = $C_{protein}$ [M] in undiluted sample

Absorption maxima of aromatic residues:

Tryptophane (Trp, W) 280nm ε_{280} = 5600 M^{-1} cm^{-1}

Tyrosine (Tyr, Y) 274nm ε_{280} = 1400 M^{-1} cm^{-1}

Phenylalanine (Phe, F) 257nm ε_{280} = 200 M^{-1} cm^{-1}

10.3 Coomassie Blue Stain

Fixing Solution
50 % Methanol
10 % Acetic acid
→ 30min or overnight
Staining Solution
10 % Acetic acid
44 % Methanol
0.05 % Coomassie Blue G-250
→ 1-2h
Destaining Solution
10 % Acetic acid
→ renew destain every ~30min
Recycling:
1) Fixing solution: Use multiple times
2) Staining solution: Use multiple times
3) Destaining solution: Filter through active charcoal, use multiple times

10.4 Silver Stain

USE A SHAKING PLATFORM FOR ALL STEPS!!!
◘ fix gel in **50% EtOH, 10% acetic acid** → 1h or better overnight
◘ incubate in **30% EtOH** → 15min
◘ wash 3x with **ddH$_2$O** → 5min each
◘ sensitize gel with **0.02g Na$_2$S$_2$O$_3$/100mL** → 1.5min
(freshly prepared, save small amount for the developing solution)
◘ wash 3x with **ddH$_2$O** → 0.5min each
◘ incubate with 1**60mg AgNO$_3$/80mL** → 25min
(in the dark, wrap in aluminium foil)
◘ wash 3x with **ddH$_2$O** → 0.5min each
◘ develop gel with
4.8g Na$_2$CO$_3$, 1.6mL of the saved Na$_2$S$_2$O$_3$ solution, 50µL 30% HCHO / 80mL (in the dark, wrap in aluminium foil) → 15min + (till desired staining is reached)
◘ stop development by discarding developing solution and incubation in
6mL acetic acid /100mL → 10min
◘ wash at least 4x with **ddH$_2$O** → 30min each and then overnight
Recycling:
AgNO$_3$ solution: Collect, add 1 platelet of NaOH, let precipitate overnight and collect precipitated Ag$_2$O by filtration (G3)
Dissolve in HNO$_3$ and recrystallize

10.5 Tris-Tricine Gel Electrophoresis

Stock solutions	**20% (2mL)**	**16.5% (6mL)**	**10% (2ml)**	**4% (4mL)**
49.5% (32:1) acrylamide sol.	0.808	2.000	0.404	0.323
3x Tris-tricine gel buffer	0.667	2.000	0.667	1.333
50% glycerol	0.400	1.200	0.400	-
water	0.121	0.800	0.523	2.329
25% APS sol. [µL]	3.3	10	5	12
TEMED [µL]	0.75	2.25	1	3

→ 1h at 30V, each 10min +15V 🕙🡅 100V, then 100V

Stock solutions	**12% (10mL)**	**12% (5mL)**
49.5% (32:1) acrylamide sol.	3* 0.808	2* 0.606
3x Tris-tricine gel buffer	4* 0.833	2* 0.833
50% glycerol	2* 1.000	1.000
water	3* 0.747	2* 0.560
25% APS sol. [µL]	20	10
TEMED [µL]	4.5	2.25

→ 15-20min at 90V, then 120V

3x Tris-Tricine Gel Buffer (pH 8.45)
3 M Tris-HCl, pH 8.45
0.3 % ($^{w}/_{V}$) SDS

2x Tricine Sample Buffer (TSB)
100 mM Tris-HCl, pH 6.8
24 % ($^{w}/_{V}$) Glycerol
8 % ($^{w}/_{V}$) SDS
5 % ($^{V}/_{V}$) Mercaptoethanol
0.02 % ($^{w}/_{V}$) Bromophenol Blue
→ 30min at 40°C

Cathode Buffer (pH 8.25)
0.1 M Tris
0.1 M Tricine
0.1 % ($^{w}/_{V}$) SDS
→ don't adjust pH!!!

5x Anode Buffer
1 M Tris-HCl, pH 8.9